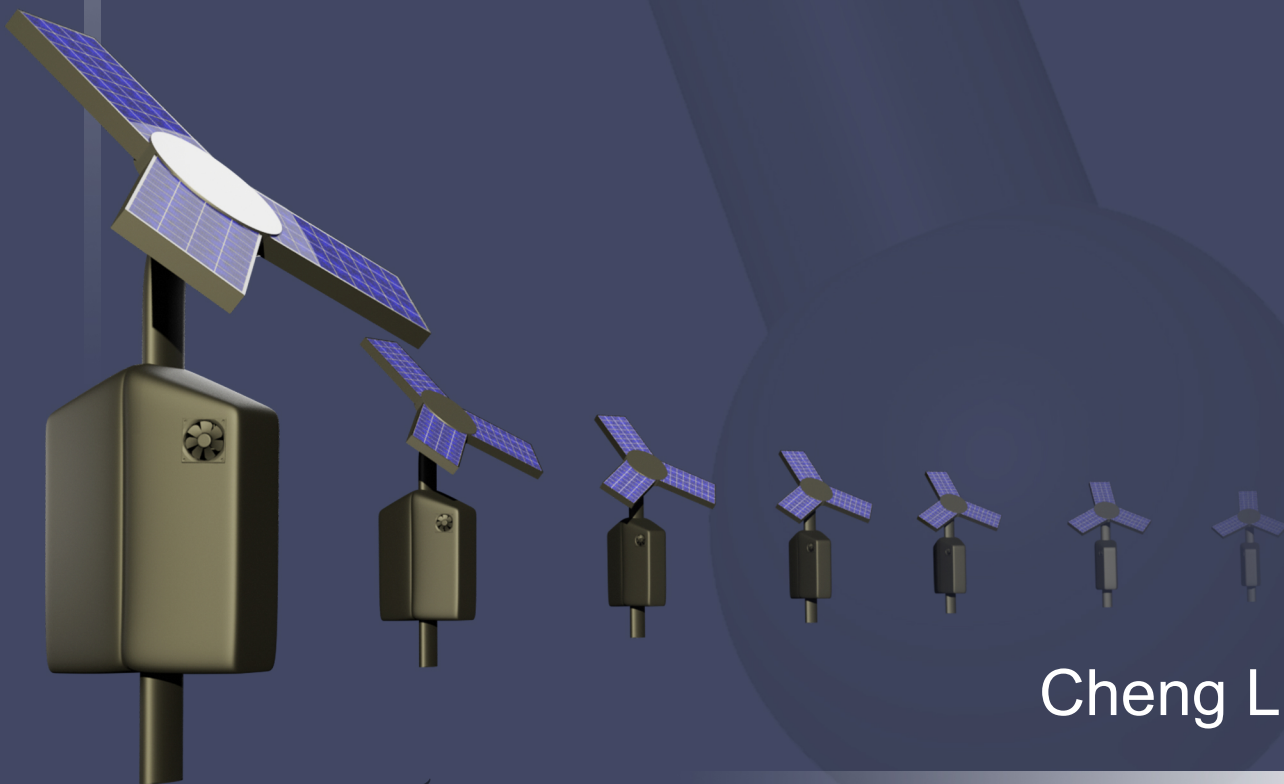
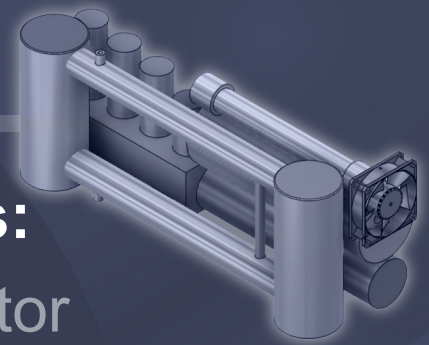


# Green Haber-Bosch Process: A Small-Scale Ammonia Reactor System Design



Cheng Liang



# Green Haber-Bosch Process: A Small-Scale Ammonia Reactor System Design

by

## Cheng Liang

to obtain the degree of Master of Science  
**in Mechanical Engineering**

at the Delft University of Technology,  
to be defended publicly on Wednesday December 18, 2019 at 11:00 AM.

Student number:	4737709	
Project duration:	March 1, 2019 – December 18, 2019	
Daily Supervisors:	Ir. Jan van Kranendonk,	ZEF B.V., Delft, The Netherlands
	Ir. Maartje Feenstra,	TNO, Delft, The Netherlands
Thesis committee:	Prof. dr. ir. Earl Goetheer,	TU Delft/TNO, supervisor
	Prof. dr. ir. Wiebren de Jong,	TU Delft
	Prof. dr. ir. Burak Eral,	TU Delft

*This thesis is confidential and cannot be made public until December 18, 2021.*

An electronic version of this thesis is available at <http://repository.tudelft.nl/>.



# Summary

The global energy transition from a fossil fuel base energy system to a renewable energy source base system is the key mission for a low-carbon future. The target of  $CO_2$  emission reduction by 2050, following the Paris Climate Agreement, is 90% compared to the  $CO_2$  level of 1990. Haber-Bosch process is the main industrial procedure for the production of ammonia today and about 80% of the global ammonia is consumed by the fertilizer industry. However, the century old Haber-Bosch process is normally energized by fossil fuel and it releases about 3% of the global carbon footprint. In light of this fact, replacing the conventional fossil fueled Haber-Bosch process for manufacturing ammonia with renewable source powered ammonia production is the main goal of this study. Instead of obtaining  $H_2$  from steam-reformed  $CH_4$ ,  $H_2$  is produced from electrolyzed  $H_2O$ . This transition enables the conventional ammonia manufacturing process transforming into a green Haber-Bosch production of ammonia. Two Dutch companies, TNO and Zero Emission Fuels, are co-operating and developing a small scale of reactor system that can convert ammonia from air and water by using solar PV panels.

In this work, a new design of ammonia reactor system is developed. Ammonia is typically formed at high pressure (150 - 250 bar) and high temperature (400 - 500°C) using a promoted iron base catalyst. High temperature ensures rapid reaction kinetics, and high pressure boosts the product yield. Here a reactor system, that is operated at lower pressure ( $\leq 100$  bar) and uses condensation to remove ammonia, is kinetically simulated in ASPEN. The effect of different operation conditions - reaction temperature (300°C, 350°C and 400°C), pressure (50, 75 and 100 bar) and feed gas ( $N_2 : H_2$ ) ratio (1 : 3 and 1 : 5) - on the production rate in a small-scale ammonia reactor have been systematically computed. The mass flow rate of the single pass reactor is set to 50 g/h in this work. With a catalyst bed length of 15 cm and inner diameter of 3.6 cm, according to the simulation, reaction temperature of 400°C and operating pressure of 100 bar can lead to the highest conversion (40%) in a single pass reactor. The average heat transfer area of the reactor system is to a great extent less than 50  $m^2$ , therefore, the double pipe heat exchanger is a favorable heat exchange system for the proposed reactor system. In the reactor design validation section, the selected optimum operation conditions are tested in the same scale reactor laboratory setup. Experimental results show that the single pass conversion of nitrogen at 400°C and 100 bar in such a small-scale reactor can reach 15.4% which is in the range of the industrial one pass conversion level. For reaction operated at 50 bar, 6% of ammonia yield is obtained. It is clear that ammonia production in small-scale and in milder operation condition is possible and the results are promising.

The techno-economic analysis has been performed based on above mentioned outcome. The reactor system is integrated with ZEF AEC, ZEF compressor system and a membrane nitrogen separation system. With current ammonia design production (350 g/day), the cost of ammonia per kilogram can be achieved in the range of €1.8 to €2 depending on the operation condition. This is about 5 times more than fossil ammonia prices, but it is very competitive with biomass ammonia. In accordance with the sensitivity analysis, increasing the capacity of feed gas production or reducing the cost in plant equipment can remarkably reduce the ammonia price to less than 1 €/kg  $NH_3$ . Furthermore, recommendations in four categories are discussed in the last section of this work, which can lead to a further step towards a green ammonia plant in small-scale.



# Acknowledgements

I would like to express the deepest appreciation to many people who helped me throughout this project and make it a successful one in the end. First and foremost, I would like to thank my supervisor Prof. Earl Goetheer, who is a genius scientist, energetic, humored, open minded and a kind person. Without his continually guidance and persistent help, this dissertation would not have been possible. I would also like to thank Jan van Kranendonk, Hessel Jongebreur and Ulrich Starke from ZEF for sharing their knowledge, offering me advice and showing their passion in science which was enlightening to me during my thesis.

A great part of this work is experimenting. I am grateful to Arjen Huizinga, Paul Gravesteijn, Nathan Godefroij, Daphne Iwaarden-Bakker, Martin Mohana, Saskia Bubberman and Roberta Veronezi Figueiredo in TNO. They provided me a lot of support on building the setup and making sure the experiment would run safely in the laboratory. I also had the good fortune to have many nice colleagues in TNO SPESS, with whom we ate kippie together every Friday, we celebrated birthdays, we talked about personal life and we discussed about science. In particular, I would like to thank Maartje Feenstra, who has been my TNO mentor during the months of my thesis. She calmed me when I was stressed and provided me help whenever I need.

Additionally, I would like to thank my husband Itam. He is the one always encouraging me and making me laugh all the time. I would like to thank my previous colleagues, or I would say friends, in Oliver Valves. Combining work with a full time study in the first year was not an easy task for both of us, but they trusted me and even adapted a new working process with me which made me feel warmed and supported. Last but not least, I would like to thank my families in China. They made me an independent woman and gave me all the trust, love and freedom for doing things I like.

It has been a fruitful two years in TU Delft. I love this university. I had great time here with all my professors and classmates. It is a place brought out the best in me and showed me more than what I expected at the start of this second master study. The knowledge I gained here I will bring it to the next stage of my life.

*Cheng Liang*  
*Rotterdam, December 2019*



# Contents

<b>List of Figures</b>	<b>xi</b>
<b>List of Tables</b>	<b>xv</b>
<b>1 Introduction</b>	<b>1</b>
1.1 “The bread from the air”: Haber-Bosch Process . . . . .	1
1.2 Global renewable energy development . . . . .	2
1.2.1 Small-scale solar energy . . . . .	4
1.2.2 Small-scale wind turbine. . . . .	4
1.2.3 Solutions to the fluctuation of renewable sources . . . . .	4
1.3 Power to ammonia (P2A) . . . . .	4
1.4 Ammonia market . . . . .	5
1.5 Research questions . . . . .	6
1.6 Thesis methodology & outline . . . . .	6
1.6.1 Methodology. . . . .	6
1.6.2 Outline. . . . .	6
<b>2 Literature Review</b>	<b>9</b>
2.1 History of ammonia synthesis. . . . .	9
2.1.1 Nitrogen fixation before Haber-Bosch Process . . . . .	9
2.1.2 Fritz Haber, Carl Bosch and BASF . . . . .	9
2.1.3 The beginning of Haber-Bosch ammonia production . . . . .	9
2.2 Haber-Bosch Process: thermodynamic characteristics . . . . .	10
2.2.1 Chemical equilibrium . . . . .	11
2.2.2 Heat of reaction . . . . .	11
2.3 Catalysts . . . . .	12
2.4 Reaction kinetic. . . . .	13
2.4.1 Heat and mass transfer. . . . .	14
2.4.2 The reaction kinetic on the multi-promoted iron based catalyst . . . . .	14
2.4.3 Rate equations . . . . .	15
2.5 Reactors. . . . .	16
2.5.1 Ammonia synthesis reactor flow models . . . . .	16
2.5.2 Kellogg’s ammonia synthesis reactors . . . . .	16
2.5.3 Braun’s ammonia converter . . . . .	17
2.5.4 Topsoe’s radial flow reactor . . . . .	17
2.6 Heat integration: Heat pipes . . . . .	17
2.7 Heat integration: Double pipe heat exchanger . . . . .	18
2.7.1 Heat transfer coefficients for double pipe exchangers without fins. . . . .	19
2.7.2 Hydraulic calculations for double pipe exchangers without fins . . . . .	19
2.7.3 Heat transfer coefficient for un-finned multi-tube heat exchangers . . . . .	20
2.8 Ammonia separation by condensation . . . . .	20
2.9 Ammonia separation by adsorption/absorption . . . . .	21
2.9.1 Separation by absorption using magnesium chloride . . . . .	21
2.9.2 Separation by absorption using calcium chloride . . . . .	22
2.10 Worldwide current green ammonia plants/projects. . . . .	22
2.10.1 The Proton Venture’s NFUEL unit . . . . .	23
2.10.2 The SOC4NH3 project in Denmark. . . . .	23
2.10.3 Thyssenkrupp - Carbon2Chem . . . . .	24
2.10.4 Yara . . . . .	24
2.10.5 CSIRO . . . . .	25

2.10.6 Siemens . . . . .	25
2.10.7 Enaex - Chile. . . . .	26
2.10.8 ARENA's new ammonia plan . . . . .	26
2.10.9 Ballance Agri-Nutrients in New Zealand . . . . .	26
2.10.10 H <sub>2</sub> U Port Lincoln green H <sub>2</sub> /NH <sub>3</sub> project. . . . .	26
<b>3 Process Simulation</b>	<b>27</b>
3.1 Simulation methodology . . . . .	27
3.2 Reactor modelling . . . . .	28
3.2.1 Reaction equilibrium . . . . .	30
3.2.2 Conversion along the bed length. . . . .	32
3.2.3 An adiabatic or an isothermal reactor . . . . .	32
3.3 Process simulation . . . . .	34
3.3.1 Reactor. . . . .	34
3.3.2 Double pipe heat exchangers . . . . .	36
3.3.3 Condenser . . . . .	37
3.3.4 Equipment heat duty comparison . . . . .	40
<b>4 Experiment Infrastructure</b>	<b>43</b>
4.1 P&ID Design . . . . .	43
4.2 HAZOP . . . . .	44
4.2.1 Methodology. . . . .	44
4.2.2 Chemical characterization . . . . .	45
4.2.3 Materials for ammonia synthesis converter . . . . .	46
4.2.4 HAZOP worksheets . . . . .	48
4.2.5 Scenarios and risks. . . . .	48
4.2.6 Nitrogen gas line to the oven . . . . .	49
4.2.7 Ammonia absorption by sulfuric acid . . . . .	49
4.3 Setup equipment and material . . . . .	49
4.4 Setup assembly . . . . .	50
4.5 Testing procedure. . . . .	51
4.5.1 Leak test . . . . .	51
4.5.2 Catalyst activation . . . . .	51
4.5.3 Haber-Bosch ammonia synthesis reaction laboratory experiments . . . . .	51
<b>5 Reactor Design Validation</b>	<b>53</b>
5.1 Ammonia production test results . . . . .	53
5.2 Pressure decay test results . . . . .	55
5.2.1 The stabilized pressure in a small-scale ammonia reactor . . . . .	55
5.2.2 Effect of initial pressure, feed gas ratio and temperature to the reaction . . . . .	56
5.2.3 Catalyst performance . . . . .	57
5.2.4 Initial rate determination from the experiments . . . . .	58
5.3 Fixed bed pressure drop validation . . . . .	61
5.4 The experimental results comparison. . . . .	62
<b>6 Micro-Ammonia Plant Techno-Economic Analysis</b>	<b>65</b>
6.1 Methodology . . . . .	66
6.2 Micro-ammonia plant energy and mass balance . . . . .	66
6.2.1 Energy balance. . . . .	66
6.2.2 Mass balance . . . . .	66
6.3 Capital cost . . . . .	67
6.3.1 Base cases CAPEX estimation . . . . .	68
6.4 Base cases OPEX estimation . . . . .	69
6.5 Annualized capital cost and total annualized cost. . . . .	70
6.6 Micro-ammonia plant economic performance analysis. . . . .	71
6.7 Sensitivity analysis . . . . .	73
6.7.1 Scenario I: the effect of the total capital investment on the micro-plant . . . . .	73
6.7.2 Scenario II: the effect of electricity cost on the micro-plant . . . . .	73

---

6.7.3	Scenario III: the effect of $NH_3$ production on the micro-plant . . . . .	74
6.7.4	Sensitivity analysis summary . . . . .	75
6.8	Comparison of the micro-plant design . . . . .	75
6.8.1	CAPEX and OPEX variations . . . . .	75
6.8.2	Ammonia price . . . . .	75
6.8.3	Ammonia production . . . . .	76
6.9	Pro's and Con's of the proposed design . . . . .	77
6.9.1	Pro's . . . . .	77
6.9.2	Con's . . . . .	78
<b>7</b>	<b>Conclusions &amp; Recommendations</b>	<b>79</b>
7.1	Conclusions. . . . .	79
7.2	Recommendations . . . . .	81
7.2.1	Reaction experiment. . . . .	81
7.2.2	Reaction catalyst. . . . .	81
7.2.3	Double pipe exchangers . . . . .	82
7.2.4	Separation process. . . . .	82
<b>A</b>	<b>Reactor Development</b>	<b>83</b>
<b>B</b>	<b>Reactor Material Properties</b>	<b>87</b>
	<b>Bibliography</b>	<b>89</b>



# List of Figures

1.1	Anhydrous ammonia plant, ca. 1954 [94]	1
1.2	Current process of ammonia production [22]	2
1.3	World population with and without synthetic nitrogen fertilizers. Data from [73]	2
1.4	The development of the renewables [47]	3
1.5	Total global renewable energy in regions [47]	3
1.6	Ammonia market: growth rate by region, 2019 to 2024 (source:Mordor Intelligence [45])	5
1.7	Thesis methodology	6
2.1	A schematic design of the circulation system by Haber's team from the stoichiometric mixture of hydrogen and nitrogen	10
2.2	Ammonia market: volume (%), by end -user industry, global 2019 to 2024 (picture:Mordor Intelligence [45])	10
2.3	Ammonia as a hydrogen carrier distribution [90]	11
2.4	Ammonia content in equilibrium with $N_2:H_2=1:3$ (A) at various temperatures under fixed pressure (B) at different pressures at fixed temperature [60]	11
2.5	Heat of reaction for ammonia synthesis with $N_2:H_2=1:3$	12
2.6	Comparison of $Ru(10wt\%)/Ba(3\%) - Ca(NH_2)_2$ , $Cs - Ru/MgO$ and wüstite iron based catalysts under 1 bar (A) and 9 bar (B)[49]	13
2.7	Schematic energy profile of the ammonia synthesis on Fe [kJ/mol][48]	14
2.8	$NH_3$ concentration as a function of hydrogen partial pressure at various temperatures	15
2.9	Kellogg ammonia converter	17
2.10	Kellogg's horizontal converter	17
2.11	Braun ammonia converter	17
2.12	Haldor Topsoe S-200 ammonia converter	17
2.13	Temperature change in countercurrent flow	18
2.14	Conversion with $MgCl_2$ is increased. [26]	22
2.15	Comparison of reaction and reaction-separation tests at different operation pressures [55]	22
2.16	Proton Venture NFuel's basic concept	23
2.17	The Haldor Topsoe SOC4NH3 project [41]	24
2.18	Power-to-X at thyssenkrupp's process concept A: ammonia from BFG and COG [50]	24
2.19	Yara $RH_2$ integration in ammonia production [93]	24
2.20	Yara $RH_2$ integration in ammonia production road map in Pilbara [93]	25
2.21	CSIRO novel direct ammonia production [42]	25
2.22	CSIRO catalytic membrane reactor for ammonia cracking [42]	25
2.23	The system demonstration [79]	26
2.24	H2U plant layout [62]	26
3.1	Drawing of a simplified reactor system	27
3.2	$P = 50$ bar, fugacity coefficient vs. temperature	30
3.3	$P = 75$ bar, fugacity coefficient vs. temperature	30
3.4	$P = 100$ bar, fugacity coefficient vs. temperature	30
3.5	Contour of constant reaction rate for a stoichiometric inert free reaction mixture at a total pressure of 100 bar	31
3.6	Contour of constant reaction rate for 1 : 5 inert free reaction mixture at a total pressure of 100 bar	31
3.7	Contour of constant reaction rate for a stoichiometric inert free reaction mixture at a total pressure of 75 bar	31
3.8	Contour of constant reaction rate for 1 : 5 inert free reaction mixture at a total pressure of 75 bar	31
3.9	Contour of constant reaction rate for a stoichiometric inert free reaction mixture at a total pressure of 50 bar	31

3.10	Contour of constant reaction rate for 1 : 5 inert free reaction mixture at a total pressure of 50 bar	31
3.11	Fraction of nitrogen conversion vs isothermal reactor at 100 bar	32
3.12	Fraction of nitrogen conversion vs isothermal reactor at 75 bar	32
3.13	Fraction of nitrogen conversion vs isothermal reactor at 50 bar	32
3.14	Fraction of nitrogen conversion vs adiabatic reactor at 100 bar, $N_2 : H_2 = 1 : 3$	33
3.15	Fraction of nitrogen conversion vs adiabatic reactor at 100 bar, $N_2 : H_2 = 1 : 5$	33
3.16	Fraction of nitrogen conversion vs adiabatic reactor at 75 bar, $N_2 : H_2 = 1 : 3$	33
3.17	Fraction of nitrogen conversion vs adiabatic reactor at 75 bar, $N_2 : H_2 = 1 : 5$	33
3.18	Fraction of nitrogen conversion vs adiabatic reactor at 50 bar, $N_2 : H_2 = 1 : 3$	33
3.19	Fraction of nitrogen conversion vs adiabatic reactor at 50 bar, $N_2 : H_2 = 1 : 5$	33
3.20	Process modelling in ASPEN	34
3.21	Reactor simulation in Aspen	34
3.22	Reaction residence time and heat released at various pressures	35
3.23	Fixed bed pressure drop at $400^\circ C$ with $N_2 : H_2 = 1 : 3$	35
3.24	Fixed bed pressure drop at $400^\circ C$ with $N_2 : H_2 = 1 : 5$	35
3.25	Double pipe heat exchanger system simulation in Aspen	36
3.26	Polydimethylsiloxane [8]	36
3.27	Condenser simulation in Aspen	37
3.28	Steady state equivalent network of the condenser thermal resistance system [61]	38
3.29	Energy balance on the $j^{th}$ mixture and material elements	39
3.30	Steady state heat rejection along the condenser	39
3.31	Gas mixture temperature along the condenser	39
3.32	Process Fusion360 model based on the ASPEN simulation results	40
3.33	Utilities heat duty comparison for different reactor sizes at 50 bar and $400^\circ C$ (Aspen model data)	41
4.1	Experiment process flowchart	43
4.2	The setup P&ID	44
4.3	TNO HAZOP risk ranking level	44
4.4	Safe operation zones for steels in hydrogen service [14]	47
4.5	Creep rate curves for several annealed stainless steels[14]	47
4.6	Setup before experiment	50
4.7	Sulfuric acid bottles used during the experiments	52
5.1	Space time yield versus pressure	54
5.2	Pressure decay to stabilized pressures	55
5.3	Pressure vs. time under various feed gas ratios	56
5.4	Tests performed at 100 bar $400^\circ C$ and $350^\circ C$	57
5.5	Catalyst performance after 9 days	57
5.6	Catalyst performance after 14 days	57
5.7	Catalyst performance during the ammonia production test	58
5.8	Reaction order determination	59
5.9	Reaction rate constant determination at $400^\circ C$ 100 bar	60
5.10	Reaction rate constant determination at $350^\circ C$ 100 bar	60
5.11	Reaction rate constant determination at $400^\circ C$ 75 bar	60
5.12	Reaction rate constant determination at $400^\circ C$ 50 bar	60
5.13	Reaction backwards rate constants comparison with literature	61
5.14	Fresh catalyst before the experiment	61
5.15	Catalyst after weeks of experiments	61
5.16	Fixed bed pressure before the experiment ( $N_2 : H_2 = 1 : 3$ , $d_p = 2$ mm)	62
5.17	Fixed bed pressure after the experiment ( $N_2 : H_2 = 1 : 3$ , $d_p = 1$ mm)	62
5.18	Fixed bed pressure before the experiment ( $N_2 : H_2 = 1 : 5$ , $d_p = 2$ mm)	62
5.19	Fixed bed pressure after the experiment ( $N_2 : H_2 = 1 : 5$ , $d_p = 1$ mm)	62
5.20	Space-time yield vs. pressure with $N_2 : H_2 = 1 : 3$	63
5.21	Space-time yield vs. pressure with $N_2 : H_2 = 1 : 5$	63
5.22	Catalyst weight loss	63

5.23	Reactor cross section cut after experiment . . . . .	63
5.24	Reactor before the experiment . . . . .	64
5.25	Reactor after weeks of experiments . . . . .	64
6.1	Ammonia micro-plant: 350 g/day . . . . .	65
6.2	Ammonia mini-plant: 65 kg/day [70] . . . . .	65
6.3	Ammonia pilot plant: 10 tons/day[68] . . . . .	65
6.4	Ammonia industrial plant: 3300 tons/day[84] . . . . .	65
6.5	Equipment cost percentage in a 50 bar (green) and 100 bar (blue) operation reactor system . . . . .	68
6.6	Net present value of a 50 bar micro-plant system . . . . .	71
6.7	Net present value of a 100 bar micro-plant system . . . . .	72
6.8	Cum. PV of a 50 micro-plant . . . . .	72
6.9	Cum. PV of a 100 micro-plant . . . . .	72
6.10	Micro-plant sensitivity analysis on CAPEX variation . . . . .	73
6.11	Micro-plant sensitivity analysis on electricity cost variation . . . . .	74
6.12	Micro-plant sensitivity analysis on $NH_3$ production variation . . . . .	74
6.13	50 bar micro-plant sensitivity analysis . . . . .	75
6.14	Two micro-plants CAPEX comparison . . . . .	75
6.15	Two micro-plants OPEX comparison . . . . .	75
6.16	Ammonia average market cost [\$/ton] (Source: BCInsight) . . . . .	76
6.17	Ammonia global production and the top 10 producers (source:IFA) . . . . .	77
6.18	Nitrogen fertilizer application by region and product [24] . . . . .	77
7.1	Multi-bed reactor: in series or in parallel . . . . .	81
7.2	Comparison between iron base catalyst and Ru base catalyst at $400^{\circ}C$ . . . . .	82
7.3	Setup system of reactor in combination with heat exchanger system . . . . .	82
A.1	Reactor design revision 1 - single pass plug flow reactor for experiment . . . . .	83
A.2	Reactor design revision 2 with double pipe heat exchanger in accordance to ASPEN process simulation results . . . . .	84
A.3	Green ammonia micro-plant (50 bar) without solar panel . . . . .	84
A.4	Green ammonia micro-plant (50 bar) with solar panel . . . . .	85



# List of Tables

1.1	Net energy consumption of natural gas based steam reforming ammonia plant in GJ/t $NH_3$ [17]	2
1.2	Classification of HAWT based on rotor diameter and power rating [88]	4
2.1	The first reported measurements of the equilibrium between ammonia, hydrogen and nitrogen [48]	9
2.2	Ammonia synthesis catalyst development[53]	12
2.3	Kinetic parameters for nitrogen adsorption and dissociation on Fe(III) and on K/Fe.[83]	15
2.4	Rate equations for ammonia synthesis reaction[48]	16
2.5	Different flow management for adiabatic ammonia synthesis reactor	16
2.6	Ammonia absorbents and adsorbents[92]	21
2.7	Details of Proton Venture's ammonia mini plant[25]	23
2.8	Siemens green ammonia demonstrator vital statistics [79]	25
3.1	Groups of parameters used for reactor Matlab calculation	28
3.2	The kinetics constants values	30
3.3	Maximum value of nitrogen conversion at each operation condition for an isothermal reactor	32
3.4	Isothermal small-scale ammonia synthesis reactor single pass optimal conversions	34
3.5	Reactor parameters comparison under various pressures	35
3.6	Silicone oil mixture used in the Aspen model	36
3.7	Double pipe heat exchanger heat duty and heat transfer area at different operation pressures	37
3.8	$cm^3$ of gas at NPT soluble per gram of liquid ammonia per atm. partial pressure [64]	38
3.9	Condenser parameters	38
3.10	Condenser stream gas conditions in ASPEN model	39
3.11	Matlab calculation condenser results	40
4.1	Chemical NFPA ranking	45
4.2	Critical parameter of hydrogen	45
4.3	Sulfuric acid toxicity [32]	46
4.4	Setup facility data overview	48
4.5	Maximum operation values of the components	50
4.6	Testing parameters	51
5.1	Titration test with $N_2 : H_2 = 1 : 3$	54
5.2	Titration test with $N_2 : H_2 = 1 : 5$	54
5.3	Pressure decay tests duration	55
5.4	Ammonia synthesis forwards reaction order [23]	59
5.5	The kinetics forwards an backwards rate constant values with $N_2 : H_2 = 1 : 3$	60
6.1	50 bar micro-ammonia plant energy balance	66
6.2	100 bar micro-ammonia plant energy balance	66
6.3	Micro-ammonia plant mass balance	67
6.4	Reactor system shell mass	68
6.5	Overview of equipment cost	68
6.6	CAPEX estimation of a 50 bar micro-ammonia plant	69
6.7	CAPEX estimation of a 100 bar micro-ammonia plant	69
6.8	VCOP estimation of a 50 bar micro-ammonia plant	69
6.9	FCOP estimation of a 50 bar micro-ammonia plant	70
6.10	VCOP estimation of a 100 bar micro-ammonia plant	70
6.11	FCOP estimation of a 100 bar micro-ammonia plant	70

---

6.12 Annualized capital cost of the micro-plants . . . . .	71
6.13 TAC of the micro-plants . . . . .	71
6.14 Gross profit of the micro-plants . . . . .	71
6.15 Simple after tax payback time of the micro-plants . . . . .	72
6.16 Price comparison of ammonia from different sources . . . . .	76
7.1 The single pass conversion values of a small-scale ammonia synthesis reactor . . . . .	80
7.2 A green ammonia micro-plant techno-economic analysis summary . . . . .	81
B.1 Material mechanical properties in comparison with SS316L [54] . . . . .	87
B.2 Material thermal properties in comparison with SS316L [54] . . . . .	87
B.3 Alloy compositions in comparison with SS316L [54] . . . . .	87

# Nomenclature

## Abbreviations

ACC	The Annual Capital Cost
ACCR	The Annual Capital Charge Ratio
AEC	Alkaline Electrolysis Cell
Alibaba	Alibaba Group Holding Limited
ARENA	The Australian Renewable Energy Agency
ASPEN	Advanced System for Process Engineering
ASU	Air Separation Units
BASF	Badische Anilin und Soda Fabrik
BFG	Blast Furnace Gas
BP	The British Petroleum Company
CAGR	Compound Annual Growth Rate
CAPEX	Capital Expenditure
CCOP	The Cash Cost of Production
CF	The Net Cash Flow
COCO	Cape-Open to Cape-Open Simulation Software
COG	Coke Oven Gas
CSIRO	The Commonwealth Scientific and Industrial Research Organization
DR	The Debt Ratio
FCOP	The Fixed Cost of Production
H2U	Hydrogen Utility
HAZOP	Hazard and Operability Study
IFA	International Fertilizer Industry Association
IRENA	International Renewable Energy Agency
ISBL	The Inside Battery Limits Investment
KAAP	KBR Advanced Ammonia Process
LC50	Lethal Concentration 50%
LD50	Lethal Dose 50%
LEL	Lower Explosive Limit
LHHW	Langmuir-Hinshelwood-Hougen-Waston

---

Matlab	Matrix Laboratory
NPV	The Net Present Value
OPEX	Operating Expense
OSBL	The Outside Battery Limits Investment
P2A	Power to Ammonia
RKS	Redlich-Kwong Soave
SOEC	Solid Oxide Electrolysis Cell
SOFC	Solid Oxide Fuel Cell
TAC	The Total Annualized Cost of Production
TNO	Netherlands Organization for Applied Scientific Research
VCOP	The Variable Cost of Production
ZEF B.V.	Zero Emission Fuels B.V.

**Chemical formulas**

<i>AC</i>	Activated carbon
<i>Al</i>	Aluminum
<i>Ba</i>	Barium
<i>BaO</i>	Barium oxide
<i>C</i>	Carbon
<i>CaO</i>	Calcium oxide
<i>CNT</i>	Carbon nanotube metal
<i>Co</i>	Cobalt
<i>Cs</i>	Caesium
<i>Fe</i>	Iron
<i>K</i>	Potassium
<i>La</i>	Lanthanum
<i>MgO</i>	Magnesium oxide
<i>Pr</i>	Praseodymium
<i>Ru</i>	Ruthenium
<i>Al<sub>2</sub>O<sub>3</sub></i>	Aluminum oxide
<i>Ba – Ca(NH<sub>2</sub>)<sub>2</sub></i>	Barium-doped calcium amide
<i>BaCl<sub>2</sub></i>	Barium chloride
<i>C<sub>16</sub>H<sub>48</sub>Si<sub>7</sub>O<sub>6</sub></i>	Hexadecamethylheptasiloxane
<i>C<sub>18</sub>H<sub>54</sub>Si<sub>8</sub>O<sub>7</sub></i>	Octadecamethyloctasiloxane
<i>CaCl<sub>2</sub></i>	Calcium chloride

$CO_2$	Carbon dioxide
$Fe_3O_4$	Iron oxide
$H_2SO_4$	Sulfuric acid
$H_2$	Hydrogen
$K_2O$	Potassium oxide
$MgCl_2$	Magnesium chloride
$MnCl_2$	Manganese chloride
$N_2$	Nitrogen
$NaOH$	Sodium hydroxide
$NH_3$	Ammonia
$SrCl_2$	Strontium chloride

**Symbols**

$c$	Concentration	$mol/L$
$H$	Heat of reaction	$kJ/mol$
$M$	Concentration	$mol/L$
$n$	Mole	$mole$
$P$	Pressure	$bar$
$R$	The universal gas constant	$L \cdot bar \cdot K^{-1} \cdot mol^{-1}$
$T$	Temperature	$K$
$V$	Gas volume	$m^3$
$X$	Volume percentage	
$\Delta P$	The fixed bed pressure drop	$N/m^2$
$\Delta T_{lm}$	Mean temperature difference	$K$
$\dot{m}$	Mass flow rate	$g/s$
$\epsilon$	The void fraction	
$\mu$	Cold fluid temperature	$Pa \cdot s$
$\rho_f$	The fluid density	$kg/m^3$
$\theta$	Surface coverage	
$A$	Heat transfer area	$m^2$
$C_p$	The heat capacity	$J/K$
$D_e$	Equivalent diameter	$m$
$d_i$	Inner diameter	$m$
$d_o$	Outer diameter	$m$
$d_p$	The catalyst particle effective diameter	$m$

$D$	Outer shell diameter	$m$
$E_a$	Activation energy	$kJ/mol$
$E$	The welding point efficiency	
$F_t$	Correction factor	
$f$	Friction factor	
$h_a$	The heat transfer coefficient of the ambient air	$W/m^2K$
$h$	Convective heat transfer coefficient	$W/m^2K$
$K_p$	Reaction equilibrium constant	
$k$	Thermal conductivity	$W/mK$
$L_b$	The length of catalyst fixed bed	$m$
$LHV$	The lower heating value	$MJ/kg$
$L$	Length	$m$
$Nu$	The Nusselt number	
$Pr$	The Prandtl number	
$Q$	Heat transfer per unit time	$W$
$R_i$	The equivalent network of the resistances	$W/K$
$R_f$	Dirt coefficient	$W/m^2K$
$r_{NH_3}$	Reaction rate	$kmol_{NH_3}/m^3_{cat}/h$
$Re$	The Reynolds number	
$STY$	Space time yield	$g_{NH_3}/h/g_{cat}$
$S$	Shape factor	
$T_b$	The fluid bulk temperature	$K$
$T_i$	Hot fluid temperature	$K$
$t_i$	Cold fluid temperature	$K$
$t_w$	Shell wall thickness	$m$
$U$	Overall heat transfer coefficient	$W/m^2K$
$u$	The fluid superficial velocity	$m/s$

# 1

## Introduction

The 2015 Paris agreement targets a  $CO_2$  emission reduction of 85% to 90% by 2050 compared to  $CO_2$  levels in 1990. Using renewable energy, such as solar energy, wind energy, hydro-power, bio-energy or geothermal energy, instead of fossil fuels is one of the paths for reaching the carbon reduction goal.

The Haber-Bosch process, discovered by Fritz Haber and Carl Bosch, is an artificial nitrogen fixation with hydrogen to produce ammonia, which is a crucial component in production of fertilizers. It is one of the most important discoveries in history that has contributed enormously to the survival of mankind. More than 80% of the ammonia produced nowadays is used in fertilizer production. Besides, the Haber-Bosch process relies on high temperature and high pressure. It requires a lot of energy. Existing ammonia plants are still from early 20<sup>th</sup> century and gigantic. They rely on fossil fuels to produce ammonia and release loads of carbon (about 3 % of the global  $CO_2$  emissions). In the Netherlands, ammonia production emits a third of the total  $CO_2$  amount from chemical industry. Ammonia produced from renewable energy can significantly reduce the greenhouse gas emissions.



**Figure 1.1:** Anhydrous ammonia plant, ca. 1954 [94]

### 1.1. “The bread from the air”: Haber-Bosch Process

Ammonia is usually made by burning coal or natural gas to obtain nitrogen, hydrogen and other mixtures of water and carbon dioxide. After careful removal of water and carbon dioxide, the reactants (nitrogen and hydrogen) carry out the reaction at high temperature and pressure on iron based catalyst to form ammonia. The unreacted nitrogen and hydrogen are recycled after the separation of liquid ammonia. Most of the processes

are aimed at hydrogen production. Starting with fossil-fuel feedstocks, the processes applied in the ammonia production are shown in the following flow chart 1.2.

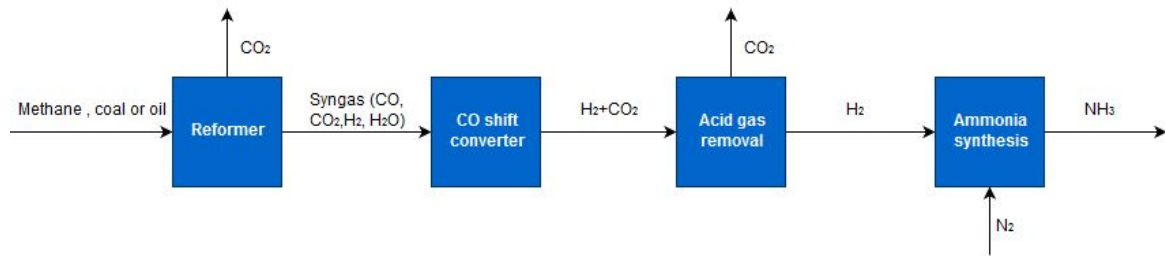


**Figure 1.2:** Current process of ammonia production [22]

There is a high level of the surplus energy available from the steam reformer and the process gas streams. Additionally, a considerable amount of mechanical energy is required for driving the compressors, pumps and blowers. The conventional plant is inefficient because of the lack of heat recovery and low efficiency in some energy consumers. The development of the plant was carried out. The decreases in energy consumption from older generation to a new technology was significant. A development of the net energy consumption of a real natural gas based steam reforming ammonia plant has been recorded from 1966 till 1991 1.1.

Year/Plant	1966	1973	1977	1980	1991
Feed	23.9	23.32	23.48	23.36	22.65
Fuel, reformer	13	9.21	7.35	5.56	5.9
Fuel, auxiliary	2.6	5.02	3.06	1.17	-
Total	39.50	37.55	33.89	30.18	28

**Table 1.1:** Net energy consumption of natural gas based steam reforming ammonia plant in GJ/t  $NH_3$  [17]

Approximately, 1.6 % of the world fossil energy consumption goes into ammonia production. As the research of Erismann et al. (2008), Smil (2002) and Stewart (2005) shows that the growth of world population was in proportion to the world population fed by synthetic fertilizer.

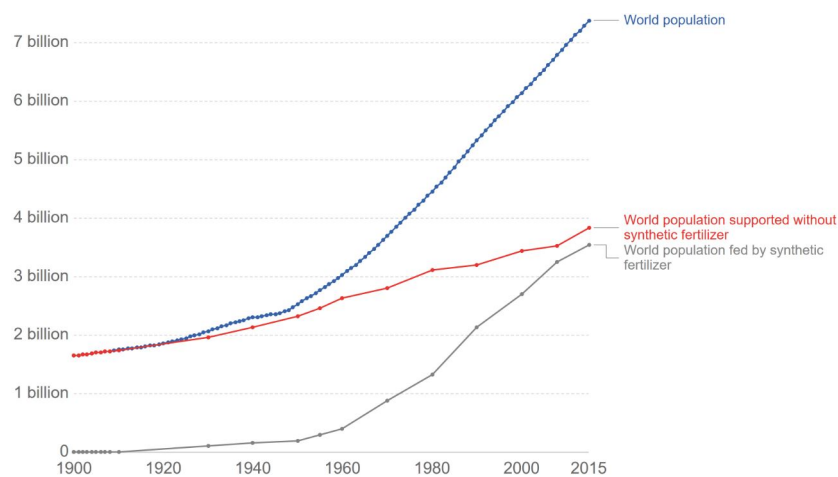


**Figure 1.3:** World population with and without synthetic nitrogen fertilizers. Data from [73]

## 1.2. Global renewable energy development

The role of energy is essential in the world's sustainability development. Energy that is generated by natural sources, such as sunlight, wind, rain, tides, waves, and geothermal heat, are named renewable energy. The

forms of the energy that are created by renewable sources are mainly electricity and heating or cooling.

From the end of 2004 the global renewable energy capacity grew at a rate of 10 - 60 % annually. In 2017 the investments in renewable energy reached to \$279.8 billion worldwide, with China accounting for \$126.6 billion (45% of the global investments), the US \$40.5 billion, and Europe for \$40.9 billion. According to the International Renewable Energy Agency (IRENA) in 2018, the costs of renewable energy dropped quickly, and will likely be equal to, or even less than, the costs of non-renewable, such as fossil fuels by 2020. Especially, the costs of solar power dropped 73% since 2010 and onshore wind power costs have decreased by 23% during the same time frame. In the report of Bloomberg New Energy Finance in 2018, wind and solar energy are expected to generate about 50% of the world energy by 2050.

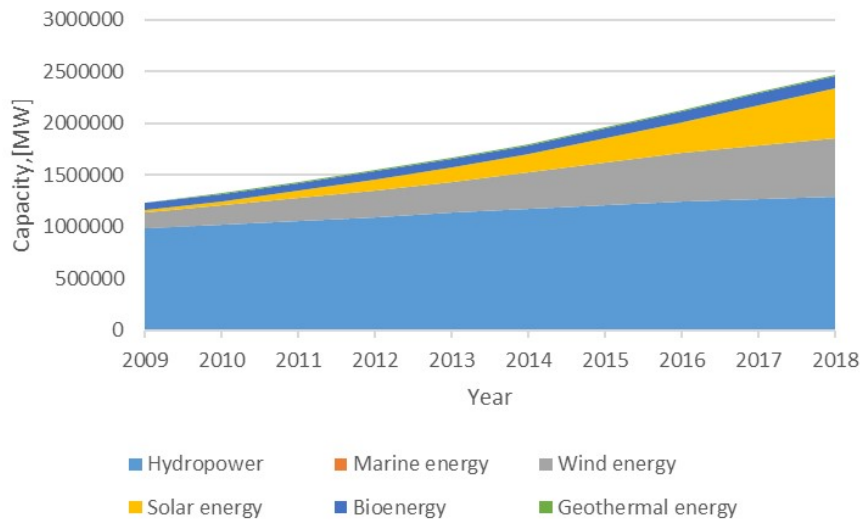


Figure 1.4: The development of the renewables [47]

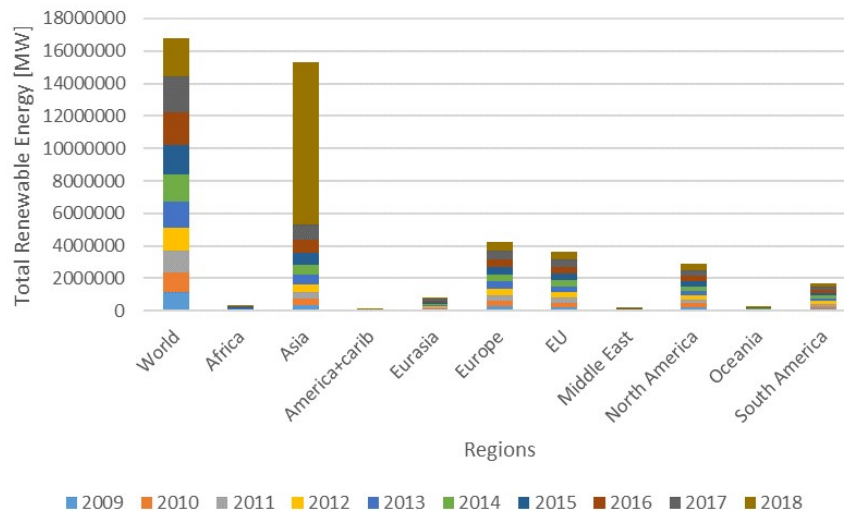


Figure 1.5: Total global renewable energy in regions [47]

The small-scale renewable energy system this thesis is about can not only use the surplus energy efficiently, decrease the energy cost and reduce the carbon footprint, but also increase the energy access. Renewable energy, such as wind power or solar photo-voltaic systems, can be easily scale up and down.

### 1.2.1. Small-scale solar energy

The costs of solar energy have declined dramatically in recent 30 years. In mid 1970s, a solar module costed \$96 per watt. And now in Dubai, a large-scale solar generated electricity is only \$2.99 cents per kWh, which is competitive with any of fossil-based electricity. A solar photovoltaic system consists of many components, such as the panels, the wiring, racks, a converter, a solar monitor and a meter[69]. A typical home use solar power system is in a power capacity of 5 kW. The application of solar energy can enhance sustainability, reduce pollution and mitigate global warming. The potential of solar energy is huge. Regionally, there is plenty amount of solar power available for this technology. For example in the Middle East and North Africa, the total amount of solar energy in these areas has a minimum value of 412.4 EJ and a maximum amount of 11060 EJ annually.

### 1.2.2. Small-scale wind turbine

Another viable renewable energy is wind. Wind turbines convert the kinetic energy in the wind to mechanical energy and eventually into electricity. A small scale wind turbine has a rotor diameter ranging from 0.5m to 10m and has a power capacity of 0.004 - 25 kW. The disadvantages of a small wind turbine are a high initial cost, effective placement, wind fluctuation, change in wind direction and also aero-acoustic noise.

Scale Size		$D_{rotor}$ [m]	Swept area [ $m^2$ ]	Standard power rating [kW]
Small scale	Mirco	0.5-1.25	0.2-1.2	0.004-0.25
	Mini	1.25-3	1.2-7.1	0.25-1.4
	Household	3-10	7-79	1.4-16
Small commercial	-	10-20	79-314	25-100

**Table 1.2:** Classification of HAWT based on rotor diameter and power rating [88]

### 1.2.3. Solutions to the fluctuation of renewable sources

Renewable energy is great, however, it suffers from fluctuation. That is because of the rotation of the earth, changes in weather conditions and seasonal fluctuations. One method to avoid fluctuation is to store surplus energy and to release it when needed. Nowadays, there are five main energy storage systems: mechanical systems such as pumped hydroelectric storage systems, chemical systems (e.g. hydrogen storage with fuel cell / electrolysis cell), batteries, electrical systems and thermal systems (e.g. heat pump) [28].

Chemical systems and batteries seem to be better options for a small-scale process due to their flexibility in size and availability of the technology. Two examples are given below:

#### (1) The storage of electricity: battery system for grid-scale energy

Batteries of various types and size are considered one of the most suitable approaches to store energy. It has smooth output and enhances renewable energy versatility in micro-generation systems and allows them to supply and distribute steady electrical power. However, battery use has significant social and environmental impact during different processes, such as mining, manufacturing, use, transportation, collection, storage and treatment [28]. It also causes hazards during disposal and recycling processes.

#### (2) Battolyser

A battolyser is designed to store surplus wind and solar energy in the form of electricity in a battery and to split water into hydrogen and oxygen by electrolysis. The first battolyser has been made in Eemshaven beginning of 2019[29]. The generated hydrogen can be used as feedstock for various chemical reactions since it has an important role in greening chemical processes.

## 1.3. Power to ammonia (P2A)

A combined application of water electrolysis and the Haber-Bosch process is called power-to-ammonia (P2A) technology [44]. A basic model of a power-to-ammonia plant consists of four parts, which are air separation, electrolysis, intermediate hydrogen buffer and ammonia synthesis. P2A can play two major roles in our sustainability development. First of all, it provides renewable feedstock for the fertilizer industry or other chemical processes. Secondly, power to ammonia enables us to store and transport the energy for a longer period

and with less space. Besides, nitrogen is abundant in the atmosphere and the nitrogen separation from air technology is rather mature. The surplus renewable energy can be used to generate the green feedstocks and produce ammonia. The ammonia product can be stored in liquid. A standard tank of  $60,000\text{ m}^3$  contains around 211 GWh of energy, which is equivalent to the annual production of about 30 wind turbines onshore. The stored ammonia can also be burned in the engines or fuel cells (e.g. SOFCs) for new energy generation. Due to its high energy density, the transportation of ammonia in a larger volume is more feasible than that of hydrogen. Additionally, by catalytic cracking ammonia can produce hydrogen which can then be combusted in fuel cells or gas turbines.

As a synthetic fuel, ammonia has the following clear advantages:

- Its combustion produces zero  $\text{CO}_2$ ;
- It can be easily stored as liquid in atmospheric pressure with the temperature of  $-33^\circ\text{C}$  or pressurized to 10 bar in room temperature;
- It contains large weight fraction of hydrogen. By catalytic cracking, ammonia can be converted to hydrogen as fuel;
- A large infrastructure for the ammonia transportation and storage already exists;
- It has low storage cost and can be densely stored for large energy amount without significant losses.

However, there are also disadvantages, which are:

- Ammonia is corrosive. The anhydrous state of ammonia can cause cracking of carbon steel or high strength low alloy steels;
- It is flammable. When it is exposed to fire in high concentrations, it may cause explosion;
- Ammonia is toxic if inhaled. It can cause chemical burns to skin and cornea.

## 1.4. Ammonia market

The global ammonia market is expected to record a CAGR (Compound Annual Growth Rate) of over 5% in the period of 2019 to 2024. By the end of 2025, it is anticipated to achieve \$70.75 billion. The main reason of the growth is the demand in the agriculture industry and its increasing usage for explosive production. The forecasted largest and fastest growing ammonia market is in Asia Pacific. Ammonia at present is mainly produced from fossil fuels (predominant by natural gas 77%, then coal 23%), air and water. It has a wide range of applications, such as agriculture, textiles, mining, pharmaceutical, refrigeration and other industries. The agriculture industry (for fertilizers) is the most dominates field and has an estimated market share of 80% in 2018.

As the most populous country in the world, China is the major consumer of ammonia and fertilizer (about 56 Mt/year) in both the Asia Pacific region and in the global market in 2018. Ammonia in China is mainly produced from partial oxidation of coal which brings the largest percentage of global  $\text{CO}_2$  emissions (about 200 Mt/year) [46]. Because of the large population, it still has a huge demand for agricultural products [45]. However, due to the less and less arable land (11.3%) in the country, there is an increase need for an ammonia production system that can utilize the land in the most efficient way.



**Figure 1.6:** Ammonia market: growth rate by region, 2019 to 2024 (source:Mordor Intelligence [45])

According to Mordor Intelligence's research, Chinese farmers use an average of 305 kg of nitrogen per year per hectare (0.0305 kg of nitrogen per year per square meter), which is more than 4 times of the global average. Overall, the Asia-Pacific market has high potential and will have a significant growth in its ammonia demand.

## 1.5. Research questions

This thesis focus on the design of a small-scale green Haber-Bosch reactor system. The feedstocks of the reaction are hydrogen and nitrogen. Nitrogen is captured from the air and hydrogen is formed from water in the electrolysis cell. The produced ammonia is condensed to the liquid phase and then stored in large tanks for other applications. A series of selected parameters will be centralized in this work. The feasibility of the concept will be depicted experimentally and economically. To do so, a set of research questions are addressed:

1. What is the feasible operation conditions for a small-scale ammonia synthesis reactor?
2. What is the most favorable heat exchange network?
3. What is the capital and operation cost for such an integrated small-scale green Haber-Bosch micro-plant?

## 1.6. Thesis methodology & outline

### 1.6.1. Methodology

In order to thoroughly research the concept feasibility of a small-scale green Haber-Bosch reactor system, the below methodology is followed in this work 1.7.

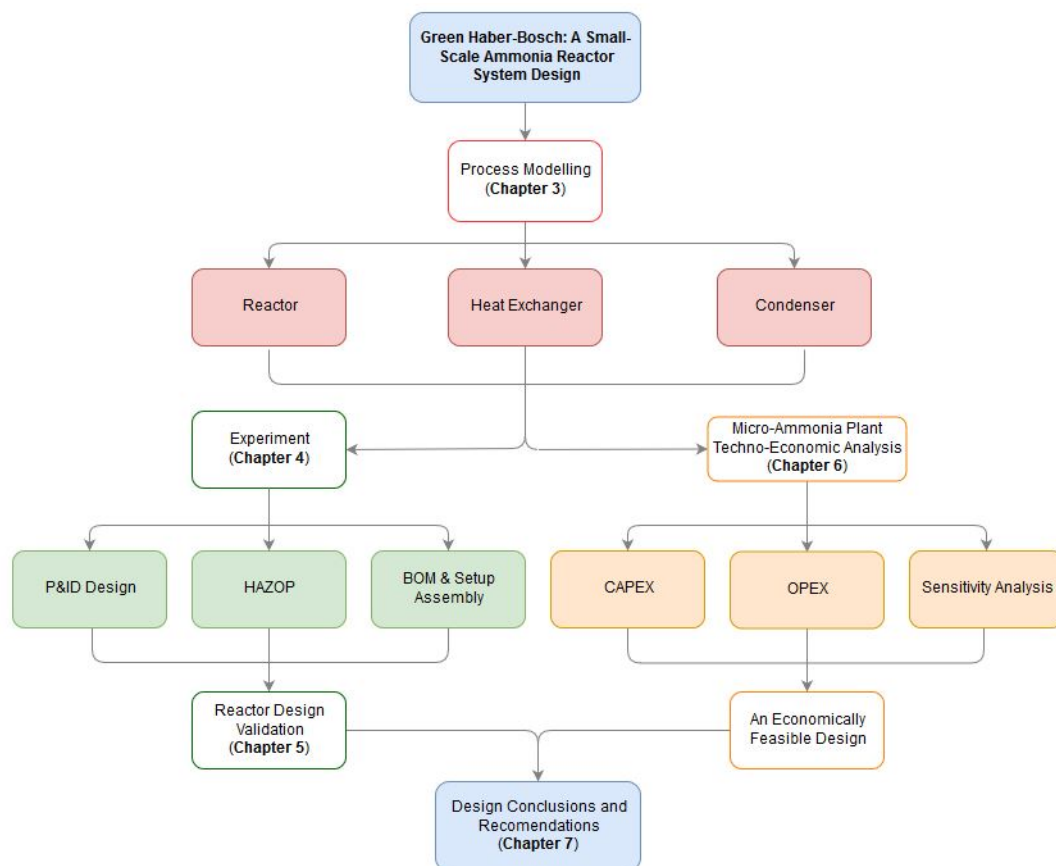


Figure 1.7: Thesis methodology

### 1.6.2. Outline

The thesis is structured in the following outline:

**Chapter 1** illustrates a background story line with the research questions of this project.

**Chapter 2** provides a theoretical background about ammonia synthesis and its separation systems. Besides that, in this chapter the author also summarized the major running green ammonia projects worldwide.

**Chapter 3** a series of selected parameters are simulated in a single pass plug flow reactor, two heat exchangers and a condenser kinetically by using COCO, Matlab and Aspen software. The simulation data helps in defining the directions for experimental activities.

**Chapter 4** since the ammonia production process is under high temperature and high pressure, a comprehensive HAZOP study needs to be executed before the real experiment. The whole setup material and equipment should meet the design operation conditions of the reaction. Several extreme explosive scenarios are interpreted. The detection, safeguards and mitigation actions are provided.

**Chapter 5** two sets of experiments are performed. One is the ammonia production test, another one is a closed system pressure decay test. Data recorded from both experiments are finalized. An optimum reaction condition is selected.

**Chapter 6** the techno-economic analysis is accomplished for an integrated micro-ammonia plant with two operation conditions. An economically feasible process plant is chosen.

**Chapter 7** the research questions as conclusions are drawn based on the work. The corresponding recommendations of future work are addressed based on the lessons learned during this work.



# 2

## Literature Review

### 2.1. History of ammonia synthesis

#### 2.1.1. Nitrogen fixation before Haber-Bosch Process

The “father of the fertilizer industry” - German scientist Justus Freiherr von Liebig firstly emphasized in the year of 1840 that the “fixed” nitrogen is one of the three most important components of a fertilizer. In the 19<sup>th</sup> century, nitrogen-containing fertilizer was obtained as ammonium sulfate, which is a by-product of the destructive distillation of coal to produce coke and town gas. Part of nitrogenous fertilizer was obtained from Chile, which contained mainly sodium nitrate and Guano, where solidified bird excrement accumulated on the tropical islands. The fertilizer was exported in elevated amount to other European countries. However, the nitrate in nature was then considered to be exhausted after exploiting. In 1898, the British chemist and physicist William Crookes’ speech to the British Association for the Advancement of Science addressed that the shortage in food was a threat to mankind and the solution to this problem would be the fixation of atmospheric nitrogen. In 1900, the German chemist Friedrich Wilhelm Ostwald invented the Ostwald Process which was used in the manufacturing of nitric acid and it provided the main raw material for the most common type of fertilizer production. During the same time frame, Caro patented an atmospheric nitrogen fixation process for generating ammonia from cyanamide by hydrolysis. Another process of fixing atmospheric nitrogen using electric arc was also developed commercially at the same time by Birkeland and Eyde. Both of the routes became commercially available, however, the large energy requirement was one of the biggest drawbacks of the process. It took a long time till Haber-Bosch replaced them in the market [48].

#### 2.1.2. Fritz Haber, Carl Bosch and BASF

Fritz Haber was born in a rich German chemical and dye merchant family in 1868. He had worked in the chemical industry and business for a period of time. In his later life, he involved himself purely in science with the help of his industrial experience. Carl Bosch, is also a German chemist, who was born in a piping materials business family. He had started his career in ammonia synthesis in BASF (Badische Anilin und Soda Fabrik) since 1899. BASF as the largest chemical producer in the world had gained great success in the development of the Haber Bosch process with capable scientists and engineers such as Bosch and Mittasch from 1908 to 1912. It started making an ammonia production plant after acquiring exclusive rights to the process in 1913[1].

#### 2.1.3. The beginning of Haber-Bosch ammonia production

Haber’s first experiment for the concentration of ammonia in equilibrium with a stoichiometric mixture of hydrogen and nitrogen under atmospheric pressure show as follows:

$^{\circ}C$	27	327	627	927	1020
% $NH_3$	98.51	8.72	0.21	0.024	0.012

**Table 2.1:** The first reported measurements of the equilibrium between ammonia, hydrogen and nitrogen [48]

It was of great importance to know that ammonia could be formed by hydrogen and nitrogen at room temperature. Later after the Deutsche Bunsen Gesellschaft meeting in 1907, he started another experiment to determine the equilibrium concentrations of ammonia at the pressure of 30 bar using iron based catalyst, which turned out to have good agreement with those data obtained at atmospheric pressure. However, according to their measurement, the equilibrium concentration of ammonia was only 8% at 600 °C and 200 bar, which was too low for the industrial application. A suitable catalyst was required to make the process feasible to the industry. Haber and his team developed further a closed circulation system to form ammonia after discovering the first suitable catalyst for the reaction - osmium (and later uranium). The steel autoclave reactor was operated under 175 bar and at the temperature of 550 °C. The closed system consisted of the synthesis reactor, a heat exchanger to heat the feed gas using the exothermic heat released by the reaction. Liquid ammonia was obtained as end product in the circulation system. The weight of the catalyst was about 98 g osmium. Ammonia was obtained at the rate of 80 g/hr. The involvement of Bosch and Mittasch from BASF later on with ammonia synthesis enabled Haber and his team to establish high-pressure technology and development of the commercial catalysts for the synthetic process, respectively. Both of Haber and Bosch were awarded Nobel Prizes for their contribution on ammonia synthesis (Haber, 1919) and in high-pressure technology (Bosch, 1931) [48].

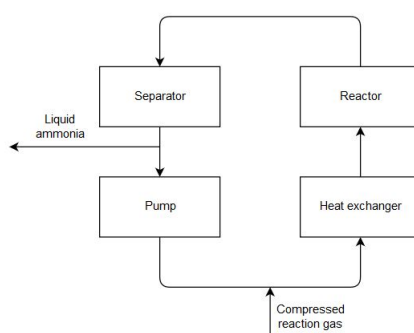
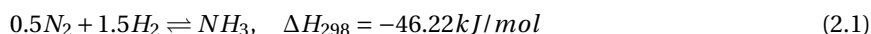


**Figure 2.1:** A schematic design of the circulation system by Haber's team from the stoichiometric mixture of hydrogen and nitrogen

## 2.2. Haber-Bosch Process: thermodynamic characteristics

Haber-Bosch process follows below chemical reaction 2.1:



Ammonia is used everywhere in our daily life. It is mainly used in fertilizer production, and then, in textiles industry, mining, pharmaceutical, refrigeration and other industries. Besides, ammonia as a hydrogen carrier can be directly used in diesel engines (ships, trucks) (short term), gas turbines, furnaces (short-medium term), fuel cells (long term) and can be cracked back to hydrogen for direct hydrogen use.

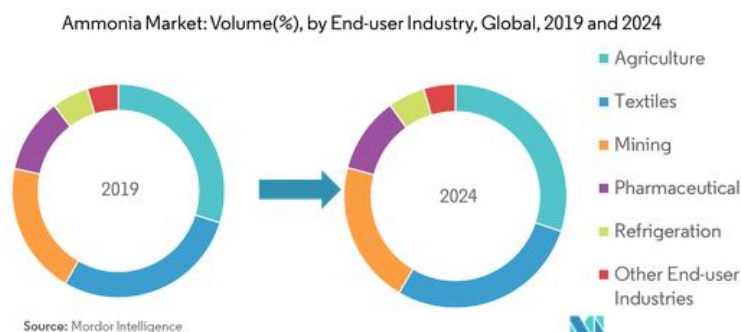


**Figure 2.2:** Ammonia market: volume (%), by end -user industry, global 2019 to 2024 (picture:Mordor Intelligence [45])



Figure 2.3: Ammonia as a hydrogen carrier distribution [90]

### 2.2.1. Chemical equilibrium

According to Gillespie and Beattie's (1930) investigation[39], the reaction equilibrium constants of Haber-Bosch process is:

$$\log K_p = \log x - \frac{1}{2} \log x_N - \frac{3}{2} \log x_H - \log P \quad (2.2)$$

$$\log \left( \frac{K_p}{K_p^*} \right) = P \left[ \frac{0.1191849}{T} + \frac{25122730}{T^4} + 38.76816 \frac{\sum (x_i A_{oi}^{1/2})}{T^2} + 64.49429 \frac{(\sum x_i A_{oi}^{1/2})^2}{T^2} \right] \quad (2.3)$$

$$\log K_p^* = -2.691122 \log T - 5.519265 \cdot 10^{-5} T + 1.848863 \cdot 10^{-7} T^2 + \frac{2001.6}{T} + 2.6899 \quad (2.4)$$

where the  $A_{oi}^{1/2}$  for ammonia, nitrogen and hydrogen are 1.546932, 1.159526, and 0.4444097 liter- $atm^{1/2}$  per mole, respectively and  $\log$  refers to the base 10.

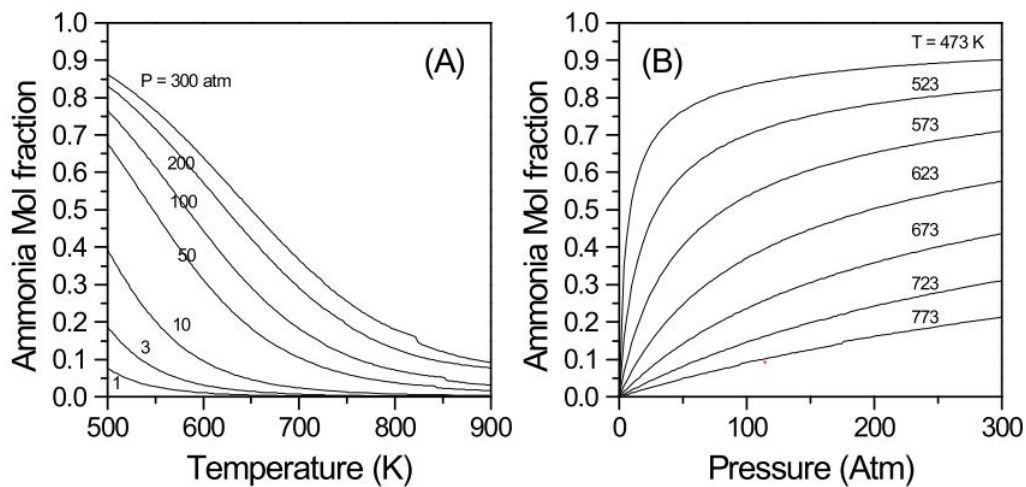


Figure 2.4: Ammonia content in equilibrium with  $N_2:H_2=1:3$  (A) at various temperatures under fixed pressure (B) at different pressures at fixed temperature [60]

Due to the exothermic character of the reaction, the equilibrium value is higher at higher pressure and lower temperature. As figure 2.4 shows, the increasing temperature leads to lower ammonia mole fraction at the outlet of the reactor.

### 2.2.2. Heat of reaction

The most used heat of reaction relation these days is the Gillespie-Beattie equation [38]:

$$\Delta H = - \left[ 0.54526 + \frac{840.609}{T} + \frac{459.734 \times 10^6}{T^3} \right] P - 5.34685 T - 0.2525 \times 10^{-3} T^2 + 1.69167 \times 10^{-6} T^3 - 9157.09 \quad (2.5)$$

Where  $\Delta H$  is the heat absorbed in the formation of one mole of ammonia from its elements in  $15^\circ\text{C}$  calories,  $P$  is in atm and  $T$  is in degrees Kelvins.

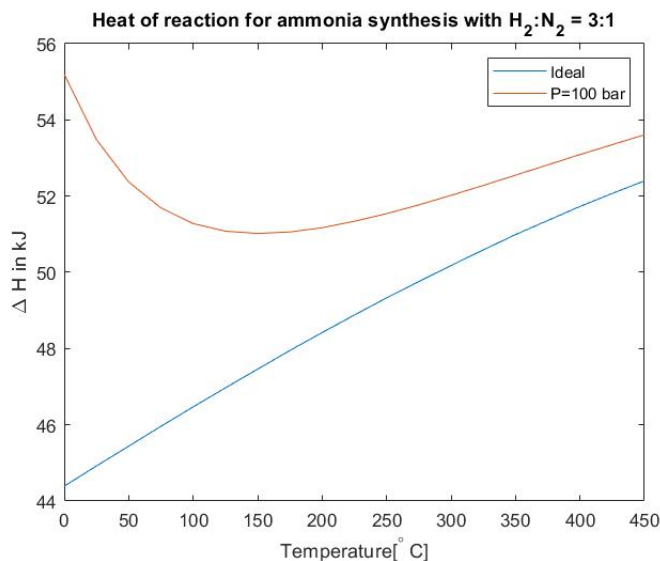


Figure 2.5: Heat of reaction for ammonia synthesis with  $N_2:H_2=1:3$

### 2.3. Catalysts

Ammonia synthesis from nitrogen and hydrogen is an exothermic reaction which is thermodynamically allowed at ambient pressure and temperature. However, due to the strong triple bonds of nitrogen molecules, it requires large activation energy to break the bonds and to proceed the reaction. Therefore, the ammonia synthesis relies on the catalyst in order to increase the reaction rate with a lower activation energy barrier.

As the heart of the ammonia synthesis reaction, the catalyst for ammonia formation has been studied intensively since the beginning of the 20<sup>th</sup> century. In 1904-1907, Haber discovered the first well performed catalyst for ammonia synthesis, which were osmium and uranium-uranium carbide. At the period of 1910-1912, Mitsch and his co-workers in BASF had tested more than 2500 kinds of catalyst in more than 6500 experiment runs[59]. They found out that many of pure metals have little or no catalytic effect to the reaction, however, with additives it could improve its catalytic activity. The best catalyst was proved to be a multi-component mixture [53]. One of the most successful catalysts of ammonia synthesis is the magnetite-based fused iron catalyst with a small amount of promoters. It requires high pressure (150 to 300 bar) and high temperature (400 to 500°C) due to the thermodynamic limitations.

Catalyst	Year	Inventor	Catalyst type	Chemical composition
$Fe_3O_4$ -based catalyst	1913	BASF	S6-10, KM	$Fe_3O_4+Al_2O_3+K_2O+CaO$
$Fe_{1-x}O_4$ -based catalyst	1986	Zhejiang University	A301, ZA-5	$Fe_{1-x}O_4+Al_2O_3+K_2O+CaO$
Ru-based catalyst	1992	UK-BP, Japan	KAAP	Ru-Ba-K/AC

Table 2.2: Ammonia synthesis catalyst development[53]

For years, researchers have been studying the alternatives for the catalytic ammonia synthesis. As a small-scale  $NH_3$  plant is gaining more and more attention to the industry, new catalyst which can operate at milder conditions are in demand. Pure cobalt has negligible activity in catalyzing ammonia synthesis due to its strong affinity with H resulting in the inhibition of  $N_2$  [59]. This can be improved by adding additional metals, such as Fe or Ni [36] or by addition BaO as promoter, which increases ammonia synthesis activity by more than 2 orders of magnitude on a Co/C catalyst[37]. Gao et al. [37] reported a much better ammonia synthesis activity catalyst  $BaH_2 - Co/CNT$  in 2017, which has approximately 2 and 2.5 times higher catalytic activity

than that of BaO-Co/CNTs and Cs-Ru/MgO at 250 and 300°C, respectively. Although, Ru-based catalyst performs better under milder reaction than iron based catalyst. However, its activity is much lower than that of Fe-based catalyst at lower temperature. Ru-based catalyst also are strongly inhibited by  $H_2$  adsorption under milder reaction condition. M. Kitano et al.[49] has developed a new type of Ru catalyst, which is a Ru catalyst with Barium-doped calcium amide ( $Ba - Ca(NH_2)_2$ ) as promoter, that can form ammonia at temperature below 300°C. This catalyst is superior to conventional Ru catalyst as well as to the wüstite-based Fe catalyst. Their data shows that a small amount of Ba-doping (3%) has effectively enhanced the activity of the  $Ru/Bu - Ca(NH_2)_2$  catalyst and the ammonia concentration reaches thermodynamic equilibrium at temperature above 340°C.

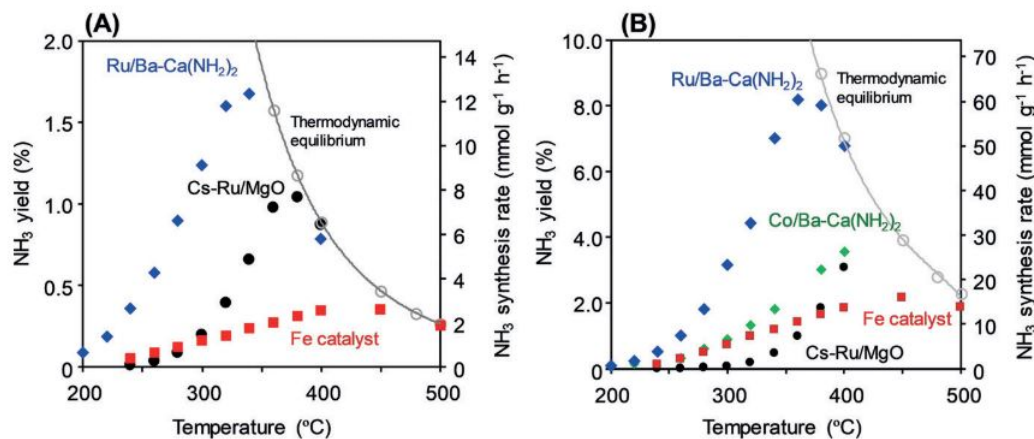


**Figure 2.6:** Comparison of  $Ru(10wt\%)/Ba(3\%) - Ca(NH_2)_2$ ,  $Cs - Ru/MgO$  and wüstite iron based catalysts under 1 bar (A) and 9 bar (B)[49]

Yuta Ogura et al. in Japan, show a  $Ru/La_{0.5}Pr_{0.5}O_{1.75}$  catalyst that has extraordinary high activity for ammonia synthesis at 650°C under 10 barg and effectively suppressed hydrogen poisoning which is a typical drawback for oxide-supported Ru catalyst (e.g.  $Cs^+ / Ru/MgO$ ) [67].

## 2.4. Reaction kinetic

Based on the experimental results, the ammonia synthesis can be formulated in the following sequence of individual steps:

1.  $N_2(g) + * \rightleftharpoons N_{2,ad}^*$
2.  $N_{2,ad}^* + * \rightleftharpoons 2N_{ad}^*$
3.  $N_{ad}^* + H_{ad}^* \rightleftharpoons NH_{ad}^* + *$
4.  $NH_{ad}^* + H_{ad}^* \rightleftharpoons NH_{2,ad}^* + *$
5.  $NH_{2,ad}^* + H_{ad}^* \rightleftharpoons NH_{3,ad}^* + *$
6.  $NH_{3,ad}^* \rightleftharpoons NH_3(g) + *$
7.  $H_2(g) + * \rightleftharpoons 2H_{ad}^*$

Homogeneous reaction of ammonia synthesis is unfavorable due to the large nitrogen dissociation energy involved in the first two steps. Adding a catalyst to the reaction can avoid this problem because the energy gain associated with the formation of the surface atom bonds overcompensate the relevant dissociating energies, and the first two steps become exothermic. The progress can be also described in an energy profile 2.7. As the figure shows, the nitrogen dissociation (step 2) is the rate determining step for ammonia synthesis on Fe. It is not because of the high activation energy barrier, but because of the very unfavorable pre-exponential factor in its rate constant. The hydrogenation steps demand also high energy, however, it can be overcome by elevating the temperature to approximately 700K. Apparently, if the reaction temperature is too low, then the rate-limiting step may switch from nitrogen dissociation to hydrogenation of the adsorbed atomic nitrogen

[48]. Provided that the rate-limitation of the reaction is step two, the rest of the steps are in equilibrium. Then, the overall synthesis rate can be given by:

$$r = k_f \theta_{N_{2,ad}}^* \theta_* - k_b \theta_{N_{ad}}^{*2} \quad (2.6)$$

Where  $\theta$  denotes surface coverage,  $k_f$  and  $k_b$  are the forward and backward rate of step 2. The equilibrium constant of step 2 is then [83]:

$$K_p = \frac{k_f}{k_b}, \quad k_f = A \exp \frac{-E_a}{RT} \quad (2.7)$$

Where  $k_f$  is the rate constant for step 2. The net activation energy for ammonia synthesis can be interpreted as the activation energy for dissociative nitrogen adsorption plus the energy required for two free adsorption sites creation, which depends on temperature and pressure [48].

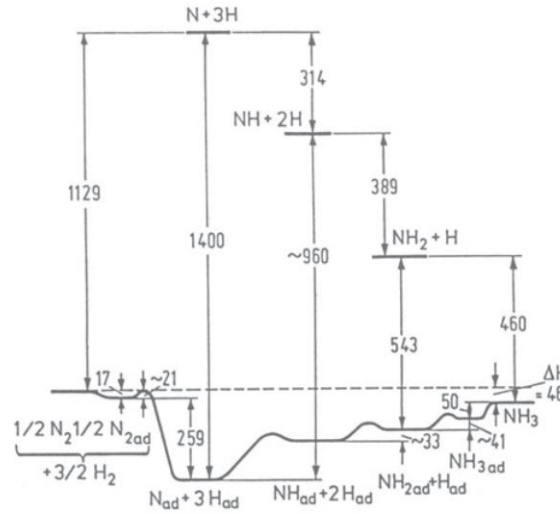


Figure 2.7: Schematic energy profile of the ammonia synthesis on Fe [kJ/mol][48]

#### 2.4.1. Heat and mass transfer

Heat and mass transfer through the stagnant film surrounding the catalyst particles. For smaller catalyst particle size ( $<1.5$  mm), if the flow velocity is high enough, the gas passes through the fixed bed and creates sufficient turbulence to keep the boundary layer around the particle thinner compared to that of the catalyst size. Besides, the iron based catalyst has better thermal conductivity than the synthesis gas, which leads to the main temperature gradient lies in the external gas film. The catalyst particle itself maintains in an almost isothermal condition.

Research shows that there are little temperature difference and  $NH_3$  concentration variation between the bulk gas stream and the external catalyst surface for small catalyst particles. For larger catalyst particle size ( $\geq 1.5$  mm), the reaction is limited by the ammonia diffusion through the catalyst pores. The increasing of catalyst particle size leads to the decrease of the activation apparent energy, reaction order and ammonia production per unit volume of catalyst. A pore effectiveness is often used as a correction factor for the rate equation constants of the ammonia converter design [17].

#### 2.4.2. The reaction kinetic on the multi-promoted iron based catalyst

There are numerous studies in multi-promoted iron based catalyst for ammonia synthesis. J. Sehested et al.[74] studied a micro-kinetic model of ammonia synthesis on a KM1R (Haldor Topsoe A/S) multi-promoted (94% Fe, 2.8% CaO, 0.6%  $K_2O$  and 2.5%  $Al_2O_3$ ) iron catalyst. Their tests were performed under temperature ranges of  $320^\circ C$  (circles),  $360^\circ C$  (triangles) and  $400^\circ C$  (squares) and pressure of 100 bar. They discovered that at low temperature and low ammonia partial pressure, the multi-promoted iron catalyst is inhibited by hydrogen (figure.2.8) and water poisoning of the catalyst is negligible.

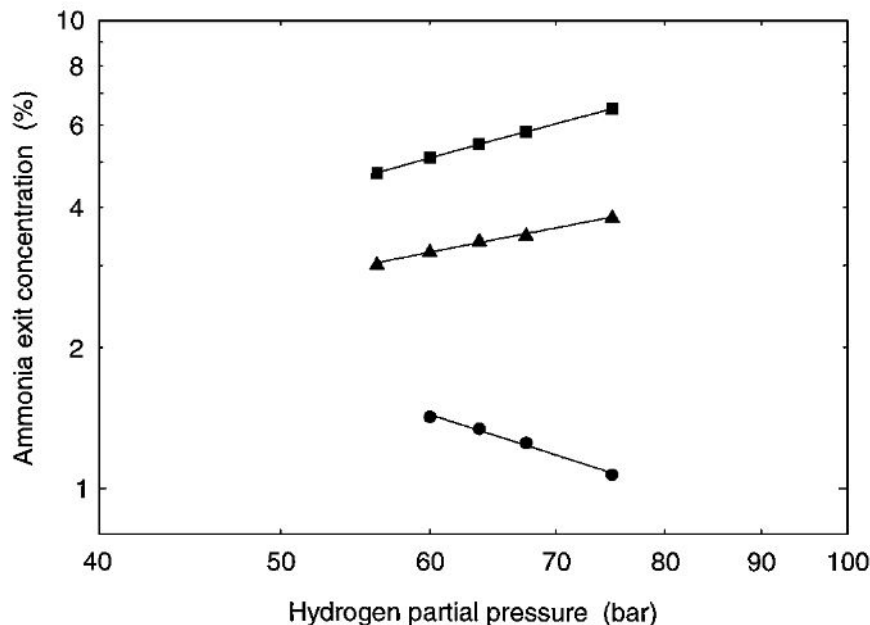


**Figure 2.8:**  $NH_3$  concentration as a function of hydrogen partial pressure at various temperatures

John U. et al. discovered that ammonia synthesis reaction, which entails the dissociation of dinitrogen, takes place readily even at 350 °C and lower over KIMR type catalyst [66]. Stoltze et al.[82] suggested that the surface coverage of atomic hydrogen is an order of  $10^{-3}$  compared to that of atomic nitrogen which has a value of 0.5 at 10 MPa (100 bar) and 350 °C. In the presence of atomic hydrogen which does not strongly compete for the active sites, the adsorbed N-intermediates prefers to exit with  $NH_3$  (g) rather than  $N_2$  (g). Their study also shows that the adsorbed K on ironed based catalyst can considerably increase  $N_2$  dissociation by means of decreasing the activation energy of step 2.

	Fe (III)	K/Fe
$E_{N_2^*}$	-38 kJ/mol	-51 kJ/mol
$E_{N^*}$	-91 kJ/mol	-91 kJ/mol
Step II $E_a$	47.7 kJ/mol	47.7 kJ/mol
Step II pre-factor A	$1.37 \times 10^{11} s^{-1}$	$5.89 \times 10^{10} s^{-1}$

**Table 2.3:** Kinetic parameters for nitrogen adsorption and dissociation on Fe(III) and on K/Fe.[83]

For common commercial iron based catalyst, the maximum allowable temperature is about 540 °C. Once the operation temperature exceeds the maximum allowable value, the catalyst loses its activity quickly because of its surface structure reorganization.

### 2.4.3. Rate equations

Synthetic ammonia reaction is a relatively simple reaction without any byproducts. The most used kinetic equation for ammonia synthesis was developed by Temkin about 50 years ago and is still being used by many engineers. Temkin's rate equation was constructed under the basic assumption that the nitrogen adsorption is the rate determining step in ammonia synthesis. Later on, Temkin developed his equation by incorporation of hydrogen addition to adsorbed nitrogen as a second rate-determining step. He further modified his equation taking the effect of small amount of water in the feed gas into account. Ozaki, Taylor and Boudart derived an equation for low temperature and pressure synthesis operation which considered that the catalyst surface is mainly covered by NH species. Nielsen and his co-workers defined the best  $\alpha$  value to the rate equation which is 0.75. Brill proposed a rate equation that takes ammonia synthesis as rate determining step instead of dissociation of nitrogen chemisorption. This equation should be valid for low conversion values. Besides, Buzzi Ferraris and his co-workers built 23 different kinetic models and evaluated them using data generated by Nielsen. Most of their models gave a better fit than the classical Temkin equation[48]. The development of

Temkin equation can be shown as followed. They are applicable to the ammonia synthesis over commercial iron based catalyst.

Author	Rate equations	Operation condition
Temkin et al.	$r_s = K_1 P_N \left( \frac{P_H^3}{P_A^2} \right)^\alpha - K_2 \left( \frac{P_A^2}{P_H^3} \right)^{1-\alpha}$	Industrial range
Temkin	$r_s = \frac{K_1 P_N^{1-\alpha} [1 - (1/K_{eq})(P_A^2/P_N P_H^3)]}{[(K_{-1}/P_H) + (1/K_{eq})(P_A^2/P_N P_H^3)]^\alpha [(K_{-1}/P_H) + 1]^{1-\alpha}}$	Industrial range
Temkin and co-workers	$r_w = \frac{k_1 P_N - k_2 (P_A^2/P_H^3)}{[(P_A^2/P_H^3) + C(P_w/P_H)]^\alpha}$	Water vapor in the feed gas
Brunauer and co-workers	$r_s = K_A P_N / (1 + b K_{eq} P_A / P_H^{1.5})^{2\alpha}$	Low ammonia concentration
Ozaki, Taylor and Boudart	$r_s = K_A P_N / (1 + K_A P_A / P_H)^2$	Low T and low P
Nielsen and co-workers	$r_s = \frac{K_2 (K_{eq} P_N - P_A^2 / P_H^3)}{(1 + k_3 P_A / P_H^w)^{2\alpha}}$	Industrial range
Brill	$r_s = K_A P_N / (1 + K_A P_A^2 / P_H^3)$	Low conversion range
Buzzi Ferraris and co-workers	$r_s = \frac{P_N P_H^2 - K_{eq}^2 P_A^2 / P_H}{C_1 P_H^2 + C_2 P_A^2 / P_H + C_3 P_H P_A}$	The Hougen-Watson approach

**Table 2.4:** Rate equations for ammonia synthesis reaction[48]

where A denotes ammonia, N represents nitrogen and H is for hydrogen.

## 2.5. Reactors

### 2.5.1. Ammonia synthesis reactor flow models

All modern ammonia converters are based on adiabatic catalyst beds with intermediate cooling [48]. There are five types of flow arrangements for the adiabatic reactors. They are axial flow reactor, radial flow reactor, axial-radial flow reactor, multi-axial flow reactor and transverse flow reactor respectively. They have different advantages and also drawbacks.

Flow type	Advantages	Disadvantages
Axial flow	Best utilization of the internal volume	1. Require large vessel wall thickness or diameter 2. Require large size catalyst for lower $\Delta P$
Radial flow	Lower pressure drop	1. Gas distribution problem 2. Require sealed compensation top chamber

**Table 2.5:** Different flow management for adiabatic ammonia synthesis reactor

The axial-radial flow model is aimed to recover the catalyst dead volume. Because it has an open top flow, the top sealing as the axial flow is no more needed. In the multi-axial flow, the bed pressure can be easily adjusted by changing the number of modules or its dimensions, which eliminates the gas distribution problem as in the radial flow model. The transverse flow model is usually used in large capacity converters.

### 2.5.2. Kellogg's ammonia synthesis reactors

The axial flow model reactor (figure 2.9) was introduced in the mid 1960s. It contains four axial flow catalyst beds with an interchanger at the top bed. A typical inlet synthesis gas composition for Kellogg reactor is 74.2% of hydrogen, 24.7% of nitrogen, 0.8% of methane and about 0.3% of Argon gas. They flow into the reactor from the bottom, then up to the top-mounted interchanger. The gas is preheated by the interchanger and then enters the first catalyst bed. The leaving gas at the outlet consists about 10 - 12% of ammonia. It uses conventional iron based catalyst with the size range of 6 to 10 mm. Ammonia is separated by a refrigeration system at the leaving temperature of  $-25^\circ\text{C}$ . Kellogg's horizontal ammonia synthesis reactor is introduced in the year of 1980s (figure 2.10). Their horizontal catalyst bed arrangement enables the use of smaller catalyst particle, which leads to lower pressure drop[35].

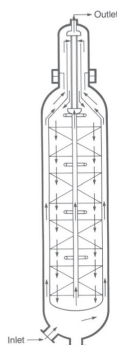


Figure 2.9: Kellogg ammonia converter

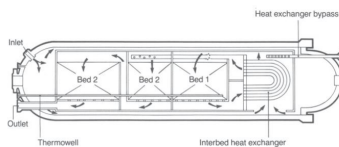


Figure 2.10: Kellogg's horizontal converter

### 2.5.3. Braun's ammonia converter

This is a type of reactor with two axial flow catalyst beds and one heat exchanger between the beds. The feed gas enters from the bottom of the vessel and flows up between the vessel shell and the catalyst beds. Then, it flows downwards through the two beds and exits from the bottom nozzles [40].

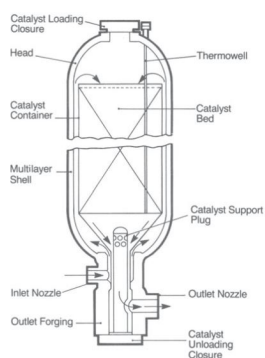


Figure 2.11: Braun ammonia converter

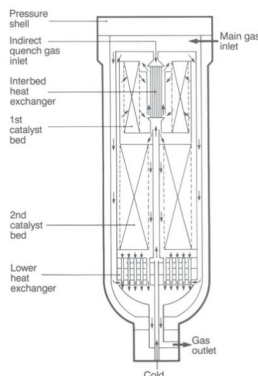


Figure 2.12: Haldor Topsoe S-200 ammonia converter

### 2.5.4. Topsoe's radial flow reactor

The typical synthesis gas composition for Topsoe inlet feed gas is 3 : 1 stoichiometric hydrogen/nitrogen mixture, which also contains about 0.3% argon and 0.8% of methane. The Topsoe S-100, S-200 and S-300 reactors are radial flow converters. This flow model was first introduced by Haldor Topsoe in the mid 1960s. The Topsoe's ammonia converter contains usually two radial flow catalyst beds. Due to the low pressure drop, the catalyst are used with size range of 1.5 - 3 mm. The S-100 has quench gas added between the two beds and a feed effluent exchanger installed under the second bed. The S-200 type of converter uses two heat exchangers. One is under the second bed, another one is located in the center of the first bed. The latest reactor version from Topsoe is S-300. It consists of three catalyst beds which provide a much higher conversion compared to that of S-200 [86].

## 2.6. Heat integration: Heat pipes

Heat pipe is a heat transfer device that transfers heat from one side to another side. It combines the principle of both thermal conductivity and the phase transition by using the latent heat of the working fluid to achieve certain amount of energy transportation. A heat pipe vessel is firstly vacuumed, then charged with a working fluid, and hermetically sealed. The latent heat of evaporation is the energy required for the working fluid phase change. The author [52] has done her research in a small-scale Haber-Bosch reactor by using heat pipe as a heat integration network. Because of the large temperature difference between the outlet of the reactor and the temperature of the condenser, using one working fluid is not thermal dynamically sufficient. An additional working fluid, such as Dowtherm A, is required to completely remove or transfer the energy from the hot side to the cold side gas stream.

## 2.7. Heat integration: Double pipe heat exchanger

The simplest form of a two-fluid heat exchanger is a double pipe made up of two concentric circular tubes. One fluid flows through the inside tube and the other in co-current or counter-current flow through the annular passage [81]. There is no problem for flow distribution and cleaning is done easily by disassembly. This type of heat exchanger configuration is also suitable for one or both of the fluids are at high pressure because containment in the small-diameter pipe or tubing is less costly than containment in a large-diameter shell. A double pipe heat exchanger is generally used for small-capacity application where the total heat transfer surface area required is  $50 \text{ m}^2$  or less. Stacks of double tubes or multi-tube heat exchangers are used in some process applications with radial or longitudinal fins. The exchanger with a bundle of U tubes in a pipe of 150 mm diameter and above uses segmental baffles and is referred to variously as a hairpin or jacketed U-tube exchanger [77]. The general equation for heat transfer across a surface is:

$$Q = UA\Delta T_m \quad (2.8)$$

For a double pipe heat exchanger, the overall heat transfer coefficient  $U$  can be expressed as [75]:

$$\frac{1}{U \cdot A} = \frac{1}{h_i \cdot A_i} + \frac{R_{fi}}{A_i} + \frac{1}{2k_{pipe}\pi l} \ln \frac{d_o}{d_i} + \frac{1}{h_o \eta_w A} + \frac{R_{fo}}{\eta_w \cdot A_i} \quad (2.9)$$

where  $Q$  is heat transferred per unit time [W],  $U$  is the overall heat-transfer coefficient [ $W/m^2 \cdot C$ ],  $A$  is heat transfer area of the inner pipe [ $m^2$ ],  $h_i$  is the convective heat transfer coefficient of fluid in the inner tube [ $W/m^2 \cdot C$ ],  $h_o$  the convective heat transfer coefficient of fluid in the outer tube [ $W/m^2 \cdot C$ ],  $R_{fo}$  is the outside dirt coefficient (fouling factor) [ $W/m^2 \cdot C$ ],  $R_{fi}$  is the inside dirt coefficient [ $W/m^2 \cdot C$ ],  $k$  is the thermal conductivity of the tube wall material [ $W/m \cdot C$ ],  $d_o$  is the outer diameter of the inner tube [m] and  $d_i$  is the inner diameter of the inner tube [m]. The specific duty can be defined by using the temperature difference available.

For counter-current flow, the mean temperature difference (temperature driving force) is given by:

$$\Delta T_{lm} = \frac{(T_1 - t_2) - (T_2 - t_1)}{\ln \frac{(T_1 - t_2)}{(T_2 - t_1)}}, \quad \Delta T_m = F_t \Delta T_{lm} \quad (2.10)$$

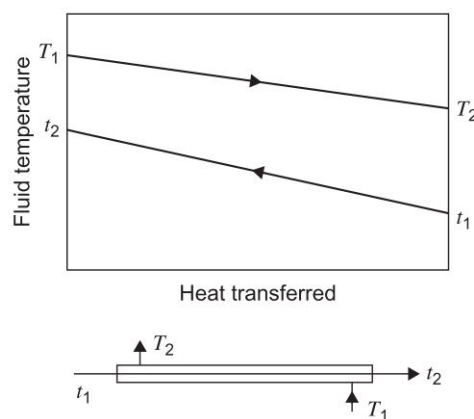


Figure 2.13: Temperature change in countercurrent flow

Where  $t_1$  and  $t_2$  are the cold fluid inlet and outlet temperatures,  $T_1$  and  $T_2$  are the hot fluid inlet and outlet temperatures and  $F_t$  is a correction factor from the “true temperature difference” in real design. For simplification, the fluid properties, such as density, viscosity and heat capacity are evaluated at the mean temperatures, which are found by using the inlet and outlet values.

$$T_{i,m} = \frac{T_{i,out} + T_{i,in}}{2} \quad (2.11)$$

$$T_{o,m} = \frac{T_{o,out} + T_{o,in}}{2} \quad (2.12)$$

In order to determine the convective heat transfer coefficient of the inner tube, the Reynolds number correlation is used to compute the heat transfer coefficient value.

$$Re_i = \frac{d_{i,i} \dot{m}_i}{\mu_i a_i} \quad (2.13)$$

### 2.7.1. Heat transfer coefficients for double pipe exchangers without fins

If the Reynolds number is greater than  $10^4$ , the flow in the pipe is turbulent and fully developed, for which the Nusselt number is given by the Seider-Tate equation[76]:

$$Nu = 0.023 Re^{4/5} Pr^{1/3} (\mu/\mu_w)^{0.14} \quad (2.14)$$

For the transition region ( $2100 < Re < 10^4$ ), the Hausen equation is used:

$$Nu = 0.116 [Re^{2/3} - 125] Pr^{1/3} (\mu/\mu_w)^{0.14} [1 + (D_i/L)^{2/3}] \quad (2.15)$$

The equations 2.14 and 2.15 are valid for both pipes and annuli. For an annulus case, the equivalent diameter is used instead of inner diameter of the outer pipe. For laminar flow ( $Re \leq 2100$ ) in pipes, the Seider-Tate equation is used:

$$Nu = 1.86 [Re Pr D_i/L]^{1/3} (\mu/\mu_w)^{0.14} \quad (2.16)$$

For laminar flow in annuli, the Gnielinski equation is used:

$$Nu = 3.66 + 1.2(D_2/D_1)^{0.8} + \frac{0.19[1 + 0.14(D_2/D_1)^{0.5}][Re Pr D_e/L]^{0.8}}{1 + 0.117[Re Pr D_e/L]^{0.467}} \quad (2.17)$$

Where  $D_1$  is the outside diameter of the inner pipe,  $D_2$  is the inside diameter of the outer pipe and  $D_e$  is the equivalent diameter =  $D_2 - D_1$ . An alternative equation proposed by Gnielinski 2.18 for transition and turbulent regimes in annuli is to be used for the replacement of the Seider-Tate and Hausen correlations.

$$Nu = \frac{(f/8)(Re - 1000)Pr}{1 + 12.7\sqrt{f/8}(Pr^{2/3} - 1)} [1 + (D/L)^{2/3}], \quad 2100 < Re < 10^6, \quad 0.6 < Pr < 2000 \quad (2.18)$$

where  $f$  is the Darcy friction factor, which can be computed from the Colebrook equation:

$$f = (0.782 \ln Re - 1.51)^{-2} \quad (2.19)$$

$$D_e = 4 \times \text{hydraulic radius} = 4 \times \text{flow area/wetted perimeter} \quad (2.20)$$

From the calculated Nusselt number, the corresponding convective heat transfer coefficient can be obtained.

$$Nu_i = \frac{h_i d_{i,j}}{k_i} \quad (2.21)$$

### 2.7.2. Hydraulic calculations for double pipe exchangers without fins

The fluid friction in the pipe generates the pressure drop in the line. With taking the viscosity correction factor into account, which creates the effect of variable fluid properties on the friction factor in non-isothermal flow. The pressure can be computed from following equation [76].

$$\Delta P_f = \frac{f L G^2}{7.5 \times 10^{12} D_i s \phi} \quad (2.22)$$

$$\phi = \begin{cases} \left(\frac{\mu}{\mu_w}\right)^{0.14}, & \text{for turbulent flow} \\ \left(\frac{\mu}{\mu_w}\right)^{0.25}, & \text{for laminar flow} \end{cases}$$

The friction factor used in equation 2.22 is computed as follows:

$$f = \begin{cases} \frac{64}{Re}, & \text{for inner pipe laminar flow} \\ \frac{64}{Re} \left[ \frac{(1-\kappa^2)}{1+\kappa^2+(1-\kappa^2)/\ln \kappa} \right], & \text{for laminar flow in the annulus} \\ 0.3673 Re^{-0.2314}, & \text{for turbulent flow with } Re \geq 3000 \end{cases}$$

where  $L$  is the pipe length,  $D_i$  is the pipe inner diameter,  $G$  is the mass flow,  $s$  ( $s = \rho/\rho_{water}$ ) is specific gravity with reference to water at  $4^\circ C$  which has density of  $1 \text{ g/cm}^3$ ,  $\kappa = D_1/D_2$

### 2.7.3. Heat transfer coefficient for un-finned multi-tube heat exchangers

A tube in tube heat exchanger with an outer shell inner diameter equals to  $D_2$  and it contains  $n_t$  tubes that have an outside diameter of  $D_1$ . The flow area and wetted perimeter can be obtained from following equations:

$$A_f = (\pi/4)(D_2^2 - n_t D_1^2), \quad \text{Wetted perimeter} = \pi(D_2 + n_t D_1) \quad (2.23)$$

The equivalent diameter is given by:

$$D_e = 4A_f / \text{wetted perimeter} \quad (2.24)$$

The heat transfer coefficient can be computed using above mentioned methods with an appropriate value of the equivalent diameter [76].

## 2.8. Ammonia separation by condensation

A typical condensation temperature in the current ammonia process plants is in the range of  $-10^\circ\text{C}$  to  $-25^\circ\text{C}$ . Araki et al. [18] investigated the steam condensation in a vertical tube with presence of noncondensable gases. The effect of noncondensable gas and the thermal resistance of the condensate film contributed to the overall heat transfer coefficient. In their study, the degradation of the heat transfer coefficient was observed in accordance to the increment of the air partial pressure ratio as the effect of non-condensables. Each element of the condenser was considered to be in saturated conditions and the non-condensables' partial pressure was determined by subtracting the ammonia partial pressure from the total pressure measured. The thermal resistance of the film for the  $i^{\text{th}}$  condenser element was obtained from [61]:

$$\frac{1}{h_{\delta,i}} = \frac{\left(\frac{3\Gamma_i\mu_i}{g\rho_l(\rho_l-\rho_v)}\right)^{1/3}}{1.28k_l} \quad (2.25)$$

The thermal resistance of the non-condensable gas is calculated by subtracting  $1/h_{\delta,i}$  from the total resistance  $1/h_{tot,i}$ . A general equation can be shown as follows:

$$\frac{1}{h_{tot,i}} = \frac{1}{h_{\delta,i}} + \frac{1}{h_{conv,i} + h_{c,i}} \quad (2.26)$$

where  $h_{tot}$  is the overall heat transfer coefficient,  $h_{\delta}$  is the heat transfer coefficient due to condensate liquid film,  $h_{conv,i}$  is the heat transfer coefficient of the convective gas and  $h_{c,i}$  is the condensation heat transfer coefficient of the mixed gas. The heat transfer coefficients can be computed from below correlation functions:

$$Nu = \begin{cases} 0.23Re^{0.8}Pr^{1/3}, & \text{for turbulent flow} \\ 3.66, & \text{for laminar flow} \end{cases}$$

$$h_{conv} = \frac{Nuk_{mix}}{L} \quad (2.27)$$

And  $h_c$  can be obtained from a function which is correlated to the mixture Re and noncondensables partial pressure ratio  $Pa/Pt$  (air / non-condensables).

$$h_c = \begin{cases} 0.33\left(\frac{Pa}{Pt}\right)^{-0.67}, & \text{for Re} < 2300 \\ 2.11 \times 10^{-4} Re^{0.8}\left(\frac{Pa}{Pt}\right)^{-0.99}, & \text{for Re} > 2300 \end{cases}$$

The material resistance can be found by taking the shape factor of the condenser into account. The shape factor for the concentric cylinders is taken from [58]:

$$S = \frac{2\pi H}{\ln(r_2/r_1)} \quad (2.28)$$

where  $r_1$  is the radius of the circular hole and  $r_2$  is the outer radius of the cylinder. The force convection correlation for the external heat transfer along the condenser has a correlation function [89]:

$$\overline{Nu} = cRe^m Pr^{(1/3)} \quad (2.29)$$

where  $c$  equals to 0.246 and  $m$  has the value of 0.588.

## 2.9. Ammonia separation by adsorption/absorption

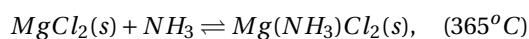
Ammonia can also be separated either by adsorption or by absorption. Adsorption captures ammonia on the solid surface. There are four pre-dominant types of ammonia adsorbents, which are zeolites, alumina, acid treated clay and activated carbon modified by inorganic acid and some metal salts. By absorption, ammonia diffuses into a solid or solvent and forms other components. Ammonia absorption can have much higher capacity, especially in a higher temperature range, however, its solid absorbent has low diffusion coefficients compared to that of liquid form. Timely capture of ammonia via absorption or adsorption can increase the conversion in the ammonia synthesis reactor. Table 1.1 shows the main absorbents and adsorbents for ammonia separation. Most of the literature studies find that replacing the condensation process by an absorption-based process can produce ammonia at a similar rate but at lower pressure, which leads to a smaller compressor and less energy consumption.

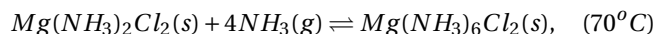
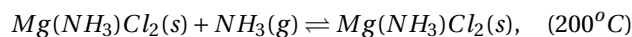
Material	Capacity g $NH_3$ per g sorbent	Temperature $^{\circ}C$
$CaCl_2$	1.228	Room
$MgCl_2$	1.073	Room
$SrCl_2$	0.859	Room
$MnCl_2$	0.812	Room
$BaCl_2$	0.654	Room
$Al_2O_3$ [78]	0.013	25
	0.003	300
$Al_2O_3 - MgCl_2$	0.059	25
	0.012	300
$Al_2O_3 - CaCl_2$	0.033	25
	0.007	300
$Al_2O_3 - BaCl_2$	0.016	25
	0.003	300
$Al_2O_3 - CaCl_2$ (14.5wt%)	0.15	50
$Al_2O_3 - CaCl_2$ (21.5wt%)	0.225	50
Vermiculite - $CaCl_2$ [78]	0.685	50
$Al_2O_3 - BaCl_2$ (16wt%)	0.09	30
Sibunit- $BaCl_2$ (19wt%)	0.12	30
Vermiculite - $BaCl_2$ (45wt%)	0.24	30
Activated carbon fiber felt - $CaCl_2$ (31wt%)[85]	0.37	40
Carbon-CMK8	0.78	Room
Carbon-OMC	0.60	Room
Carbon-OMC-AC	0.72	Room
COF-10	0.26	25
MCM-41- $ZnCl_2$ (50wt%)[30]	0.13	Room
MCM-41- $MgCl_2$ (50wt%)	0.07	Room
CSC- $ZnCl_2$ (50wt%)	0.1	Room
CSC- $MgCl_2$ (50wt%)	0.05	Room
$Al_2O_3$ [43]	0.022	50
Silica Gel	0.042	50
Carbon	0.042	50
Zeolite 13X	0.054	50
Zeolite 4A	0.060	50

Table 2.6: Ammonia absorbents and adsorbents[92]

### 2.9.1. Separation by absorption using magnesium chloride

Magnesium chloride can take up ammonia in three formation steps and the ammonia can be released by warming:





Mark et al. [56] studied the kinetic of ammonia absorption into magnesium chloride under 5 bar in the temperature range of 170 – 430°C. They derived a major approximated equation for isothermal absorption condition. Their results suggested that ammonia absorption by magnesium chloride has larger separation capacity compared to that of adsorption and provides ways to develop a smaller scale ammonia plant.

Heath et al.[26] further studied the ammonia synthesis enhancement by magnesium chloride absorption. They ran their reactor and the absorber at 400°C, 200°C respectively under 80 barg. They found out that at large times, ammonia conversion with Haber-Bosch process can be increased above 95% by using  $MgCl_2$  absorbent. The maximum ammonia conversion depends on the reaction overall rate constants and the absorption equilibrium that are controlled by ammonia diffusion in the solid salt. Suggestions for increasing the absorption rate are provided by Heath et al.. One is to use smaller absorbent particles on a porous inert absorbent support, which is a nice idea for designing a small-scale ammonia synthesis reactor. The second idea is to increase the rate by enhancing the absorbent volume. However, the effect of absorbent volume becomes less once overall production is controlled by chemical kinetics. Last but not least, the absorbent kinetic can be also improved by frequently regenerating the absorbent.

Furthermore, Wagner et al.[92] found out that pure magnesium chloride is not a strong absorbent for ammonia separation in a small scale Haber-Bosch plant. It loses available capacity with increase of cycles due to the fusing and deterioration of microstructure in the presence of ammonia at high temperature. They sought an inert micro-porous solid to support the sub-micron-sized  $MgCl_2$  particles and they discovered alumina, which itself can also absorb ammonia at low temperature. When it combines with magnesium chloride, it remains effective at high temperature. Their study show that the absorption process goes rapidly and reversibly at 400°C, which is close to the ammonia synthesis process. The desorption process occurs at 450°C for 30 min.

### 2.9.2. Separation by absorption using calcium chloride

Calcium chloride can also selectively absorb ammonia while nitrogen and hydrogen are not absorbed [80]. Mahdi et al. proved that ammonia can be produced at high temperature and lower pressure (e.g. 25 bar) if the product ammonia is rapidly separated. They investigated this using calcium chloride in a reaction-separation process and by comparing the results with a conventional reaction test. It is found that the rapid removal of product ammonia reduces the constraint of reversible reaction and enables to reach high conversion at relatively lower pressure. It is also worth to note that the increase of flow rate can reduce the reactor temperature due to the heat loss to the gas flowing out of the reactor. Their maximum flow rate to the reactor is found 3mL/min [55].

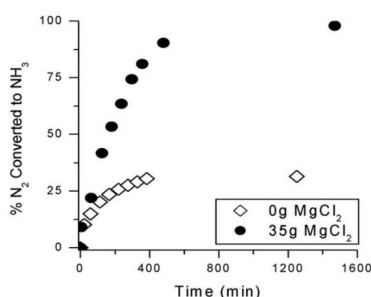


Figure 2.14: Conversion with  $MgCl_2$  is increased. [26]

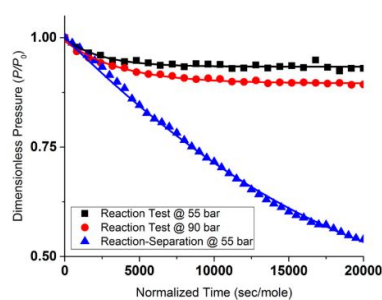


Figure 2.15: Comparison of reaction and reaction-separation tests at different operation pressures [55]

## 2.10. Worldwide current green ammonia plants/projects

Ammonia plants in smaller scale can not only reduce the environmental impact, but also diminish the safety issues due to the hazardous transportation. The standardized Haber-Bosch process becomes sustainable when it is powered by renewable energy. With the mature Haber-Bosch technology and the growing renewable energy market, a green micro-ammonia plant is possible. Furthermore, a smaller ammonia plant can

also bring more flexibility in size, in feedstock and in the market. Many of the ambitious companies have already started their path on greening the ammonia production.

### 2.10.1. The Proton Venture's NFUEL unit

The Dutch company - Proton Venture is developing a sustainable, fully automated process, remotely operated, decentralized small-scale ammonia production plant and energy storage system named NFuel unit for various applications such as fuel storage applications, chemicals and fertilizers [68]. It can be powered by using surplus electricity from renewable energy, natural gas, biogas, recycle waste from landfills or anaerobic digesters. As one of the feedstocks for ammonia production - hydrogen is rather costly. The NFuel unit uses also economical and fatal hydrogen or polluted hydrogen from chemical process besides from the electrolyzer process, such as chlorine, silicium carbide and formaldehyde. The current NFuel unit is designed for a production rate of 120 kg/hr  $NH_3$  and its ammonia reactor skid is about a 40 ft standard container (volume of  $64 m^3$ ) (figure 2.16).

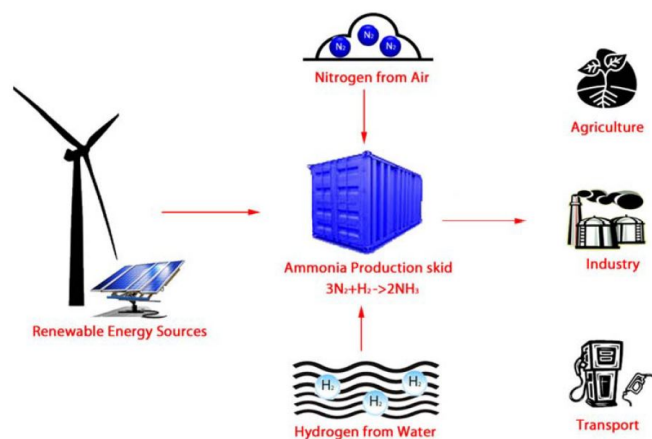


Figure 2.16: Proton Venture NFuel's basic concept

The completed NFuel unit in Proton Venture consists of six parts:

- Nitrogen generator skid;
- Hydrogen generator skid based on electrolyzers;
- Ammonia compressor skid;
- Ammonia synthesis loop skid;
- Storage tank for ammonia;
- Utility skid: operator station stand, control panel and motor control center.

The ammonia reaction skid of Proton Venture applies Casal's Haber-Bosch ammonia synthesis loop and takes only 8% to 17% of the system's total energy consumption.

	NFUEL 1	NFUEL 4	NFUEL 20
Capacity, tons/day	3	10	60
Power consumption, MW	1.5	5-6	25-30

Table 2.7: Details of Proton Venture's ammonia mini plant[25]

### 2.10.2. The SOC4NH3 project in Denmark

The new EUDP collaboration project from Haldor Topsoe A/S is aimed to use 1.5 kW SOFC and 50 kW SOEC production  $20 Nm^3/h NH_3$  synthesis gas by April of 2022. Haldor Topsoe is the market leader in ammonia plants and their classical ammonia process is very energy efficient, however, it emits 1.6 Mt of  $CO_2$ . Employing an electrolysis process provides the potential to decouple chemical synthesis from  $CO_2$  emissions. Besides, SOEC can separate oxygen from air directly. With a better heat integration system, the new SOC4NH3 design can significantly reduce the investment cost and increase the efficiency.

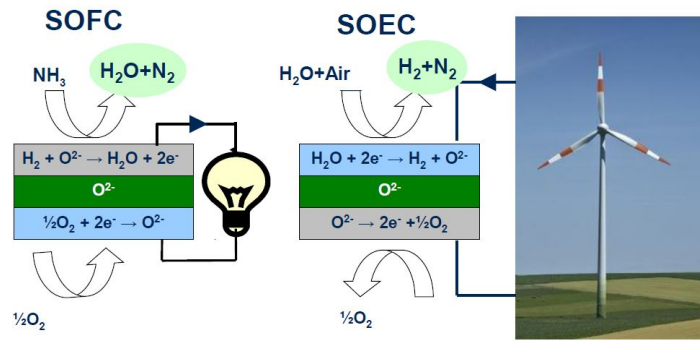


Figure 2.17: The Haldor Topsoe SOC4NH3 project [41]

### 2.10.3. Thyssenkrupp - Carbon2Chem

Thyssenkrupp AG is a German engineering company focusing on industrial engineering and steel production. The company has been researching on ammonia production from BFG and COG since June 2016. Hydrogen is obtained from COG gases as well as water electrolysis cells. Nitrogen and carbon dioxide are captured from the blast furnace gases. The new concept can not only produce ammonia but also urea due to the additional reaction sector of ammonia and carbon dioxide. The aim of urea capacity with this concept is 29000 ton/day.

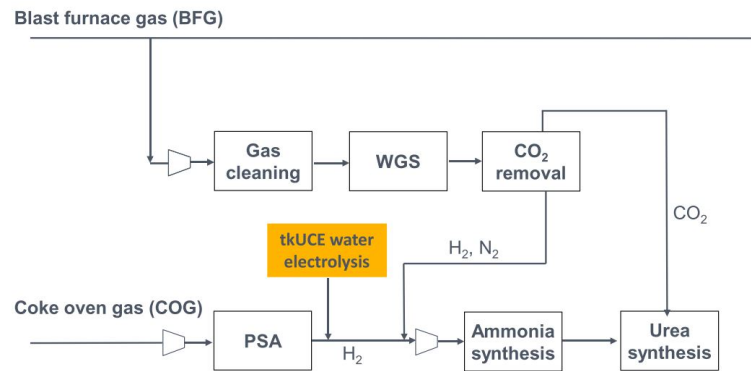


Figure 2.18: Power-to-X at thyssenkrupp's process concept A: ammonia from BFG and COG [50]

### 2.10.4. Yara

Yara is working on their next generation green fertilizer technology. It will include an integrated battery-electrolyzer (kW size) and an electrochemical ammonia production system (a Gigawatt electrolyzer design). Yara will collaborate with ENGIE on green hydrogen production linked to existing Yara Pilbara plant, which is installed with a Haber-Bosch ammonia synthesis system. The Yara Pilbara ammonia plant is close to the key import market for carbon-free energy. The area has also abundant stranded renewable energy resources. Additionally, the local opportunities are also inspiring. It has very supportive policies and care for the environment.

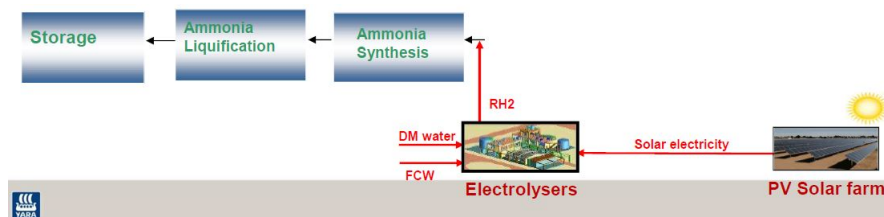


Figure 2.19: Yara  $RH_2$  integration in ammonia production [93]

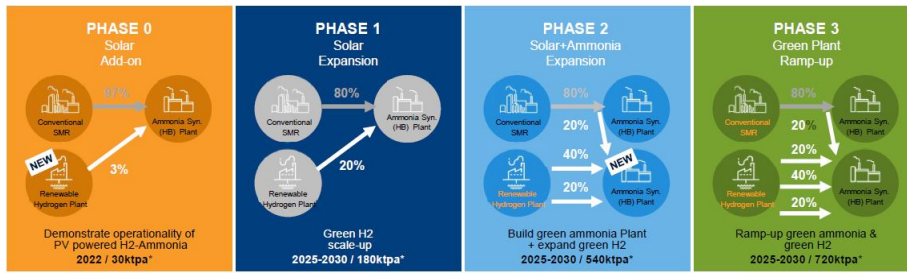


Figure 2.20: Yara  $RH_2$  integration in ammonia production road map in Pilbara [93]

2.10.5. CSIRO

CSIRO’s collaborative project with ARENA has developed a prototype proof of concept facility in Australia. The system is operated at lower pressure (10 - 30 bar), which is 25% less energy input than that of the conventional Haber-Bosch process. It is a decentralized, modular process which has a high conversion rate and ammonia yield. CSIRO has also developed a pilot ammonia cracking system for hydrogen production which can be used as car fuel for 2 to 3 days.

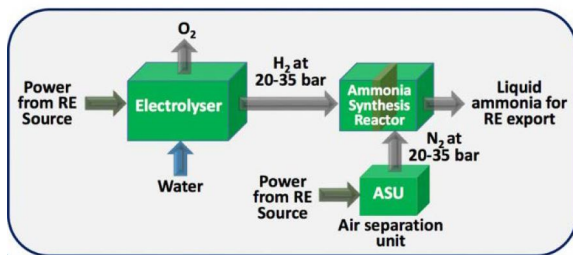


Figure 2.21: CSIRO novel direct ammonia production [42]

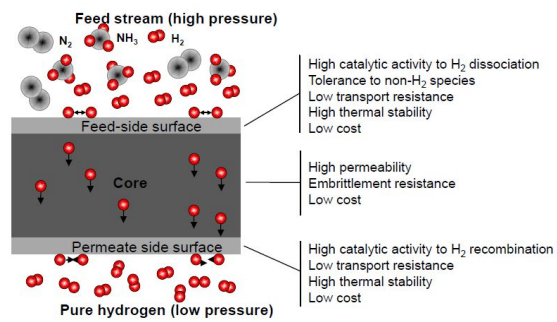


Figure 2.22: CSIRO catalytic membrane reactor for ammonia cracking [42]

2.10.6. Siemens

Siemens has built an energy storage demonstration system based on green ammonia in the UK to explore the possibility of using ammonia as an energy vector. It has a completed cycle of renewable power generator, nitrogen capturing from air, an electrolyzer for hydrogen production, an ammonia synthesis reactor, an ammonia storage tank and a combustion system that converts ammonia back to electricity.

Component	Vital data of the Siemen’s demonstrator
Wind turbine	20 kW
Electrolyzer	13 kW and producing approx. $2.4 Nm^3/h$ of hydrogen
Pressure-swing absorption	7 kW and producing $9 Nm^3/h$ of nitrogen
Haber-Bosch synthesis reactor	30 kg/day of ammonia
Storage system	350 kg of on-site ammonia
Generator set	30 $kW_e$ with ammonia as fuel
Control system	Siemens PCS7

Table 2.8: Siemens green ammonia demonstrator vital statistics [79]

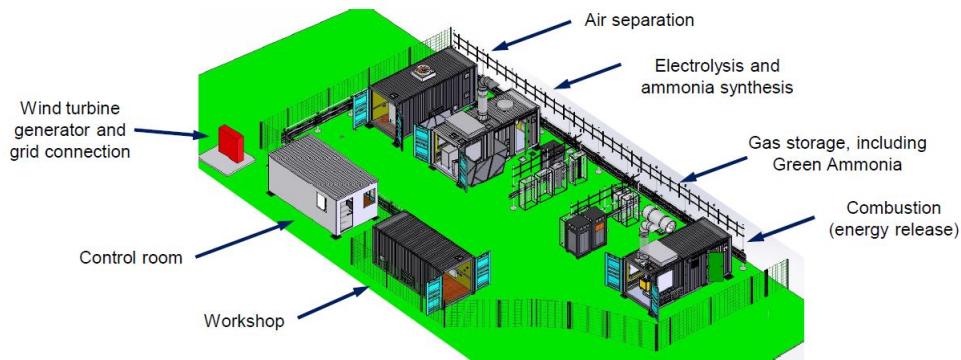


**Figure 2.23:** The system demonstration [79]

### 2.10.7. Enaex - Chile

Enaex is the largest ammonium nitrate producer in Latin-American. Ammonium nitrate is an essential chemical used in the blasting process in the mining industry. They together with ENGIE are starting a new green ammonia pilot plant that will feed the existing Prillex ammonium nitrate production plant [34].

### 2.10.8. ARENA's new ammonia plan

ARENA (the Australian Renewable Energy Agency) is going to build the world's largest green ammonia plant powered by renewable hydrogen in Queensland. The renewable ammonia facility will be built at the existing Moranbah ammonia plant. The current Dyno Nobel's Moranbah facility produces more than 360,000 tonnes of ammonium nitrate per year for their mining customers. The present plant is using natural gas as feedstock to produce hydrogen[19].

### 2.10.9. Ballance Agri-Nutrients in New Zealand

This New Zealand's fertilizer producer is planning to build a showcase green ammonia project at their Kapuni plant in Taranaki. The current plant is using natural gas to make ammonia and upgrades it to urea fertilizer. The new pilot plan will be using an electrolyzer to produce hydrogen by four wind turbines with a total capacity of 16 MW. The project is expecting to be completed by 2021 [13].

### 2.10.10. H2U Port Lincoln green $H_2/NH_3$ project

H2U is Australia's leading renewable-energy integrated hydrogen infrastructure developer. Its Port Lincoln project has a scope of developing a 35 - 40 MW electrolyzer plant, a network support service and a 60 tonne per day distributed ammonia production. The green hydrogen is produced from electrolysis cells. Nitrogen is captured from ASU and ammonia is formed by the Haber-Bosch process.

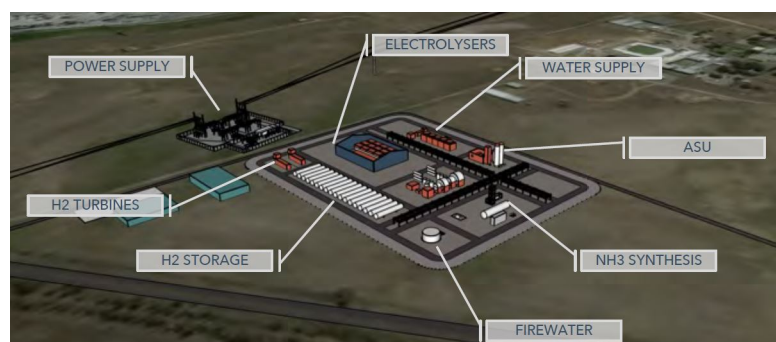


**Figure 2.24:** H2U plant layout [62]

# 3

## Process Simulation

In this chapter, process simulation of the small-scale ammonia synthesis reactor system was performed in Aspen and Matlab. The results of the process modelling were discussed. The optimal operation parameters were employed by the reactor experiments. A simplified reactor drawing is shown in figure 3.1.

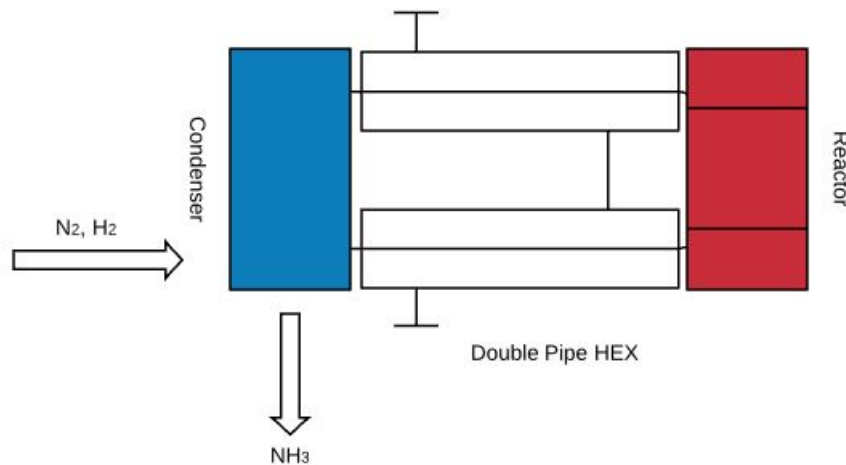


**Figure 3.1:** Drawing of a simplified reactor system

Methodology of the process simulation is illustrated in section 3.1. Modelling and simulation of the reactor, the heat exchanger system and the condenser are depicted in section 3.2 and 3.3.

### 3.1. Simulation methodology

In this section, the basic methodology of the model are described. Two approaches were used in modelling the reactor system. One was a process flowsheet simulation in ASPEN (Advanced System for Process Engineering), another approach applied Matlab CAPE-OPEN thermo import for calculating the thermodynamic and physical property of the process streams[16] in Matlab.

Chemical components (conventional and polymer) that were used in the system process were found in the ASPEN Databanks. RKS (Redlich-Kwong Soave) property method was selected for the simulation. The flowsheet consists of one mixer for the fresh feed, three shell and tube heat exchangers, one heater, one reactor, one flash for ammonia separation, one splitter for the purge, one valve and one pump for cooling oil circulation.

A plug flow reactor was picked for the solid-catalyzed exothermic reaction. The reaction kinetic form was

LHHW (Langmuir-Hinshelwood-Hougen-Waston)[15].

$$r = \frac{(\text{kinetic factor})(\text{driving force expression})}{\text{adsorption term}}$$

For reversible reaction, consider a reaction  $A + B \leftrightarrow C + D$ , the rate expression can be re-written as:

$$r = \frac{k_f[A][B] - k_b[C][D]}{\text{Adsorption expression}}$$

The rigorous heat exchanger model (HEATX) was employed in the simulation. The flow direction in the heat exchangers were countercurrent. The overall ASPEN process simulation is revealed in section 3.3.

With a constant fresh feed mass flow rate of 50 g/h, firstly six groups of parameters were analyzed in the reactor Matlab calculation and then the optimal three groups of Matlab results were studied in the ASPEN simulation. From which, a set of testing parameters from the modelling results were chosen for the reactor experiments and two of those operation conditions were selected for an optimistic micro-ammonia plant techno-economic analysis. The original six groups of parameters are displayed in table 3.1.

No.	Reactor Pressure [bar]	Reaction Temperature [ $^{\circ}C$ ]	Feed gas ( $N_2 : H_2$ ) ratio
1	100	400, 350, 300	1 : 3
2	75	400, 350, 300	1 : 3
3	50	400, 350, 300	1 : 3
4	100	400, 350, 300	1 : 5
5	75	400, 350, 300	1 : 5
6	50	400, 350, 300	1 : 5

**Table 3.1:** Groups of parameters used for reactor Matlab calculation

### 3.2. Reactor modelling

The simple form of temperature-pressure rate equation which was originally presented by Temkin and Pyzhev is used in this chapter. It is a general expression for ammonia synthesis reaction over a magnetite catalyst. The equation is given below 3.1.

$$-r_{N_2} = \frac{r_{NH_3}}{2} = k_f \cdot P_{N_2} \left( \frac{P_{H_2}^3}{P_{NH_3}^2} \right)^{\alpha} - k_b \left( \frac{P_{NH_3}^2}{P_{H_2}^3} \right)^{1-\alpha} \quad (3.1)$$

Where  $k_f$  and  $k_b$  are the rate constants for ammonia synthesis and ammonia decomposition respectively,  $\alpha$  is a positive constant that has value of 0.5 - 0.75.  $\alpha = 0.5$  was found by Livshits and Sidorove which has good agreement with experimental data and is normally taken. Temkin's kinetic equation is based on the assumption that the rate-determining step is the chemisorption of nitrogen on a nonuniform surface and all surface is dominated by  $N^*$  species. However, equation 3.1 is not valid down to zero or at a very low ammonia concentration in the gas feed. Despite this limitation, for the proposed reactor system design, the ammonia content at the inlet of the reactor is always greater than zero due to the recycle flow. The forward and backward rate constants are calculated from the Arrhenius relation:

$$k = k_0 \cdot \exp(-E_a/RT) \quad (3.2)$$

Where R is the universal gas constant 8.314 (J/mol K), T is the reaction temperature (K),  $E_a$  is the activation energy (J/mol) and  $k_0$  is the pre-exponential factor. The equilibrium constant can be then obtained:



In order to calculate  $K_{eq}$ , the activity of each component i must be introduced.

$$a_i = \frac{f_i}{f_i^*} \quad (3.4)$$

Where  $f_i^*$  is the fugacity of component  $i$  at an arbitrary chosen standard state. Here we choose  $f_i^*$  as equal to the fugacity of pure component  $i$  at a pressure of 1 atm.  $f_i$  is the fugacity of component  $i$  at the partial pressure of the component in the system. From the Lewis and Randall rule, we rearrange and get:

$$a_i = f_i = y_i \cdot f_i^o, \quad f_i^o = \gamma_i \cdot P \quad (3.5)$$

Where  $f_i^o$  is the pure component fugacity at the operation condition of the system and  $y_i$  is the mole fraction of component  $i$ ,  $\gamma_i$  is the activity coefficient of component  $i$  and  $P$  is the system total pressure. From the study of Dyson et al. [31], the activity coefficients are computed by using equations 3.6, 3.7 and 3.8.

$$\gamma_H = \exp\left(e^{-3.8402T^{0.125}+0.541} \cdot P - e^{-0.1268T^{0.5}-15.980} \cdot P^2 + 300 \cdot e^{-0.011901T-5.941} (e^{-P/300} - 1)\right) \quad (3.6)$$

$$\gamma_N = 0.93431737 + 0.3101804 \times 10^{-3}T + 0.295896 \times 10^{-3}P - 0.2707279 \times 10^{-6}T^2 + 0.4775207 \times 10^{-6}P^2 \quad (3.7)$$

$$\gamma_A = 0.1438996 + 0.2028538 \times 10^{-2}T - 0.4487672 \times 10^{-3}P - 0.1142945 \times 10^{-5}T^2 + 0.2761216 \times 10^{-6}P^2 \quad (3.8)$$

Where  $T$  is in unit of K and  $P$  is with the unit of atm. Therefore,  $K_{eq}$  can be calculated:

$$K_{eq} = \frac{a_A}{a_H^{3/2} a_N^{1/2}} = \frac{\gamma_A \cdot y_A \cdot P}{(\gamma_H \cdot y_H \cdot P)^{3/2} (\gamma_N \cdot y_N \cdot P)^{1/2}} = K_P \cdot K_{\gamma_0} \cdot K_{\gamma} \quad (3.9)$$

$$K_{eq}^2 = \frac{k_f}{k_b} \quad (3.10)$$

Where  $K_P$  is the ideal gas equilibrium constant, for standard state of 1 atm,  $K_{\gamma_0} = 1$ . The value of  $K_P$  can be determined by the Gillespie and Beattie correlation 3.11.

$$\log_{10} K_P = -2.691122 \log_{10} T - 5.519265 \cdot 10^{-5} T + 1.848863 \cdot 10^{-7} T^2 + \frac{2001.6}{T} + 2.6899 \quad (3.11)$$

$K_{\gamma}$  can be calculated from Gillespie and Beattie's correlation for ammonia synthesis:

$$\log_{10}\left(\frac{1}{K_{\gamma}}\right) = P \left( \frac{0.1191849}{T} + \frac{91.87212}{T^2} + \frac{25122730}{T^4} \right) \quad (3.12)$$

A plug flow reactor was used in both the laboratory scale model and the reactor simulation, which contained no ammonia and no inert in the feed gas. Hence, we can write the fractional conversion of nitrogen as followed equation:

$$\eta = \frac{\text{molar flow of } N_2 \text{ at the inlet} - \text{molar flow of } N_2 \text{ at across section}}{\text{molar flow of } N_2 \text{ at inlet}} \quad (3.13)$$

Assuming that the inlet flow rate is  $F_{i0}$  of component  $i$ , the relations between the mole mass of each component and the total mole mass can be derived as follows:

$$\begin{aligned} F_N &= F_{N0} - F_{N0} \cdot \eta \\ F_H &= F_{H0} - 3 \cdot F_{N0} \cdot \eta \\ F_A &= F_{A0} + 2 \cdot F_{N0} \cdot \eta \\ \hline F_{tot} &= F_{tot0} - 2 \cdot F_{N0} \cdot \eta \end{aligned}$$

The molar fractions of each component are equal to:

$$y_N = \frac{F_{N0}(1-\eta)}{F_{tot}} \quad (3.14)$$

$$y_H = \frac{F_{H0} - 3 \cdot F_{N0} \cdot \eta}{F_{tot}} \quad (3.15)$$

$$y_A = \frac{F_{A0} + 2 \cdot F_{N0} \cdot \eta}{F_{tot}} \quad (3.16)$$

$\eta_{exit}$  is the conversion value at the outlet. It equals to:

$$\eta_e = \frac{y_{Ae} \cdot F_{tot0}}{2F_{N0}(1 + y_{Ae})} \quad (3.17)$$

After several adjustments, Dyson et al. [31] derived the alternative form of the original Temkin-Phyzev rate equation, which is:

$$r_{NH_3} = k_b \left[ K_p^2 a_N \left( \frac{a_H^{3/2}}{a_A} \right) - \left( \frac{a_A}{a_H^{3/2}} \right) \right] \quad (3.18)$$

Where  $k_b = 2k$ ,  $k = 8.849 \times 10^{14} e^{-170561/RT}$  and the unit of the ammonia production rate is in kilogram-moles of ammonia formed per cubic meter of catalyst bed per hour. For ideal gases, the partial pressure is equal to its fugacity. For non-ideal gases, fugacity equals to the fugacity coefficient times the partial pressure. Below figures show the fugacity coefficients for the reaction gases vs. temperature under different total pressures by using Dyson and Simon's fugacity coefficient equations.

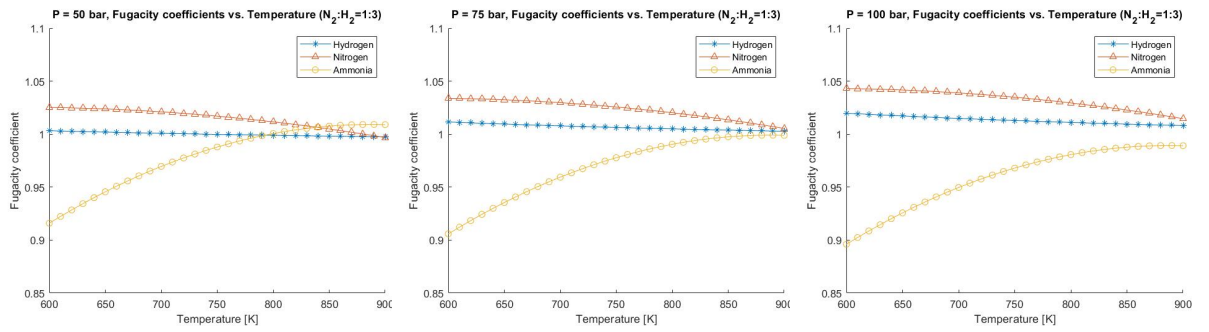


**Figure 3.2:** P = 50 bar, fugacity coefficient vs. temperature **Figure 3.3:** P = 75 bar, fugacity coefficient vs. temperature **Figure 3.4:** P = 100 bar, fugacity coefficient vs. temperature

As the figures show,  $\gamma$  is very close to 1. The lowest value of fugacity coefficient is 0.9 and the highest value of that is 1.025. For simplification, the following assumptions are used for the process simulation:

1. The fugacity coefficients for all gases are equal to 1.
2. The Temkin-Pyzhev equation for the rate expression is valid.
3. It is a one-dimensional model so that the temperature and concentration gradients in the radial direction are neglected.
4. Heat and mass diffusion in the longitudinal direction are negligible.
5. The temperature of the gas flowing around the catalyst particle is equal to the temperature of the particle itself.
6. The catalyst activity is uniform along the reactor and equal to unity.
7. The bulk density of the catalyst is  $1200 \text{ kg/m}^3$ .

The kinetics constants values used in the equation 3.1 are illustrated in the followed table:

Parameters	Value
$k_{0f} (\text{kmol/m}^3 \cdot \text{h} \cdot \text{atm}^{1.5})$	$1.78954 \times 10^4$
$E_{1f} (\text{kcal/kmol})$	20800
$k_{0b} (\text{kmol} \cdot \text{atm}^{0.5} / \text{m}^3 \cdot \text{h})$	$2.5714 \times 10^{16}$
$E_{1b} (\text{kcal/kmol})$	47400

**Table 3.2:** The kinetics constants values

### 3.2.1. Reaction equilibrium

Figures below show 1) the distribution of constant reaction rate lines (solid lines); 2) the maximum conversion for each reaction rate with iron based catalyst and operated at the pressure of 100 bar, 75 bar and 50 bar (dash line), respectively.

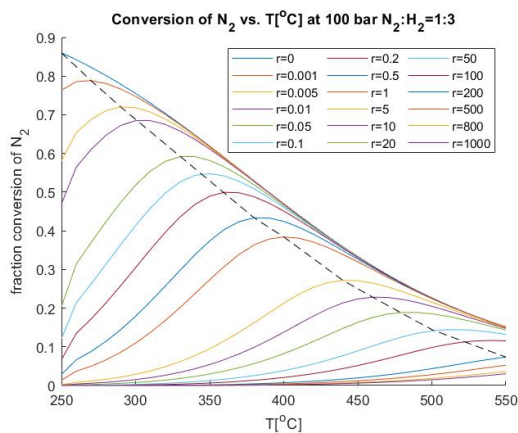


Figure 3.5: Contour of constant reaction rate for a stoichiometric inert free reaction mixture at a total pressure of 100 bar

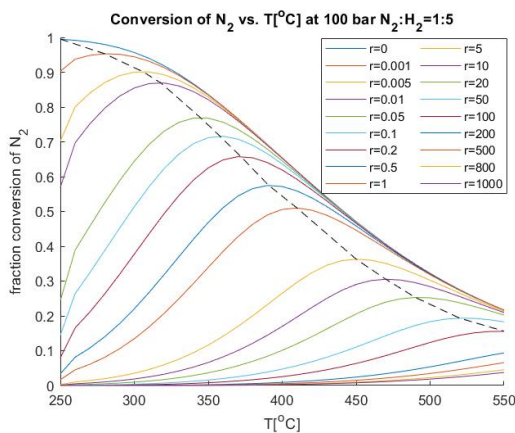


Figure 3.6: Contour of constant reaction rate for 1 : 5 inert free reaction mixture at a total pressure of 100 bar

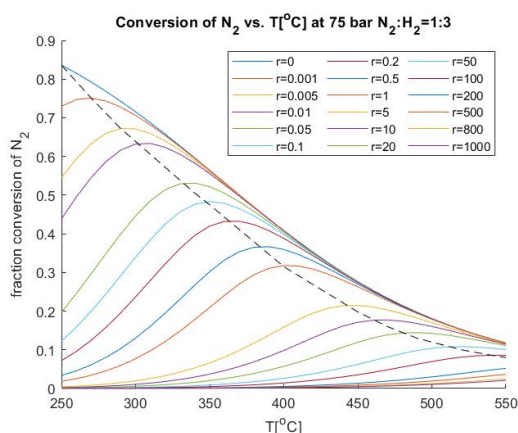


Figure 3.7: Contour of constant reaction rate for a stoichiometric inert free reaction mixture at a total pressure of 75 bar

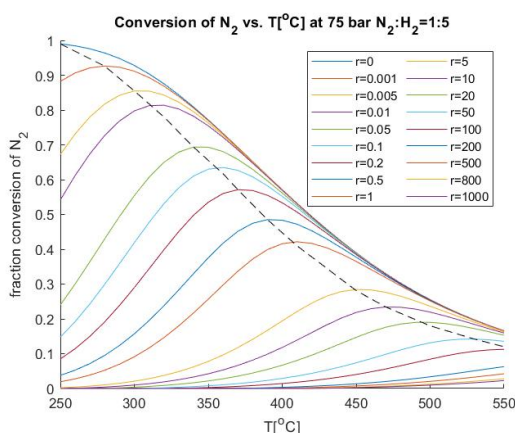


Figure 3.8: Contour of constant reaction rate for 1 : 5 inert free reaction mixture at a total pressure of 75 bar

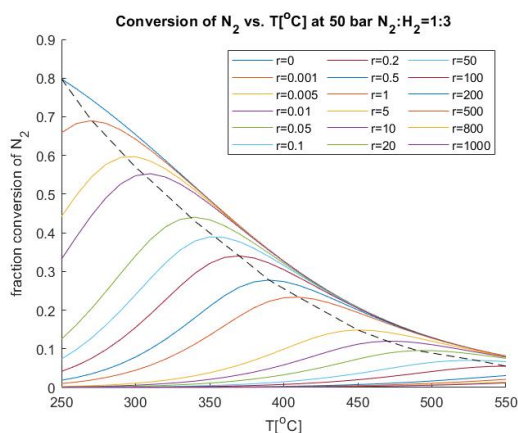


Figure 3.9: Contour of constant reaction rate for a stoichiometric inert free reaction mixture at a total pressure of 50 bar

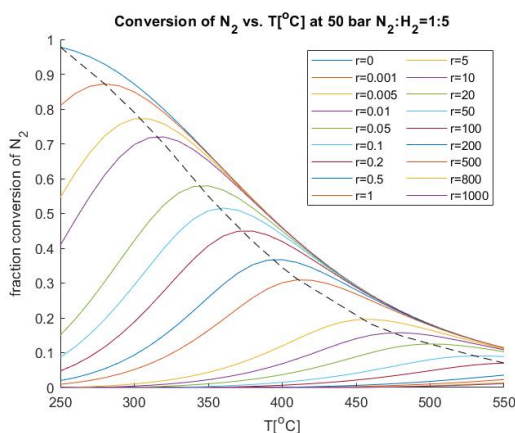


Figure 3.10: Contour of constant reaction rate for 1 : 5 inert free reaction mixture at a total pressure of 50 bar

The figures were obtained by imposing a constant value of reaction rate from zero to 1000 and used the Excel nonlinear solver solving for the conversion at a given reaction temperature and pressure. There are two different feed gas ratios. One is stoichiometric ratio (left side figures), another one is with a nitrogen and hydrogen ratio of 1 : 5 (right side figures). For an isothermal reactor, the conversion of nitrogen grows from zero

and progressively extends to a saturation value at  $r = 0$ , which is the maximum extent of the reaction. The black dash line shows  $\frac{\partial r}{\partial T} = 0$ , which is the optimal reaction temperature and conversion at a constant rate. At a constant conversion value, the reaction rate firstly increases as temperature elevates, and then decreases until it reaches equilibrium. For an isothermal reactor at different temperatures, regardless of the catalyst bed length and the residence time, the highest reaction temperature leads to the lowest equilibrium conversion. A summary of the saturated nitrogen conversion at the different operation conditions are listed below.

	50 bar	75 bar	100 bar	Feed gas ratio
300 °C	65.4%	71.5%	75.5%	1 : 3
	87.2%	92.8%	95.7%	1 : 5
350 °C	48.5%	56.4%	62%	1 : 3
	67.2%	77.2%	83.6%	1 : 5
400 °C	32.7%	40.9%	47%	1 : 3
	46%	57.1%	65.4%	1 : 5

**Table 3.3:** Maximum value of nitrogen conversion at each operation condition for an isothermal reactor

Reaction with the lowest temperature (300 °C) and the highest hydrogen partial pressure in the feed gas has the most reaction conversion.

### 3.2.2. Conversion along the bed length

Secondly, the fraction of nitrogen conversion versus bed length at various temperatures and at a constant pressure were plotted in the same graph. Since Temkin-Pyzhev equation is limited to non-zero ammonia concentration in the feed gas, a factor of  $K_3 P_{NH_3} / (1 + K_3 P_{NH_3})$  needs to be multiplied to the rate equation for an inner free single pass reactor modelling [20]. In this case, the approach to infinite low ammonia pressure can be avoided.

$$r = f K_3 \left( \frac{K_f P_N P_H^{1.5} - K_b P_A^2 / P_H^{1.5}}{1 + K_3 P_A} \right) \quad (3.19)$$

Where  $f$  is equal to 1 and  $K_3$  has a value of  $2 \text{ atm}^{-1}$ . Along the length of the reactor, as the fraction of conversion increases, the rate of reaction is progressively decreasing until it reaches equilibrium. The reaction rate has a maximum value at the beginning of the reactor.

Yet, for isothermal ammonia synthesis in small-scale with a catalyst bed length of 15 cm, the high reaction temperature, namely 400 °C, is preferred to the design in order to obtain a higher conversion in a short residence time. For reaction at the same temperature, the higher the operation pressure, the more ammonia can be produced.

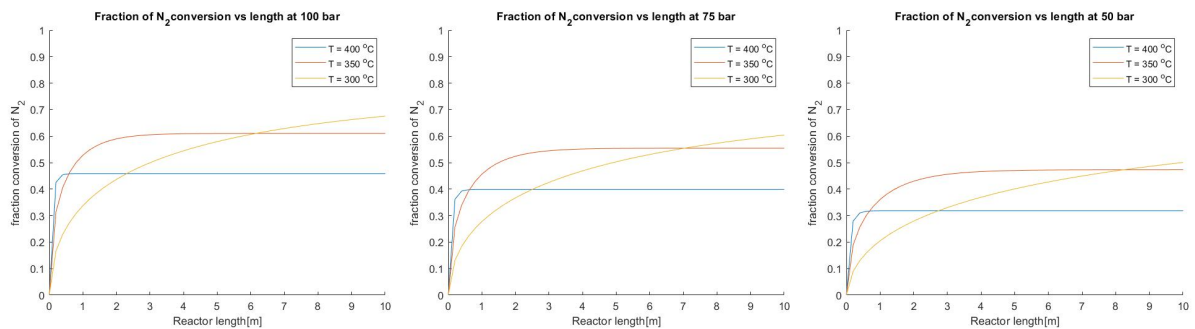


**Figure 3.11:** Fraction of nitrogen conversion vs isothermal reactor at 100 bar

**Figure 3.12:** Fraction of nitrogen conversion vs isothermal reactor at 75 bar

**Figure 3.13:** Fraction of nitrogen conversion vs isothermal reactor at 50 bar

### 3.2.3. An adiabatic or an isothermal reactor

Nitrogen conversion versus reactor bed length in adiabatic and isothermal conditions were plotted in the same graph. In adiabatic condition, as the exothermic reaction is progressing, the temperature increases. The reaction rate firstly steadily increases to the optimal value and then decreases to zero (equilibrium point).

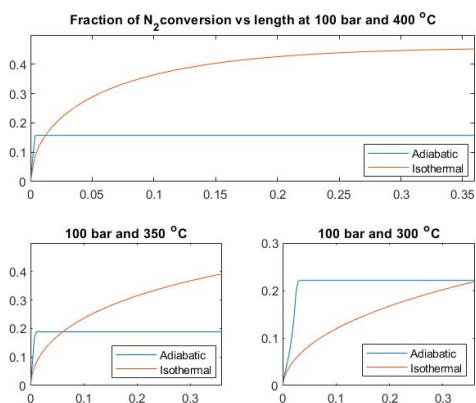


Figure 3.14: Fraction of nitrogen conversion vs adiabatic reactor at 100 bar,  $N_2 : H_2 = 1 : 3$

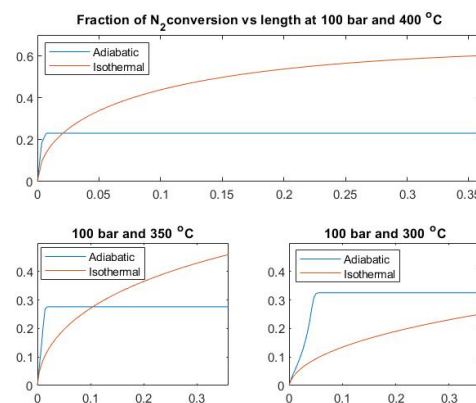


Figure 3.15: Fraction of nitrogen conversion vs adiabatic reactor at 100 bar,  $N_2 : H_2 = 1 : 5$

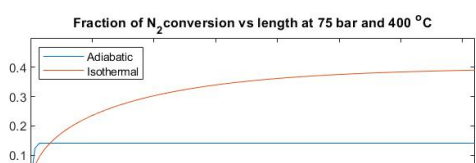
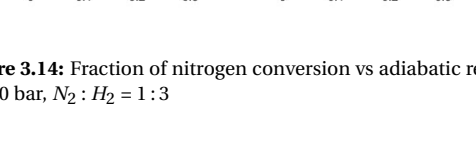
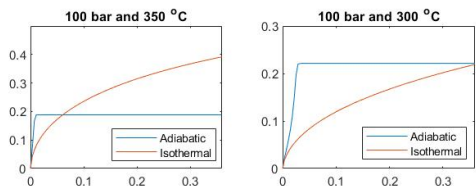


Figure 3.16: Fraction of nitrogen conversion vs adiabatic reactor at 75 bar,  $N_2 : H_2 = 1 : 3$

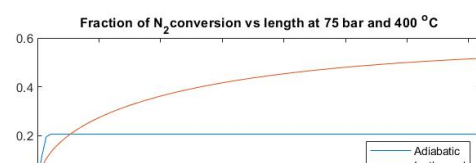
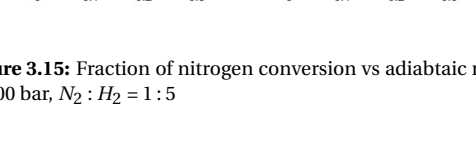
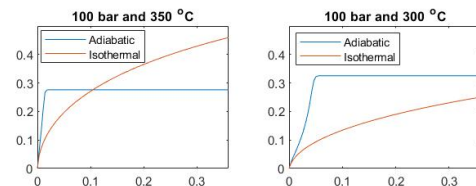


Figure 3.17: Fraction of nitrogen conversion vs adiabatic reactor at 75 bar,  $N_2 : H_2 = 1 : 5$

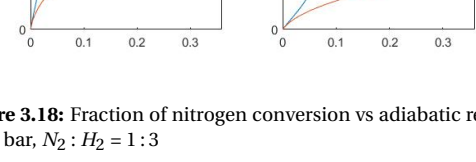
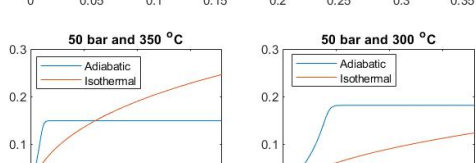
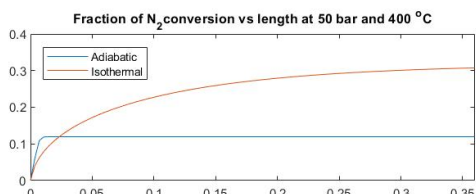


Figure 3.18: Fraction of nitrogen conversion vs adiabatic reactor at 50 bar,  $N_2 : H_2 = 1 : 3$

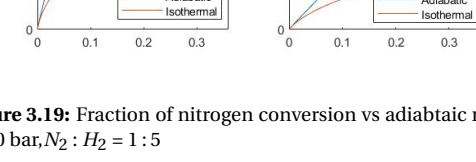
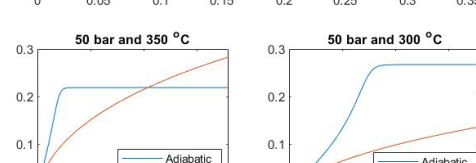
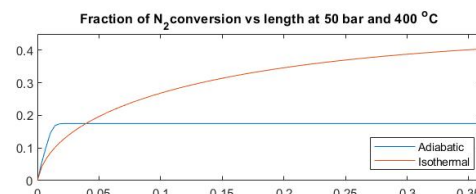


Figure 3.19: Fraction of nitrogen conversion vs adiabatic reactor at 50 bar,  $N_2 : H_2 = 1 : 5$

From figures above, it can be clearly seen that for the same operation condition, an isothermal reactor can reach much higher conversion than that of an adiabatic reactor. However, due to the lower reaction rate, it takes longer time to reach equilibrium for an isothermal reactor. As the figures show, with a catalyst bed length of 15 cm and the operation temperature of  $400^{\circ}C$ , the reaction has better conversion in isothermal



Three operation pressures were simulated. The results show that the higher the operation pressure, the sooner the reaction reaching steady state and the higher nitrogen conversion per single pass is obtained.

P [bar]	T [°C]	Mass flow [g/h]	Conversion [%]
100	400	161.562	20.3%
75	400	244.819	11.7%
50	400	358.88	5.8%

**Table 3.5:** Reactor parameters comparison under various pressures

With the increase of pressure, more heat is released due to the catalytic exothermic reaction. The resident time also becomes longer, which boosts the ammonia formation on the catalyst surfaces.

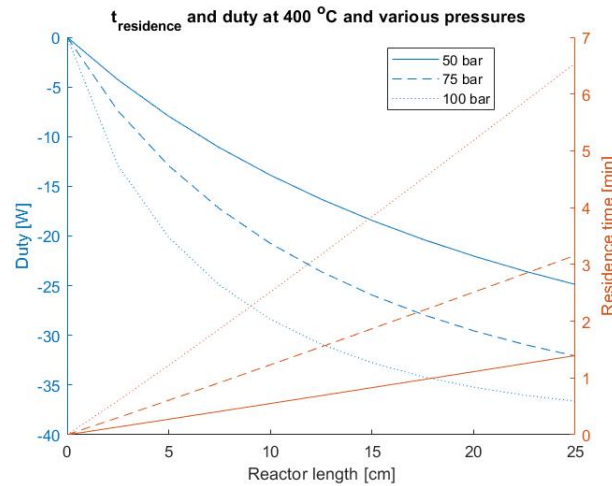


**Figure 3.22:** Reaction residence time and heat released at various pressures

The pressure drop per unit tube length in the reactor fixed bed can be calculated using the Ergun equation [87] :

$$\frac{\Delta P}{L_b} = 150 \cdot \frac{(1 - \epsilon)^2}{\epsilon^3} \cdot \frac{\mu u}{d_p^2} + 1.75 \cdot \frac{(1 - \epsilon)}{\epsilon^3} \cdot \frac{\rho_f u^2}{d_p} \tag{3.20}$$

Where  $\Delta P$  is the pressure drop ( $N/m^2$ ),  $L_b$  is the length of solid bed (m),  $\epsilon$  is the void fraction, here we take a reasonable value of 0.5,  $\mu$  is the fluid viscosity ( $Ns/m^2$ ),  $u$  is the fluid superficial velocity (m/s),  $d_p$  is the particle effective diameter. A mean value 0.0023 m of the catalyst particle size is used for the calculation.  $\rho_f$  is fluid density ( $kg/m^3$ ).

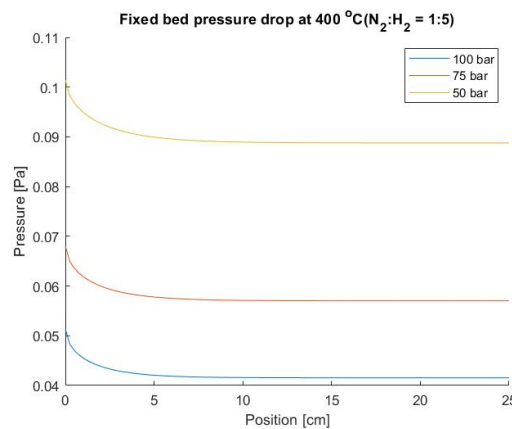
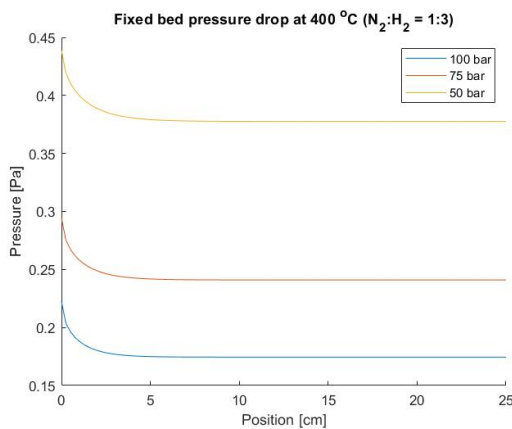


**Figure 3.23:** Fixed bed pressure drop at 400°C with  $N_2:H_2 = 1 : 3$  **Figure 3.24:** Fixed bed pressure drop at 400°C with  $N_2:H_2 = 1 : 5$

As figures 3.23 and 3.24 show, the pressure drops are very small. However, it can be significantly increased by having a longer catalyst bed or by applying much smaller catalyst particles (less than 1 mm). The pressure drop of lower operation pressure is 2 times larger than that of higher operation pressure. With the current simulated bed length (25 cm) and catalyst particle size (2 mm), operation conditions of 400°C and 50 bar is more suitable for a small-scale ammonia synthesis reactor design.

### 3.3.2. Double pipe heat exchangers

A double pipe heat exchanger is generally suitable for small-capacity applications where the total heat transfer required area is less than 50 m<sup>2</sup>. For the purpose of suitability of this type of heat exchanger system to our proposed reactor model, two shortcut counter current flow heat exchanger system were simulated in ASPEN 3.25.

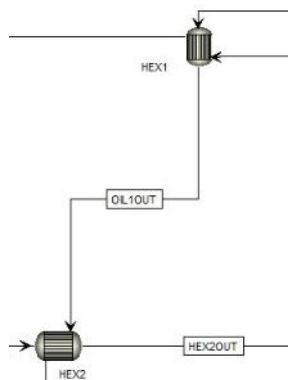


Figure 3.25: Double pipe heat exchanger system simulation in Aspen

Because of the large temperature decline from outlet mixed gas temperature to ammonia dew point with outlet gas composition, a heat transfer fluid with wider operation temperature limit is required. Silicone oil is chosen here for heating the inlet gases and cooling the outlet gases. It has relatively high thermal stability and high maximum operation temperatures. The most important member of silicone oil is polydimethylsiloxane [8].

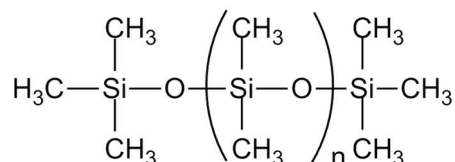


Figure 3.26: Polydimethylsiloxane [8]

Two chemicals are picked in ASPEN Databanks as silicone oil mixture for the simulation.

Name	Molecular Formula	Molecular Weight [g/mol]	Boiling point [°C]
Octadecamethyloctasiloxane	C <sub>18</sub> H <sub>54</sub> Si <sub>8</sub> O <sub>7</sub>	607.3	311.6
Hexadecamethylheptasiloxane	C <sub>16</sub> H <sub>48</sub> Si <sub>7</sub> O <sub>6</sub>	533.1	286.8

Table 3.6: Silicone oil mixture used in the Aspen model

An oil compositions of 15% of Hexadecamethylheptasiloxane and 85% of Octadecamethyloctasiloxane is used in the outer shell of the double pipe heat exchangers. The total heat exchanger duty and required heat transfer areas are displayed in table 3.7. The silicone oil is designed to be operated at the ambient pressure and to flow in a closed system.

Operation Conditions	Properties	EHX1	EHX2	Oil mass flow [g/h]
100 bar 400 °C	Heat Duty [W]	52	51	300
	Required heat transfer area [ $m^2$ ]	0.0025	0.027	
75 bar 400 °C	Heat Duty [W]	75	75	450
	Required heat transfer area [ $m^2$ ]	0.002	0.042	
50 bar 400 °C	Heat Duty [W]	115	115	600
	Required heat transfer area [ $m^2$ ]	0.005	0.013	

**Table 3.7:** Double pipe heat exchanger heat duty and heat transfer area at different operation pressures

As observed from the table above, the total heat transfer area for all three operation conditions are significantly less than  $50 m^2$ , which means the double pipe heat exchanger system can be employed to the heat transfer network for a small-scale ammonia reactor system.

A higher ammonia yield and residence time can be achieved by up-scaling the reactor size or by elevating the operation pressure. Consequently, the dew point of ammonia in the mixed gas also increases. In this case, the total heat duty of the double pipe heat exchangers reduces, therefore, less heat transfer area is required and less materials is needed for building the reactor system.

### 3.3.3. Condenser

The condenser for a small-scale ammonia reactor system depending on its operation pressure can be a concentric cylinder cooling by ambient air (e.g. at 100 bar) or a simple tube in tube heat exchanger with refrigerant in the outer tube cooling the hot gases (e.g. at 50 bar).

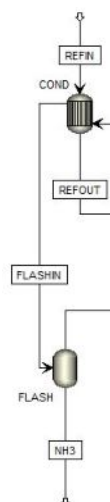


**Figure 3.27:** Condenser simulation in Aspen

In this section, both types of the condenser were discussed. For the two types of the condenser, the cooling fluid is operated at an ambient pressure.

#### Condensation with R-404A refrigerant

Refrigerant was chosen from literature [71]. R-404A consists of 52 wt% R-143A, 44 wt% R-125, 4 wt% R-134A and is usually used for low and medium temperature refrigeration applications, such as industrial refrigeration, commercial refrigeration and transport refrigeration. However, this working fluid is under great scrutiny due to its high global warming potential. The fluid is used now only for simulation.

The inlet temperature of the R-404A was set to  $-48 ^\circ C$  with a mass flow rate of 500 g/h. The heat of the hot gases was removed by the cooling fluid and ammonia was condensed. The liquid ammonia was separated from the remaining gases at the bottom of the condenser. Because the solubility of hydrogen and nitrogen in liquid ammonia are very low [64], it is assumed that pure ammonia is obtained after condensation.

Gases	5 <sup>o</sup> C	30 <sup>o</sup> C
Hydrogen	0.095	0.112
Nitrogen	0.117	0.126

**Table 3.8:**  $cm^3$  of gas at NPT soluble per gram of liquid ammonia per atm. partial pressure [64]

For operation at higher pressure, more ammonia can be obtained at the outlet of the reactor, which can increase the dew point of ammonia in the mixture and raise the condenser temperature. As the simulation results in table 3.9 show, ammonia synthesis at 400<sup>o</sup>C and 100 bar can have a minimum condensation temperature of 25<sup>o</sup>C. Little heat transfer area is required for the cooling system and extra liquid ammonia can be gained after condensation.

Operation Conditions	T [ <sup>o</sup> C]	Duty [W]	A [ $m^2$ ]	Vapor fraction [%]	NH <sub>3</sub> Condensed [%]
100 bar 400 <sup>o</sup> C	25	14	0.0002	0.84	49.5%
75 bar 400 <sup>o</sup> C	20	18	0.00027	0.92	32.1%
50 bar 400 <sup>o</sup> C	5	20	0.00037	0.963	20.8%

**Table 3.9:** Condenser parameters

### Air cooling concentric cylinder condenser for reactor at high pressure

As previous stated, for operation pressure of 100 bar, condensation at higher temperature can be achieved. Correspondingly, a more environmental friendly heat transfer fluid for the condenser can be selected. The most accessible natural cooling fluid is ambient air. For instance, the average temperature in Saudi Arabia during the winter period is about 25<sup>o</sup>C with an average of 8 sun hours [7]. The Netherlands has an annual temperature of 10<sup>o</sup>C, but it has only half of the sun hours per day compared to that of winter time in Saudi Arabia [11]. In order to see the feasibility of this type of condenser for an ammonia synthesis reactor operated at high pressure calculations were performed in Matlab [61]. The fluid properties, such as density, thermal conductivity and viscosity as a function of pressure, temperature and composition, were calculated using COCO software. The length of the condenser is the same as the reactor model in ASPEN, 25 cm. The inner diameter of the cylinder is taken as 10 cm. Inconel 600 is used as the condenser cylinder material, which has a thermal conductivity value of 14 W/m – K. The mass flow rate of the gases is very low and it is in the laminar flow range. The condensation occurs on the inner wall. In the heat transfer model, since the Biot number for a internal fluid-solid element is larger than 0.1, the lumped system is not valid here. For simplification, the axial heat conduction within the fluid is neglected. The equivalent network of the resistances is shown as follows.

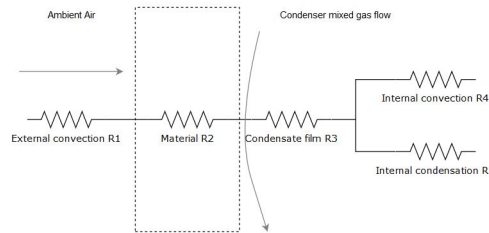


**Figure 3.28:** Steady state equivalent network of the condenser thermal resistance system [61]

$$R_1 = \frac{1}{h_a A}, \quad R_2 = \frac{d_o - d_i}{KS}, \quad R_3 = \frac{1}{h_\delta A}, \quad R_4 = \frac{1}{h_{conv} A}, \quad R_5 = \frac{1}{h_c A}$$

$$\sum R = R_1 + R_2 + R_3 + \frac{1}{\frac{1}{R_4} + \frac{1}{R_5}}, \quad UA = \frac{1}{\sum R} \quad (3.21)$$

The energy balance of the  $j^{th}$  element can be drawn as figure 3.29.  $Q_1$  and  $Q_2$  are the mixed gas heat flows in and out of the element  $j$ .  $Q_3$  is the heat flow from the internal system to the material and  $Q_4$  is the heat flow from the material to the external system. For simplification, the axial heat conduction for both fluid and

material is negligible here and the grid spacing of the steady state simulation is constant.

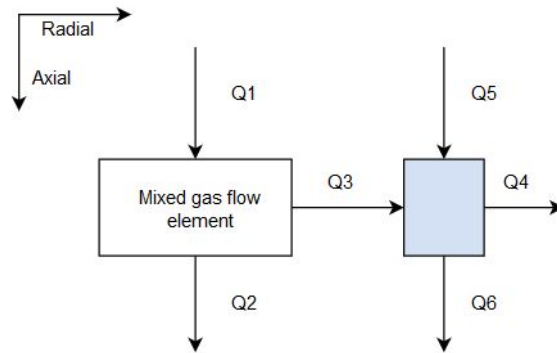


Figure 3.29: Energy balance on the  $j^{th}$  mixture and material elements

The governing equation for the mixed gases and material energy balance are:

$$Q_1 = Q_2 + Q_3, \quad m_{inconel} C_p \frac{dT}{dt} = Q_3 + Q_5 - Q_4 - Q_6 \tag{3.22}$$

where,

$$Q_1 = h_{int,j} A_1 (T_{j-1} - T_j), \quad Q_2 = h_{int,j+1} A_2 (T_j - T_{j+1}), \quad Q_3 = h_{int,j} A_3 (T_{b,j} - T_{inconel,j})$$

$$Q_4 = h_a A_4 (T_{inconel,j} - T_a), \quad Q_5 = \frac{K_{inconel} A_5 (T_{inconel,j-1} - T_{inconel,j})}{\Delta y}, \quad Q_6 = \frac{K_{inconel} A_6 (T_{inconel,j} - T_{inconel,j+1})}{\Delta y}$$

$T_b$  is the temperature of the fluid (bulk temperature) and  $h_a$  is the heat transfer coefficient of the ambient air. According to the ASPEN model at 100 bar, the condenser inlet and outlet mixed gas conditions are displayed in table 3.10.

Gas composition	Mole fraction	$T_{inlet}$ [ $^{\circ}C$ ]	$T_{outlet}$ [ $^{\circ}C$ ]	$\dot{Q}_{cond}$ [W]	Steady state $\dot{m}$ [g/h]
Nitrogen	18%	47.8	24.8	14	162
Hydrogen	55%				
Ammonia	27%				

Table 3.10: Condenser stream gas conditions in ASPEN model

The calculation results in Matlab are as below figures. The ambient air temperatures in the calculation are ranged from  $5^{\circ}C$  to  $45^{\circ}C$ .

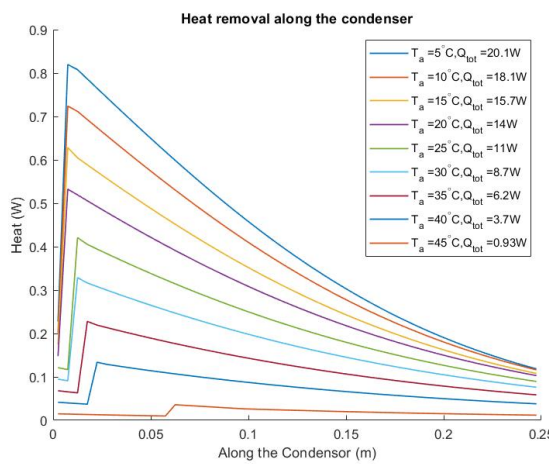


Figure 3.30: Steady state heat rejection along the condenser

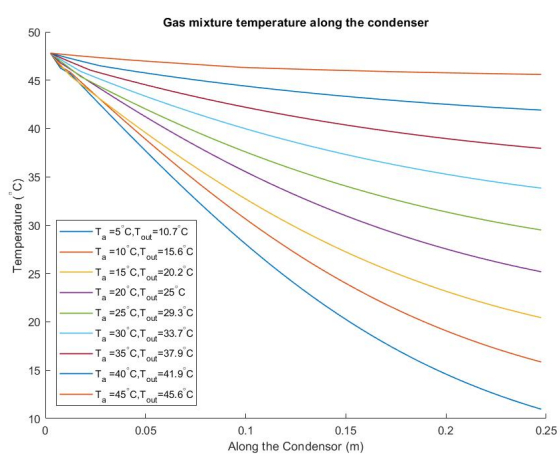


Figure 3.31: Gas mixture temperature along the condenser

The dew point of mixed gas with composition stated in table 3.10 in accordance to COCO thermal import is 47 °C. Thus, the condenser inlet gas flow temperature was slightly above the dew point. As observed from the figures, the condensation started at the point when the dew point temperature was reached. The jumps of the heat rejection lines at the beginning of the heat plot are due to the neglecting of axial heat conduction within the wall and the material. The calculation results of ambient gas temperature of 20 °C from the Matlab are coincident with ASPEN results. 14 W of heat was removed by the condenser and the outlet gas temperature was 25 °C. A summary of the results are illustrated in the table 3.11.

Ambient air temperature °C	Outlet gas temperature °C	Heat rejection [W]
5	10.7	20.1
10	15.6	18.1
15	20.2	15.7
20	24.9	13.8
25	29.3	11
30	33.7	8.7
35	37.9	6.15
40	41.9	3.7
45	45.6	0.93

**Table 3.11:** Matlab calculation condenser results

### 3.3.4. Equipment heat duty comparison

Based on the ASPEN results, the reactor system can be illustrated in Fusion360 (figure: 3.32)

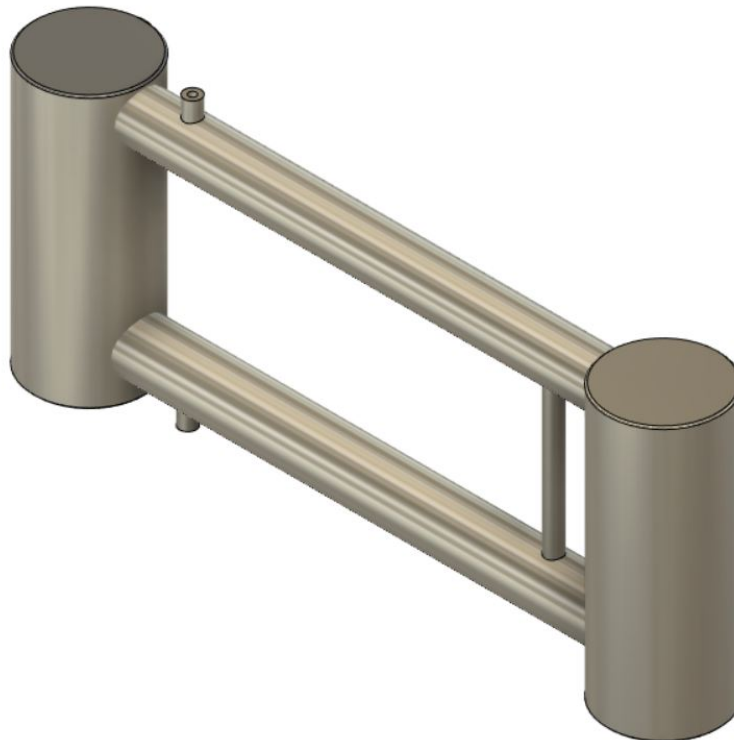


**Figure 3.32:** Process Fusion360 model based on the ASPEN simulation results

The increase of reactor size has effect on the heat exchanger sizing in the production loop. A comparison of the utilities duty with different reactor size are shown as followed:

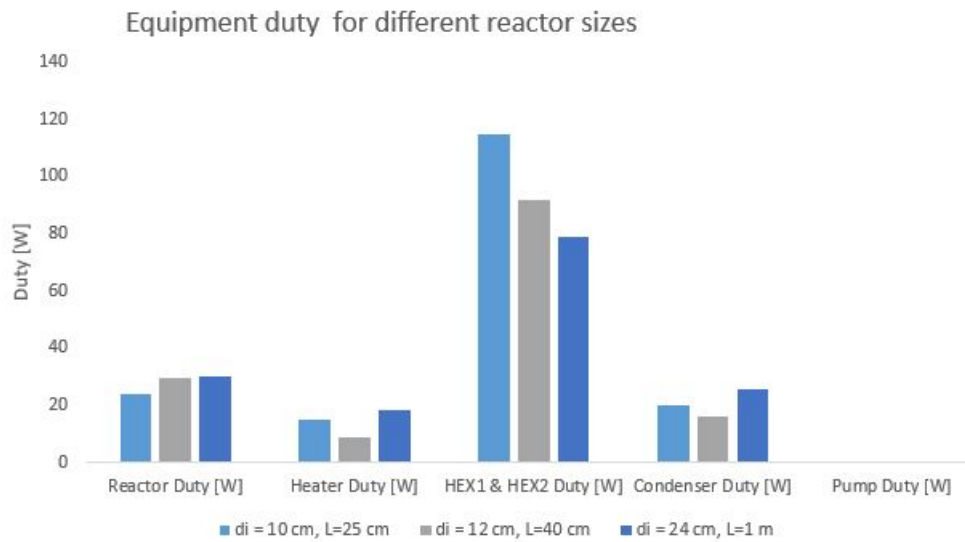


**Figure 3.33:** Utilities heat duty comparison for different reactor sizes at 50 bar and 400 °C (Aspen model data)

It can be clearly seen that the pump required net work is almost negligible compared to that of other components. The bigger the reactor, the less heat transfer area required for the double pipe heat exchangers.



# 4

## Experiment Infrastructure

In this chapter, an introduction of the experiment infrastructure and testing procedures are depicted. In order to test the parameters that were chosen from the process simulation, a laboratory scale reactor setup with the same dimensions as the design model was built. Because the reactor was operated at high temperature and high pressure with hydrogen and ammonia, a comprehensive HAZOP study was carried out and approved before the performance of any experimental testing. The process flowchart for the experiment setup design and building are shown in the following figure.



**Figure 4.1:** Experiment process flowchart

### 4.1. P&ID Design

The laboratory scale ammonia synthesis reactor setup has a size of approximately 1 m wide, 1 m deep and 2 m high. The heart of the apparatus is the stainless steel (316SS) fixed bed reactor which is placed in an oven. The reactor has a height of 368 mm and has a total bed volume of  $300\text{cm}^3 \pm 5\%$ . The catalyst bed length is 15 cm long and the bed volume is  $153\text{cm}^3 \pm 5\%$ . The total weight of the catalyst filled in the reactor is 300 g. A gas or a mixture of gases is led through the reactor with a volumetric flow rate of 2.5 NL/min. The maximum operation pressure during the experiment is 125 bar and the maximum operation temperature is  $400^\circ\text{C}$ . The gas cylinders are placed in the gas cylinder cabinet. All cylinders are fitted with an approved pressure regulator. One hydrogen sensor (10% LEL) and one ammonia sensor (25 ppm) are placed near the reactor. The engineering piping and instrument diagram of the experiment setup is shown in figure 4.2.

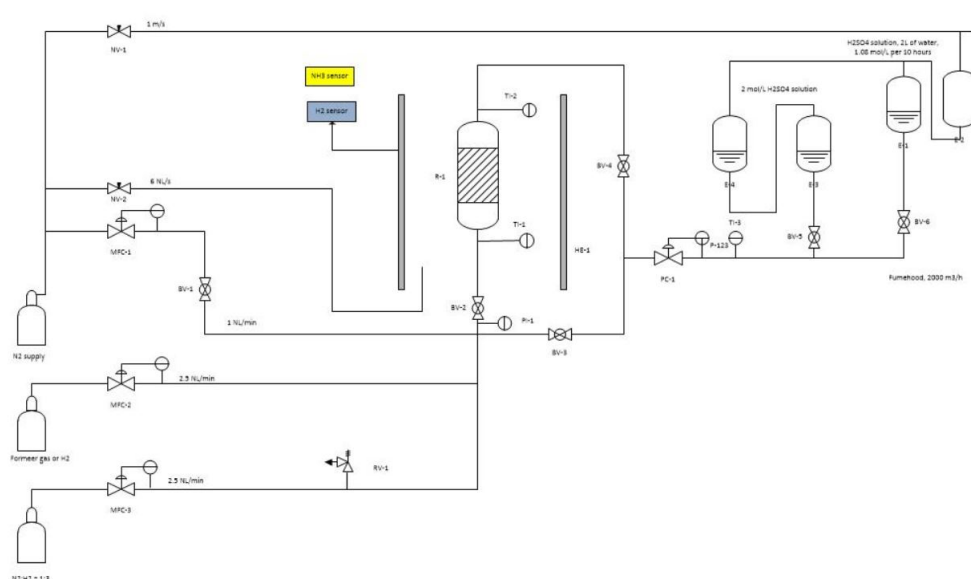


Figure 4.2: The setup P&ID

## 4.2. HAZOP

### 4.2.1. Methodology

At first, the main chemicals that were used during the experiment were rated in NFPA (National Fire Protection Association) Hazard standard. The NFPA rating identifies the hazards of materials in four principal categories: health (blue), flammability (red), reactivity (yellow) and unusual hazards (white). The degree of severity is indicated by a number between zero and four (0 - 4), where zero stands for no hazard and four for severe hazard (table 4.1).

Secondly, each process line and vessel of the setup are thoroughly analyzed. The what-if questions are formulated and answered to evaluate the effect of component failures or procedural errors. This risk assessment is a team effort. The consequences and accordingly mitigation actions are summarized in the HAZOP worksheets based on the TNO risk ratings. The general idea of the TNO risk rating is based on a quantitative methodology that analyses and estimates risks. The rating is a function of the consequences of an incident and the frequency of the incident. A combination of the two factors results in a risk ranking level table is given below (figure 4.3).

		Likelihood				
		L5	L4	L3	L2	L1
		Very Unlikely	Unlikely	Possible	Likely	Very Likely
Consequence	C1 Very high	2	2	1	1	1
	C2 High	3	2	2	1	1
	C3 Moderate	4	3	2	2	1
	C4 Low	4	4	3	2	2
	C5 Very Low	4	4	4	3	3

Figure 4.3: TNO HAZOP risk ranking level

Where 1 and 2 denote unacceptable and undesirable risk level respectively. Both risk levels should be reduced to level 3. Level 3 is an almost acceptable risk level and level 4 is an accepted risk level.

Last but not least, a series of normal and abnormal operation conditions are assessed. The explosion or instantaneous release due to the extreme scenarios are carefully calculated and compared with the minimum explosive levels. The parameters, the components and the testing procedure are adjusted accordingly to the HAZOP study results. The final approved HAZOP makes sure the coming laboratory experiments can be

performed correctly and safely.

#### 4.2.2. Chemical characterization

Table 4.1 gives a NFPA rating overview of the chemicals appearing in the process. Then, more details of the chemical safety, hazard information, physical properties and precaution on safe handling are following.

Chemical	NFPA			
	Health	Flammability	Reactivity	Unusual
Hydrogen	0	4	0	SA
Nitrogen	0	0	0	SA
Ammonia	3	1	0	
Iron based catalyst	1	0	0	
Sulfuric acid	3	0	2	W & OX
Sodium hydroxide	3	0	1	ALK

**Table 4.1:** Chemical NFPA ranking

Where OX stands for oxidizer, which allows chemicals to burn without air supply. W denotes that the chemical can react with water in an unusual or dangerous manner. SA represents the simple asphyxiant gas and ALK is alkaline [3].

#### Hydrogen gas

Hydrogen is a colorless, odorless and highly flammable gas even with small amount of ordinary air. But it is not toxic. It can be stored as a compressed gas in cylinders. In high concentration, it may cause asphyxiant because of the reduced oxygen available for breathing. No adverse effects are expected from hydrogen in case of eye and skin contact. Some critical parameters of hydrogen safety is show in table 4.2.

Critical parameters for hydrogen safety	Value
Flammability limit - lower(%)	4%(V)
Flammability limit - upper(%)	77%(V)
Auto-ignition temperature	560°C

**Table 4.2:** Critical parameter of hydrogen

#### Nitrogen gas

Nitrogen is an inert gas. It makes up 78% of the atmosphere. It is odorless, colorless, tasteless and nonirritating gas. It is commonly used to purge equipment and process lines. It is also used as protective gas in experimental environment with flammable gases. The compressed nitrogen gas can be stored in cylinders or tanks. In high concentration, it may cause asphyxiant because of reduced oxygen available for breathing. No adverse effects are expected from nitrogen gas in case of eye and skin contact.

#### Ammonia

Ammonia is a colorless gas with a characteristic pungent smell . It is also a flammable gas with flammability range of 15.4%(V) to 30%(V). The auto-ignition temperature of ammonia is 651°C. The U.S. OSHA (Occupational Safety and Health Administration) has set a 15 minute exposure limit for gaseous ammonia of 35 ppm by volume in the air and 8 hours exposure limit of 25 ppm by volume. The average odor threshold is 5 ppm, which is below any danger or damage. In high concentration, inhalation can cause lung damage. Liquid ammonia is dangerous because it is hygroscopic and it can freeze flesh. Ammonia even at diluted concentration (e.g. 0.05 mg/L) is highly toxic to aquatic animals. It can cause severe burns/damage to skin/eyes if one is in contact with the chemical [5].

#### Iron based catalyst

The iron based catalyst is a dark gray solid granular form particle. It consists of Fe and CaO,  $K_2O$ ,  $Al_2O_3$  as promoters. The size of the particles are in the range from 1.5 to 3 mm. It is classified as non-hazardous to health or to the environment. It is also not flammable. It may cause irritation in the event of inhalation, eyes/skin contact or ingestion. The catalyst should be stored in a dry, well ventilated and cool place. No decomposition will occur under normal usage and storage. The solid should be kept away from oxidizing agents and metal oxide fumes [72].

### Sulfuric acid

Sulfuric acid is a colorless, odorless and syrupy liquid. It is soluble in water and highly exothermic during mixing. It may be corrosive to metals, but it can cause severe skin burn and eye damage in case of contact. The product container should be well labeled. When the concentration of the solution is higher than 1.5 M, it should be labeled 'corrosive', while solution concentration between 0.5 M and 1.5 M are labeled 'irritant'. In the preparation of the diluted acid, it can be dangerous due to the heat release during the dilution process. To avoid splattering, the concentrated acid is usually added to water and not the other way around [6]. Do wear protective gloves / clothing / eye protection / face protection before handling. Make sure hands are washed thoroughly after handling. In case of inhalation, remove the victim to fresh air and keep him or her at rest. In case of contact, rinse cautiously with water or shower for 15 to 20 minutes. The chemical should be stored in a nonreactive material container and in a cool location with a good ventilation system and kept away from food and beverages. Some other critical data are illustrated in the table below [32].

Acute Toxicity	
Inhalation	Oral
510 $mg/m^3$ per 2 hours (LC50 Rat)	2140 mg/kg (LD50 Rat)
Ecotoxicity	
Freshwater Fish	Fish
> 500 mg/L (static)	42 mg/L (96 hours)

**Table 4.3:** Sulfuric acid toxicity [32]

### Sodium hydroxide

Sodium hydroxide is a highly caustic base and alkali that can decompose proteins at room temperature and may cause severe chemical burns. It is very soluble in water and easily absorbs moisture and carbon dioxide from the air. In case of eyes contact, it may induce permanent blindness. The protective equipment should always be used in handling the chemical or its solutions. In the event of sodium hydroxide spills to the skin or eyes, continuously wash the burning part for at least 10 to 15 minutes. Sodium hydroxide should be stored in airtight and nonreactive material containers [4].

#### 4.2.3. Materials for ammonia synthesis converter

The vessels and pipes that are in contact with hydrogen and ammonia under elevated pressure and temperature have potential risk of material deterioration [17]. There are two types of hydrogen attacks to the material. One is decarburization, another one is hydrogen embrittlement. The blistering or cracking that is caused by ammonia is called nitriding.

The commercial ammonia converters are usually operated at a temperature of max. 530 °C and at a pressure of max. 350 bar. The material of the converter should be highly resistant to both of the hydrogen and ammonia attacks since they are the main components in the reactants and the product. One of the common solutions is to use two concentric vessels. The inner shell uses stainless steel and the outer shell uses a less expensive steel since the attacks to the outer shell is much less compared to that of the inner shell.

#### Decarburization - chemical hydrogen attack

When metals are being exposed to hydrogen under high temperature and high pressure, the ability of hydrogen diffusion to the solid metal becomes severer. It reacts with the carbon, which is responsible for the strength of the material, and forms methane. Because of the higher molecular volume of methane, it cannot diffuse out of the metal. The methane gas accumulates inside the metal, which causes the increase of inner pressure of the material and generates cavities along the grain boundaries. The metal is transformed from a ductile to a brittle state. And finally, the vessel or the pipes rupture at a certain point. This risk of attack may exist at a moderate temperature (ca. 200 °C) and a hydrogen partial pressure as low as 7 bar [17].

#### Hydrogen embrittlement - physical hydrogen attack

The embrittlement may occur simultaneously with decarburization. At higher temperature, the adsorbed molecular hydrogen dissociates into atomic hydrogen, which can diffuse through the material structure. The diffused atomic hydrogen recombines to molecules inside the material structure which causes the growth of the internal stress and ultimately creates progressive deterioration of the material [17]. It is most likely to occur in welds that not received proper PWHT (Pre-weld heat treatment) [63].

### Nitriding

Nitriding is a specific problem for an ammonia converter. Under elevated temperature (above 300°C) and high pressure (varying from atmospheric to 1034 bar), in the unalloyed and low-alloy steels, ammonia in the reactor is dissociated to atomic nitrogen and penetrates the material. Once the atomic nitrogen diffuses into the metal, it reacts with the iron and forms a stable iron nitride, which may result in blisters or cracks[14].

### Damage inspection

For hydrogen damage, a reference with a thickness of 6 mm is flattened through an angle of 180°. If there is evidence of cracking, the sample of the material will break at a much lower angle. On the other hand, the ultrasonic inspection method can be applied. A piece of sample is projected through by the beam. If the metal is perfect, a distinct sharp reflection is returned from the opposite wall. If the metal has cracks, a fuzzy or scattered signal is returned[91].

For ammonia damage, the part can be inspected by its external appearance, weight and metallographical investigation. Take a perfect material as reference and compare the two parts. If the part is damaged, there should be blisters, pimples, weak/dense film of corrosion products or increased weight. Additionally, by employing the x-ray diffraction analysis, the iron nitride can be also detected[91].

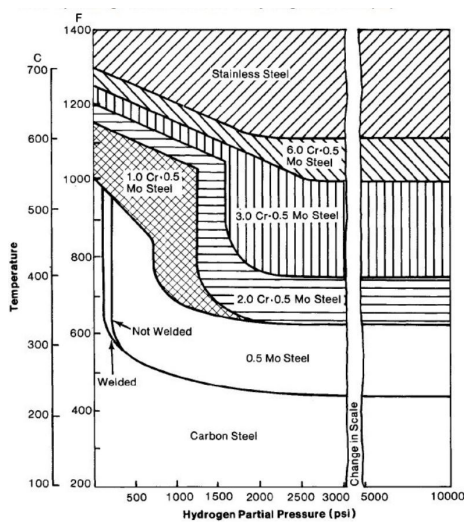


Figure 4.4: Safe operation zones for steels in hydrogen service [14]

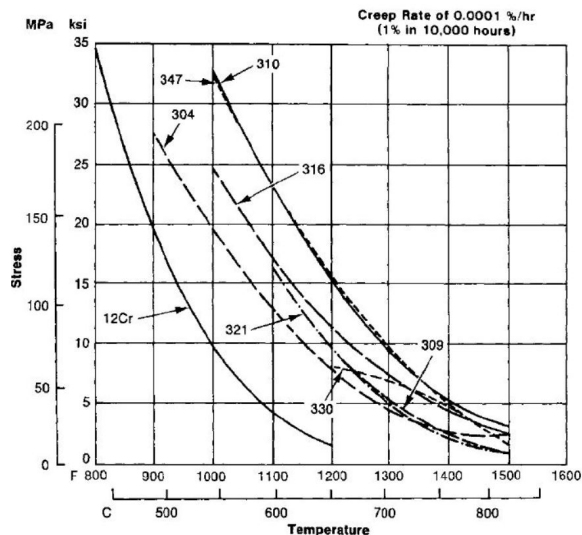


Figure 4.5: Creep rate curves for several annealed stainless steels[14]

### Overall prevention

- Adding carbide-stabilizing elements, such as manganese, chromium, tungsten, molybdenum, vanadium, titanium, and columbium. Nickel and silicon are non-carbide-forming elements. They have no effect in preventing interior damage to steels by hydrogen.
- The use of alloy steels for the vessel;
- The use of specialized design and fabrication techniques, for instant multi-wall or layer-built vessels;
- Increase of the vessel wall thickness;
- The use of superior quality welding with near complete elimination of slag inclusions and blow holes;
- Avoidance of rapid temperature fluctuations in order to keep hydrogen away from trapping within the steels;
- The use of low carbon content vessel material;
- The use of high chromium content (> 12 %) material which can prevent the selective penetration and reduce the depth of attack;

- The use of additional of tungsten;
- The use of nickel instead of iron steel since nickel nitride is unstable compared to that of iron nitride.

#### 4.2.4. HAZOP worksheets

The experiment is aimed at finding out the optimum operation condition for a small-scale ammonia reactor. A thorough risk assessment of the experimental setup supply lines, reaction vessel, analytical system and the ventilation system was summarized in the HAZOP worksheets by the team and has been approved by the research manager in the form of a complete TNO HAZOP report.

#### 4.2.5. Scenarios and risks

Before carrying out the extreme risk scenarios analysis, an overview of the setup facility data is given below.

Gas volumetric flow rate [NL/min]	2.5
Cabine volume [ $m^3$ ]	6
Fumehood suction volume [ $m^3/h$ ]	2000
Nitrogen flow rate to the oven [NL/min]	6
Mass flow controller max. flow rate [NL/min]	10
Hydrogen sensor max. allowable value [ppm]	4000 (0.4%)
Ammonia sensor max. allowable value [ppm]	25

**Table 4.4:** Setup facility data overview

##### Scenario 1: content of hydrogen release into fume hood during reaction

The reactor has a volume of 300 mL and the maximum hydrogen mole fraction inside the reactor during the reaction is 86.3%. The maximum reaction pressure is 100 bar and the maximum reaction temperature is 400 °C. In accordance to ideal gas law, we have:

$$V_{H_2, released} = 0.3L \times 0.863 \times 100 \times \frac{20 + 273.15}{400 + 273.15} = 11.3L$$

$$X_{H_2} = \frac{11.3L}{6 \times 1000L} = \frac{11.3}{6000} = 0.19\% < 0.4\% (10\%LEL)$$

Conclusion: in case of sudden release of all the gases inside the reactor, the content of hydrogen in the fume hood is far below LEL.

##### Scenario 2: content of hydrogen release into fume hood during activation process

The synthesis gas with stoichiometric ratio of hydrogen and nitrogen were used for the catalyst activation process. The operation pressure and temperature are 80 bar and 400 °C, respectively.

$$V_{H_2, released} = 0.3L \times 0.75 \times 80 \times \frac{20 + 273.15}{400 + 273.15} = 7.84L$$

$$X_{H_2} = \frac{7.84L}{6 \times 1000L} = \frac{7.84}{6000} = 0.13\% < 0.4\% (10\%LEL)$$

Conclusion: in case of sudden release of all the gases inside the reactor, the content of hydrogen in the fume hood is still less than LEL value.

##### Scenario 3: content of ammonia release into fume hood during reaction

The maximum mole fraction of ammonia during reaction at different operation conditions can be obtained from its equilibrium nitrogen conversions.

$$x_{NH_3} = \frac{e}{2 - e}$$

where e is the conversion value at equilibrium. The maximum ammonia mole fraction can be found at 100 bar and 300 °C with feed gas ratio of  $N_2 : H_2 = 1 : 5$  and a conversion value of 91.8%. Then, the content of ammonia release into the fume hood can be calculated:

$$V_{NH_3, released} = 0.3L \times 0.92 \times 100 \times \frac{20 + 273.15}{400 + 273.15} = 12L$$

$$X_{NH_3} = \frac{12L}{6 \times 1000L} = \frac{12}{6000} = 0.2\% < 15\%(\text{LEL})$$

Conclusion: in case of sudden release of all the gases inside the reactor, the content of ammonia in the fume hood is far below LEL.

#### 4.2.6. Nitrogen gas line to the oven

The single zone tube furnace has an inner diameter of 0.11 m and a height of 0.62 m. It has a volume of 6 liter. The nitrogen volumetric flow rate to the oven is set to be 6 NL/min in order to fill the oven environment completely with protective nitrogen gas.

#### 4.2.7. Ammonia absorption by sulfuric acid

As ammonia is a soft base, sulfuric acid as gas washer is used to capture the ammonia that is produced during the reaction. The neutralization reaction between ammonia and sulfuric acid is exothermic and salt is formed.



The maximum flow rate of ammonia in the outlet stream at atmospheric condition is:

$$V_{NH_3} = 0.042NL/s \times 0.92 = 0.038NL/s$$

The total amount of ammonia released after 5 hours of operation:

$$V_{NH_3,tot} = 2 \times 3600 \times 0.039 = 276NL$$

$$n_{NH_3,tot} = \frac{PV}{RT} = \frac{101325Pa \times 103.8 \times 10^{-3}m^3}{8.314J/(mol \cdot K) \times (20 + 273.15)K} = 11.5mol/2hr$$

From above data, we can compute the concentration of the sulfuric acid solution required for 10 hours of operation.

$$n_{H_2SO_4} = 0.5 \times n_{NH_3,tot} = 0.5 \times 11.7 = 5.7mol/5hr$$

$$c_{H_2SO_4} = \frac{5.7mol}{2L} = 2.8mol/L$$

### 4.3. Setup equipment and material

The reactant mixed gases  $H_2$  and  $N_2$  from 200 bar, of ultrahigh purity, were purchased from Linde Gas Benelux B.V. (Dieren, the Netherlands). The stainless steel reactor is a double-ended Swagelok sample cylinder (316L-50DF4-300). The first and the last 100 mm sections of the reactor were filled with glass wool and the iron-based catalyst was packed in the middle. The catalyst (item No.: 2510-ASFe-GPDrC-1P5KG), a commercial standard iron type, was purchased from Riogen Inc (Monmouth Junction, USA). The catalyst was pre-reduced by the supplier and stabilized with an oxygen-rich protective layer at delivery. The Carbolite oven (type: VST 12/600, England) was used to control the temperature. The inlet and outlet gas temperatures were measured by using K-type thermocouples (Type: 405-053, TC Direct, the Netherlands).

The flow rate of the system was controlled by Bronkhorst F-231M mass flow controller (model key: F-231M-RAD-22-L) with E-8501-R-10 control unit. The reactor back pressure was regulated by an Equilibar precision back pressure regulator valve (item code: H3P2SNN8-NSBP3000T300S5LLB-G) in combination with a Bronkhorst pressure control unit (item code: P-822CV-M40A-RAD-22-W). The experiments were carried out in batches at different reaction conditions. A WIKA pressure sensor recorded the pressure data during the experiment which was used for analysis. The maximum allowable operation conditions of each component are listed in table ??.

Component	Max. operation temperature ( $^{\circ}\text{C}$ )	Max. operation pressure (bar)
Reactor	454	181
Needle valves	232	236
Tubing	537	392
Pressure relief valve	148	321
Couplings	537	551
Mass flow controller	20	200
Back pressure regulator	300	206
Tube oven	1200	1
Thermocouples	1100	-

**Table 4.5:** Maximum operation values of the components

Graphite thread sealant paste (APSO parts, Germany) is applied to the thread connections of the setup. The paste is made to seal small diameters (less than 2 inch) and used in critical service applications to 635  $^{\circ}\text{C}$  and 160 bar.

#### 4.4. Setup assembly

The parts were purchased in June and the assembly of the experimental setup was completed in mid of September 2019.



**Figure 4.6:** Setup before experiment

## 4.5. Testing procedure

Fresh catalyst was added to the reactor and then the reactor was sealed. After every test, the catalyst was always kept under nitrogen or synthesis gas environment.

### 4.5.1. Leak test

To start up the reactor, a successful leak test needs to be accomplished. The forming gas (hydrogen as tracer gas - 5% and nitrogen as solvent gas -95%) was used as testing flow. A hydrogen sniffer was used to detect leakage along the process lines and the connections of the apparatus. The pressure data was record for observing possible pressure decay in the system during the leak test. The procedure of the test is as follows:

1. Feed the system with the forming gas and slowly elevate the pressure to 25 bar at room temperature. Then stop the flow once the system reaches the desired pressure. Record the pressure data for 20 min. Timely check if there is any leakage in the setup;
2. Depressurize the system to 1 bar. Slowly increase the temperature of the reactor to 400°C. During the heating, the gases expand and the back pressure regulator responds correspondingly to the system to make sure that the reactor is at the set pressure point. Once it reaches the desired temperature, keep the system at this condition for another 20 min and record the pressure data.
3. Next, gently rise the pressure to 125 bar by feeding the forming gas to the reactor. Then, stop the flow and leave the closed system for 1 extra hour and timely check if any leakage occurs;
4. In case of leakage detection, depressurize the system and then cool down the reactor to room temperature. Hereafter, fix the leakage section and restart the leak test from step 1;
5. Once the leak test is completed, reduce the pressure and then increase the temperature to the subsequent catalyst activation operation condition.

### 4.5.2. Catalyst activation

The employed catalyst is a standard commercial iron based catalyst, which consists of Fe and CaO,  $K_2O$ ,  $Al_2O_3$  as promoters. In order to remove the oxidized protective layer around the catalyst particles and activate the catalyst before reaction, an activation process needs to be followed. A stoichiometric ratio of nitrogen and hydrogen were fed to the reactor. The operation pressure of this process was constant at 80 bar and temperature was 400°C. The volumetric flow rate of the mixed gas to the reactor was 2.5 NL/min. Activation procedure:

1. Slowly heat up the reactor filled with synthesis gas to 400°C overnight;
2. Start the flow and gradually pressurize the system to 80 bar;
3. Once it reaches the objected set points, keep the flow running at the operation conditions for 24 hours;
4. In the event of accomplishment of the activation process, adjust the temperature and pressure to the next reaction condition or keep the catalyst under nitrogen/synthesis gas environment.

### 4.5.3. Haber-Bosch ammonia synthesis reaction laboratory experiments

Groups of parameters were chosen from the modeling results to see the feasibility of the concept and the optimum results under the achievable conditions. The testing parameters that were used during the experiments were:

$N_2 : H_2$ gas ratio	Temperature [°C]	Pressure [bar]
1 : 3	400	50, 75, 100
1 : 5	400	50, 75, 100

**Table 4.6:** Testing parameters

### Ammonia production test

To perform the experiment, the following steps were followed:

1. Prepare two bottles of 2 M sulfuric acid solution and take the reference of the solution before starting the experiment;
2. Feed the system with reactant gases and then slowly heat up the reactor;
3. After attaining the desired temperature, gradually increase the pressure of the system;
4. Once the operation conditions are gained, keep the flow running for about 30 min until the system is stabilized;
5. Open valve BV-5, lead the outlet flow to the sulfuric acid bottles and start capturing the produced ammonia;
6. Run the test for 2 hours, then switch off valve BV-5 and open valve BV-6;
7. Remove the sulfuric acid bottles from the setup, and take samples for titration analysis.
8. Once the experiment is finished, stop the flow and reduce the system pressure to about 1.5 bar. Keep the catalyst under this condition overnight till next day's experiment.

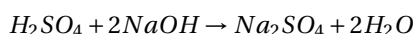
### Pressure decay test

The pressure decay test was performed right after the ammonia production test. The testing steps are given below:

1. Stop the synthesis gas flow and close valves BV-5 and BV-6;
2. Record the pressure data of the closed system for 7 hours;
3. Release the pressure to about 1.5 bar and flush the system with fresh synthesis gas for 5 min, stop the flow then keep the apparatus under the same condition overnight for next day's testing.

### Titration analysis

To measure the amount of sulfuric acid that has reacted with ammonia, the titration method is applied to determine the amount of ammonia that was produced by the Haber-Bosch reaction. Since sulfuric acid is diprotic, a titration curve with two plateaux and two end points could be expected. The simple neutralization reaction with sodium hydroxide is:



5 mL of the sulfuric acid reference and sample volume were taken from the sample bottles. 0.1 M of sodium hydroxide solution was prepared for the titration. The diluted base solution was titrated with sulfuric acid solution till the second color change.



**Figure 4.7:** Sulfuric acid bottles used during the experiments

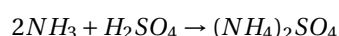
# 5

## Reactor Design Validation

In this chapter, the performance of the laboratory reactor is presented and discussed. Comparisons are made between the experimental data and the modelling outcomes. The first research question is addressed and evaluated here. In the final section of this chapter, the combined experimental and modeling results are examined with the literature data.

### 5.1. Ammonia production test results

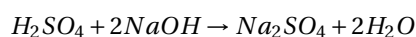
Ammonia from the reactor was captured by the sulfuric acid solution and formed ammonium sulfate.



Titration method was used to determine the amount of sulfuric acid that reacted with ammonia. Sodium hydroxide with known concentration was used as a reagent in the titration. The two stages reaction between the acid and the base are as follows:



Net reaction (1) + (2):



The mole of sodium hydroxide used to reach the second equivalence point in the titration can be calculated from below equations. Here, letter A and B denote 'Acid ( $H_2SO_4$ )' and 'Base ( $NaOH$ )' respectively.  $c_{Bref}$  equals to 0.1 M. The volume of the acid in titration was 0.5 mL and the total volume of the acid is 900 mL. The mass of the catalyst in the experiment was 300 g.

$$n_B = c_{Bref} \times V_{Badded}, \quad c_{Aref} = n_{Bref} / 2V_A$$

The mole of acid that reacted with the base:

$$n_A = n_B / 2$$

Accordingly, the mole difference between the sample sulfuric acid and the reference sulfuric acid can be computed, from which the amount of ammonia that has been captured by the solution is obtained.

$$\Delta n_A = n_{Aref} - n_{Asample}, \quad n_{NH_3} = 2\Delta n_A \times 1800$$

After that, the space time yield of the reaction can be calculated by taking the ammonia flow rate per hour and dividing it by the total mass of catalyst inside the reactor. The percent yield is the percentage ratio of the actual experimental yield to the theoretical yield. The results of the calculations are shown below,

$N_2 : H_2 = 1 : 3$ at $400^\circ C$					
Sample No.	P [bar]	Duration [h]	$n_{H_2SO_4}$ [mol]	$n_{NH_3}$ [mol]	Percent yield
Sample 1	50	2	0.13941	0.27882	4.8%
Sample 2	50	2	0.19386	0.38772	6.6%
Sample 3	50	2	0.20106	0.40212	6.8%
Sample 1	75	2	0.16263	0.32526	5.5%
Sample 1	100	2	0.25794	0.51588	9%
Sample 2	100	2	0.45261	0.90522	15.4%

**Table 5.1:** Titration test with  $N_2 : H_2 = 1 : 3$

As table 5.1 shows, with higher operation pressure, greater ammonia yield can be achieved. At pressure of 100 bar, the percent yield of the second sample is in the range of the industrial level (15%). For feed gas ratio ( $N_2 : H_2 = 1 : 5$ ), the titration results are displayed in table 5.2.

$N_2 : H_2 = 1 : 5$ at $400^\circ C$					
Sample No.	P [bar]	Duration [h]	$n_{H_2SO_4}$ [mol]	$n_{NH_3}$ [mol]	Percent yield
Sample 1	50	2	0.03069	0.06138	1.3%
Sample 1	75	2	0.21735	0.4347	8.2%
Sample 1	100	2	0.30501	0.61002	12%

**Table 5.2:** Titration test with  $N_2 : H_2 = 1 : 5$

The relation between space time yield of sample 1 and operation pressure under different feed gas ratio is illustrated in the graph 5.1. Where the horizontal axial is the testing pressure and the vertical axial is the space time yield value with unit  $g_{NH_3}/h/g_{cat}$ .

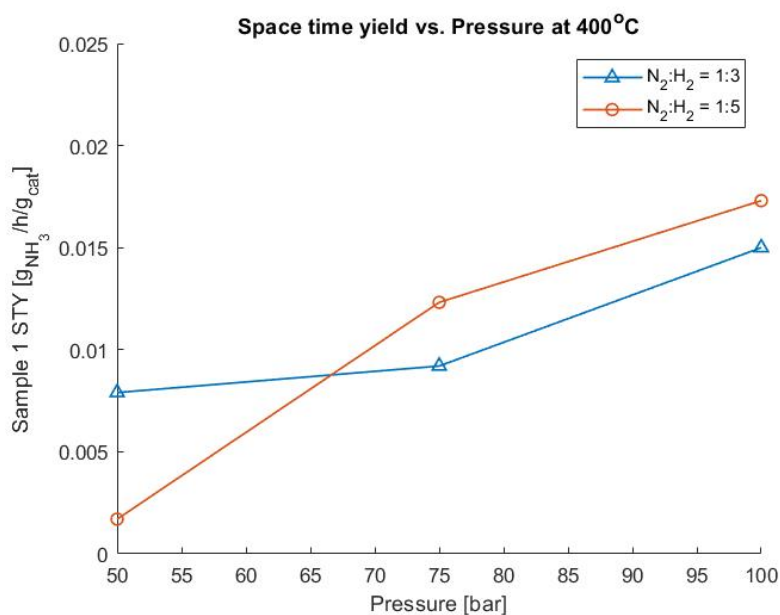


**Figure 5.1:** Space time yield versus pressure

As observed from figure 5.1, the extra hydrogen partial pressure in the feed gas can increase the yield of ammonia at the same temperature and pressure conditions. For instance, the ammonia produced at 1 : 5 feed gas ratio at 75 bar is 1.35 times more than that of at stoichiometric feed gas ratio. The same conclusion can be drawn for operation at 100 bar. However, the results at 50 bar are relatively low. In section 3 of this chapter, it can be seen that the performance of the catalyst is better after 14 days of testing and sample 1 for 50 bar 1 : 5 gas ratio was performed on the last day. Hence, the titration results appeared to be falling and

should be retested. The expected value shall be slightly larger than that of sample 1 for 50 bar 1 : 3 space time yield result.

## 5.2. Pressure decay test results

### 5.2.1. The stabilized pressure in a small-scale ammonia reactor

The testing parameters stated in chapter 4 have been experimentally conducted in the closed ammonia synthesis reactor system. The pressure was recorded during the test. In a certain period of time, a stabilized pressure value was obtained. These values were compared with the theoretical equilibrium pressure data in order to investigate if the reaction has reached equilibrium stage.

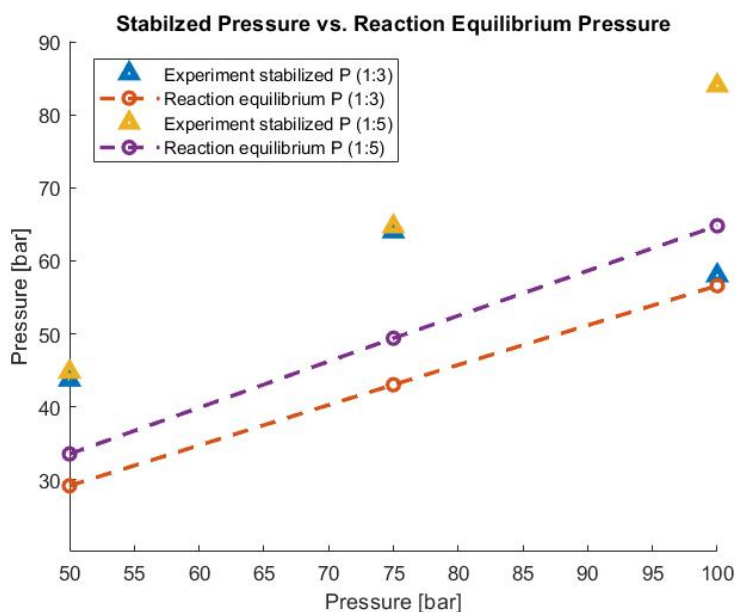


Figure 5.2: Pressure decay to stabilized pressures

During the ammonia synthesis reaction, ammonia content grows from zero and progressively extend to a saturated value where the maximum extend of the reaction is reached. Because of the reduction of the total amount of molecules, four molecules reduce to two molecules, in the closed volume, the total pressure of the system declined. At the saturation point, the pressure became stable which was also the conclusion while studying the reaction behavior after a maximum of 69 testing hours. A table with testing durations is listed below.

Initial Total Pressure [bar]	Feed gas ratio	Duration [hour]	Feed gas ratio	Duration [hour]
50		8		17
75	1 : 3	20	1 : 5	20
100		69		20

Table 5.3: Pressure decay tests duration

The equilibrium pressures were calculated from the chapter 3 reaction modelling section. As figure 5.2 shows, after about 3 days of testing for 100 bar  $P_{total}$  initial condition with stoichiometric gas ratio, the total pressure of the system was stabilizing at a value of 58 bar which is very close to its equilibrium point at the same reaction conditions. However, the rest of the testing points were far away from its equilibrium since the testing duration was too short.

For the initial total system pressure test of 75 bar, after 20 hours of decay tests, the pressures coincided. But the pressure decay rate of the stoichiometric reaction was higher than the 1 : 5 gas ratio. The reason could be that with higher hydrogen content in the same size closed volume, there was less nitrogen inside the reactor for

ammonia formation, correspondingly, less reduction of total molecules. In other words, the stoichiometric system is able to reach the same pressure at a much shorter time.

### 5.2.2. Effect of initial pressure, feed gas ratio and temperature to the reaction

Three pressures and two feed gas ratios are plotted in the same graph, which enable us to study the impact of those parameters directly by comparison.

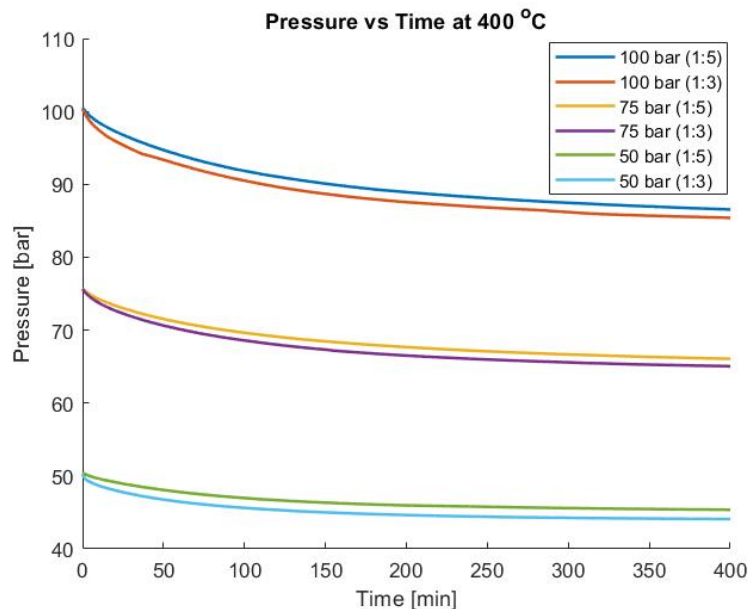


Figure 5.3: Pressure vs. time under various feed gas ratios

#### (1) Effect of initial pressure

From the slopes of the curves in the first 50 min, it can be observed that the reaction rate is much faster in 100 bar than 75 and 50 bar. The consumption speed of nitrogen and hydrogen gas inside the reactor to form ammonia is steeper in the 100 bar system. Because the reactor is small, the total amount of ammonia formed inside the reactor is limited by the total feed gas volume. Besides, it is also hindered by the type of catalyst used for the reaction. In accordance to the research (chapter 2), the iron base catalyst favors higher pressure and high temperature, which can be inspected from the overall trend of the curves.

#### (2) Effect of feed gas ratio

The pressure decay test is different from the ammonia production test. It is constrained in reaction space. No flow ran through the reactor and the only reactants for making ammonia was the original feed gas. Therefore, the predominant parameter here is the nitrogen partial pressure rather than hydrogen partial pressure. As noted from figure ??, the stoichiometric gas ratio produced more ammonia than that of the feed gas ratio with higher hydrogen content. The larger initial partial pressure of hydrogen made the system filled mostly with hydrogen and a scarcely amount of nitrogen that could be converted to ammonia. These results are in contradicting with the ammonia production test.

#### (3) Effect of the temperature

Based on the results from previous sections, the optimal operating condition for a small-scale ammonia synthesis reactor is 400 °C and 100 bar. However, the effect of temperature to the reaction still needs to be discussed. Two sets of tests were performed for this purpose. The first test was to start the pressure decay test at 400 °C and 100 bar. The second one was to conduct the test at a lower temperature of 350 °C and at the same pressure. The recorded pressure in 400 minutes are indicated in figure 5.4.

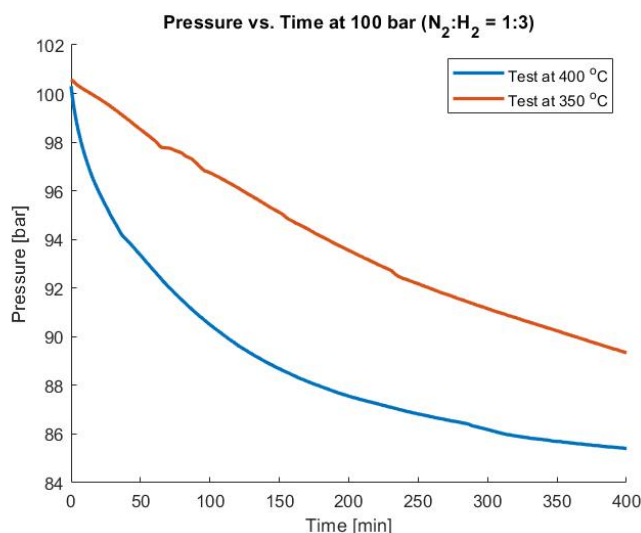


Figure 5.4: Tests performed at 100 bar 400°C and 350°C

The results reveal that the small-scale ammonia synthesis reactor has a higher reaction rate when it is operating at a higher temperature. This is consistent with the research conclusion stated in chapter 2 that the magnetite-based fused iron catalyst with small amount of promoters favors high pressure (100 to 300 bar) and high temperature (400 to 500 °C) due to the thermodynamic limitations.

### 5.2.3. Catalyst performance

In this subsection, the performance of the employed iron based catalyst is studied. The experimental results of the same tests were reviewed after 9 days and 14 days of testing in order to monitor if the results of the same test can be reproduced. Two sets of tests were chosen. One is the 100 bar (1 : 3), another one is the 50 bar test (1 : 3). The comparison results of test 1 for a 9 days catalyst performance is shown in figure 5.5. The performance of the iron based catalyst after 14 days of testing is shown in figure 5.6.

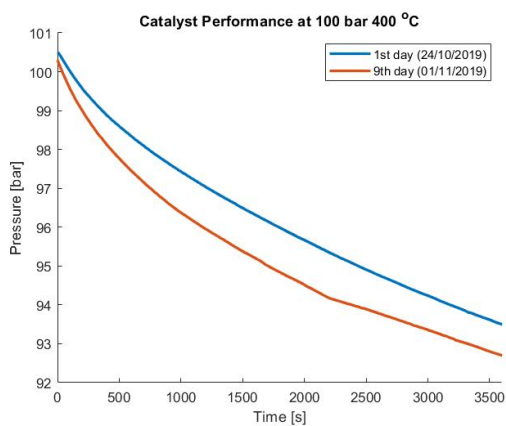


Figure 5.5: Catalyst performance after 9 days

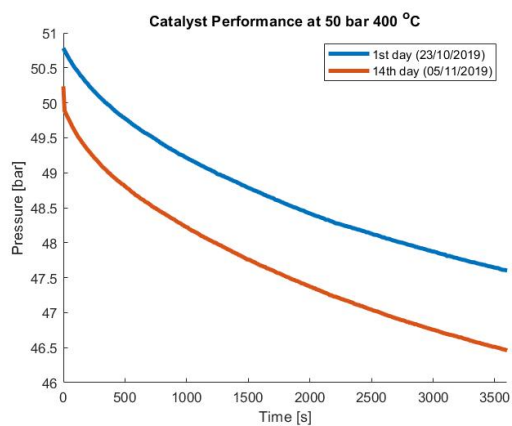


Figure 5.6: Catalyst performance after 14 days

The above figures demonstrate that the expanded time of testing improved the performance of the catalyst. The exact result of the same test cannot be obtained, but better outcomes were achieved in the later tests (red lines).

The same sets of parameters were chosen from the ammonia production test. The ammonia mole flow rate in 2 hours of reaction is plotted in the same graph for both pressure conditions. As observed from figure 5.7, the test that was performed later for both of the pressure conditions has more ammonia produced during the reaction than that of the test on the first day.

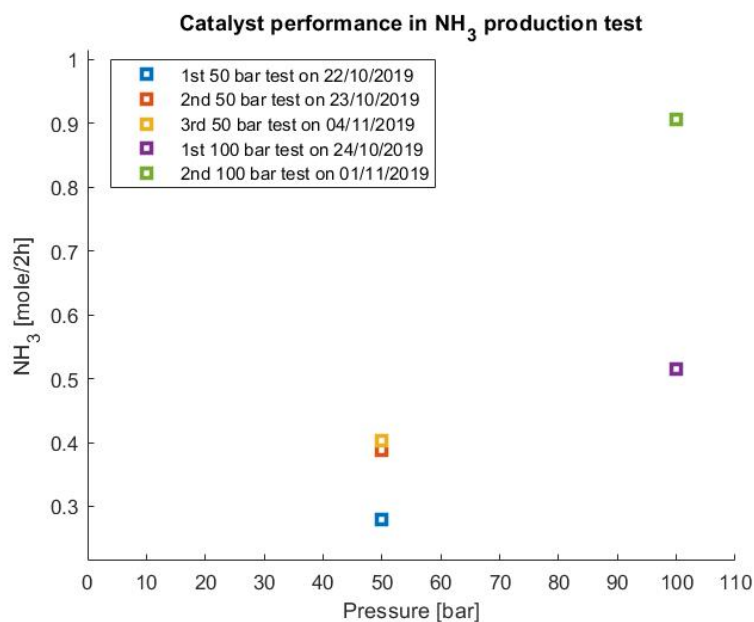
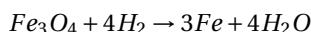


Figure 5.7: Catalyst performance during the ammonia production test

The total mass of the catalyst has changed after one month of testing. Before the experiment, the catalyst weight was 300 g in total. However, after the experiment, there was only 285 g left. One main reason for the weight loss is the activation process. During the activation, water is generated by the chemical reaction between iron oxide layer and hydrogen.



The presence of water increases the average pore diameter and decreases the activity of the catalyst. The activity of the catalyst increases with increasing space velocity during reduction [65]. The applied catalyst is prerduced for this experiment, so the only part that generates water is the surface oxide. According to the catalyst supplier, water generation for pre-reduced catalyst is about 3 -5 wt% during the activation process, which is consistent with the mass results we have (5% wt). The harmfulness of water to the catalyst depends on the reaction condition. For a sufficiently low concentration of water, the effect on the synthesis is negligible [65].

#### 5.2.4. Initial rate determination from the experiments

The results from pressure decay tests can be used for measuring the reaction rate. In the pressure vs. time graph, the rate of the reaction can be determined by measuring the slope of the graph. The steeper the slope, the faster the reaction rate. Because the most important rate section is at the beginning of the reaction, firstly the initial rate constants from the experimental results will be discussed below .

As the reaction carried out, the total pressure of the system changed. During the test, some of the parameters stayed constant, such as the reactor volume and the reaction temperature. The pressure and time during the test were recorded. Then a 'log graph' was plotted to determine the order of the reaction. The basic equation of the graph is the following:

$$\text{Rate} \propto [A]^n$$

$$\log(\text{Rate}) \propto n \log[A]$$

The slope of the straight line in the 'log graph' is equal to the order of the reaction. The first 1 hour of the reaction is selected for this analysis. The initial composition of the gas and the reactor volume are known, from which the concentration of ammonia and nitrogen can be derived by using following equations.

$$P_{NH_3,i} = P_o - P_i$$

where  $i$  denotes the time step,  $P_i$  is the total pressure at time step  $i$  and  $P_{NH_3,i}$  is the partial pressure of ammonia. The concentration value of each component can be derived from the ideal gas law, which is:

$$PV = nRT, \quad n = \frac{PV}{RT}$$

In accordance to the stoichiometric ratio between the reactants and the product, the relation among the concentrations are as follows:

$$n_{N_2,i} = n_{N_2,o} - 0.5n_{NH_3,i}, \quad n_{H_2,i} = n_{H_2,o} - 1.5n_{NH_3,i}$$

The initial feed gas ratio in the closed system is also known. The mole fraction of each component at time step  $i$  is as below equation:

$$x_{N_2,i} = \frac{P_{N_2,o} - 0.5P_{NH_3,i}}{P_i}, \quad x_{H_2,i} = \frac{P_{H_2,o} - 1.5P_{NH_3,i}}{P_i}, \quad x_{NH_3,i} = \frac{P_{NH_3,i}}{P_i}$$

From the experimental results, the 'log graph' for ammonia can be obtained.

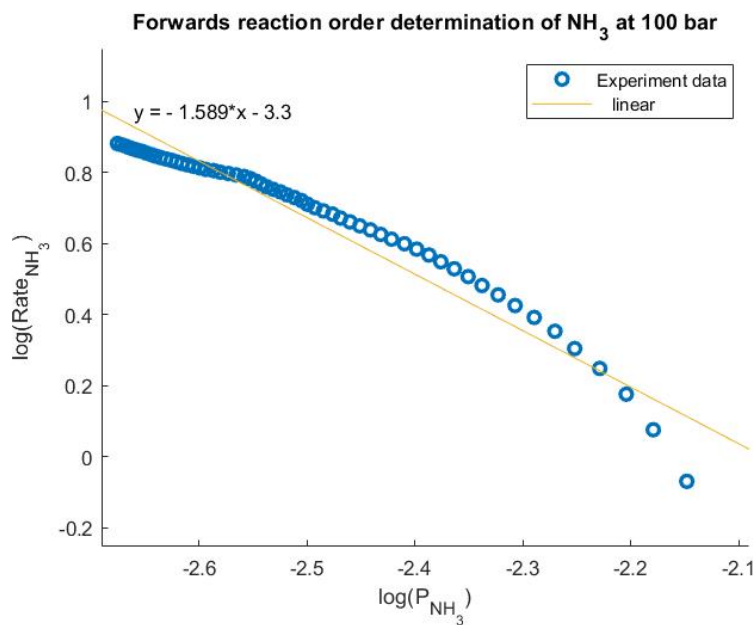


**Figure 5.8:** Reaction order determination

M. Boudart [23] had derived the reaction function of forwards ammonia synthesis. The exponent for ammonia in their forwards reaction is  $-1.5$  which is nearly equal to the one figure 5.8 obtained with a linearized slope value of  $-1.6$ .

Reaction	Rate function
$N_2 + 3H_2 \leftrightarrow 2NH_3$ (catalytic)	$k(N_2)(H_2)^{2.25}(NH_3)^{-1.5}$

**Table 5.4:** Ammonia synthesis forwards reaction order [23]

For simplification, the rate function in table 5.4 is used for the reaction rate constant calculation. Since nitrogen dissociation and chemi-absorption are the rate determined steps and the reaction order for nitrogen is 1 which is easier for the computation. The equilibrium rate constant  $k_p$  can be calculated from Gillespie and Beattie correlation 3.11.

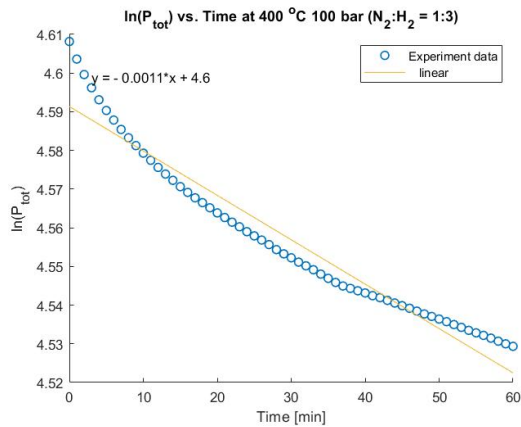


**Figure 5.9:** Reaction rate constant determination at 400°C 100 bar

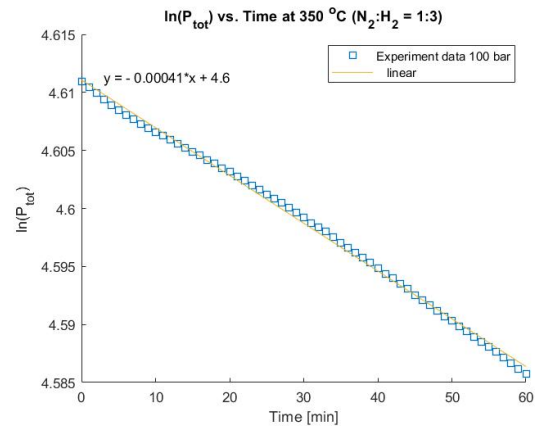


**Figure 5.10:** Reaction rate constant determination at 350°C 100 bar

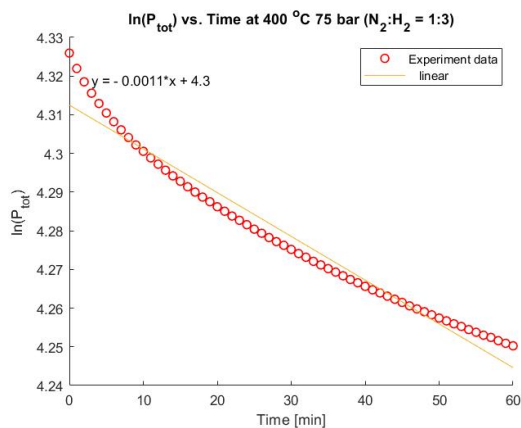


**Figure 5.11:** Reaction rate constant determination at 400°C 75 bar

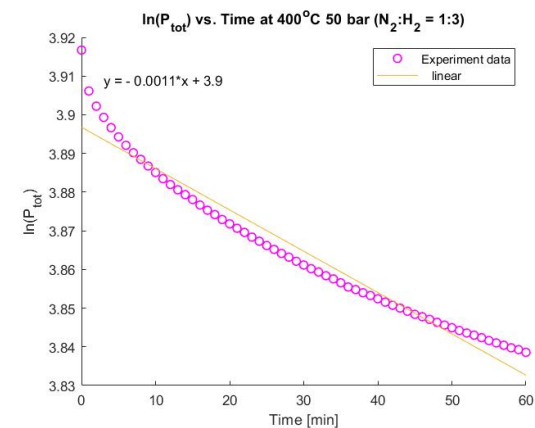


**Figure 5.12:** Reaction rate constant determination at 400°C 50 bar

The slope of the pressure versus time profiles represent the forwards rate constants of ammonia reaction at each operating condition with stoichiometric feed gas ratio. The rate of the reaction is much faster at 400°C then 350°C. The operation pressure can affect the reaction kinetics, but to a lesser degree than the temperature does. The data of the forwards and backwards rate constants from experiment results under various operation conditions are listed in table 5.5 and are compared to the values that were used during reaction modelling (chapter 3).

	$k_f$ [ $kmol \cdot /m^3 \cdot h \cdot bar^{-1.5}$ ]	$k_b$ [ $kmol \cdot bar^{0.5} / m^3 \cdot h$ ]
Modelling value used at 400°C [20]	0.0032	10.48
Experiment result at 100 bar	0.0011	6.13
Experiment result at 75 bar	0.0011	6.13
Experiment result at 50 bar	0.0011	6.13
Modelling value used at 350°C [20]	0.00091	0.61
Experiment result at 100 bar	0.00041	0.52

**Table 5.5:** The kinetics forwards an backwards rate constant values with  $N_2 : H_2 = 1 : 3$

Furthermore, the obtained experimental results shall be determined if they are consistent with the literature [20] [55] [51]. The reverse reaction rate constants are chosen for this purpose, since most of the previous literature on catalytic ammonia illustrated the value with reverse rate constants. The reverse rate constant increases with temperature, but slightly decreases with pressure.

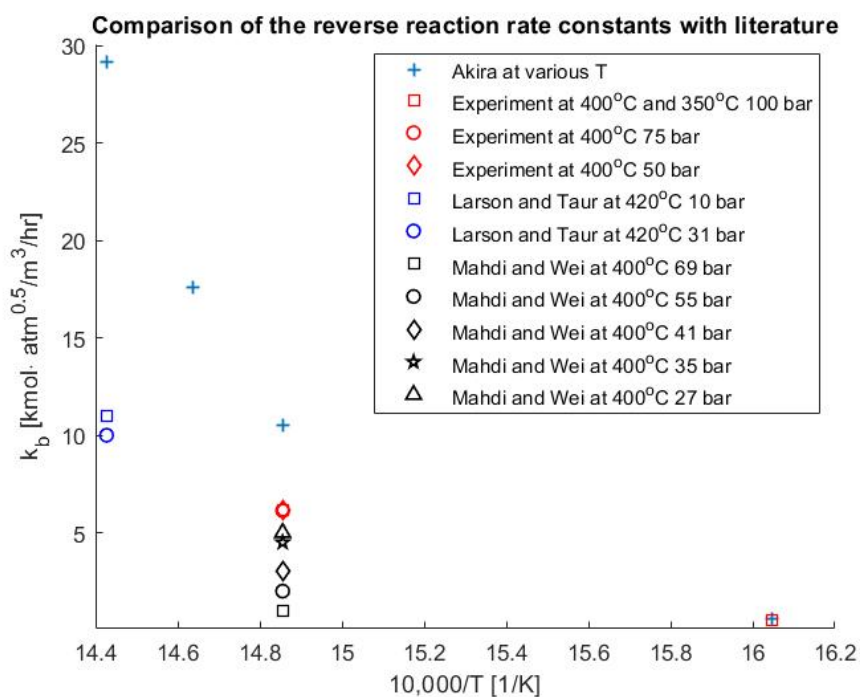


**Figure 5.13:** Reaction backwards rate constants comparison with literature

The deviation between the data of this work and the literature data could be due to the experimental error in operation timing and the temperature variation along the reactor. The results show that temperature plays a much more critical role in ammonia synthesis reaction kinetics than reaction pressure.

### 5.3. Fixed bed pressure drop validation

The laboratory small-scale ammonia synthesis reactor has a bed length of 15 cm and an inner diameter of 3.6 cm. Before the reaction, the catalyst particle size is ranged from 1.5 mm to 3 mm (figure:5.14). Here the mean value of 2 mm is taken for pre-experiment calculation. After a month of testing, the size of the catalyst particle reduced (figure: 5.15). It has a smaller average diameter of 1 mm. As chapter 3 stated, the decrease of catalyst particle size can significantly change the pressure drop across the reactor bed. The Ergun equation 3.20 [87] is employed to validate the pressure drop difference before and after the experiment.



**Figure 5.14:** Fresh catalyst before the experiment



**Figure 5.15:** Catalyst after weeks of experiments

The results of the pressure drop calculation are shown in the figures below:

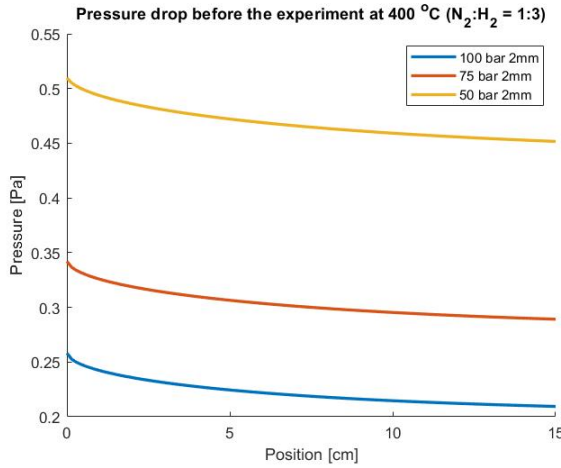


**Figure 5.16:** Fixed bed pressure before the experiment ( $N_2 : H_2 = 1 : 3$ ,  $d_p = 2$  mm)

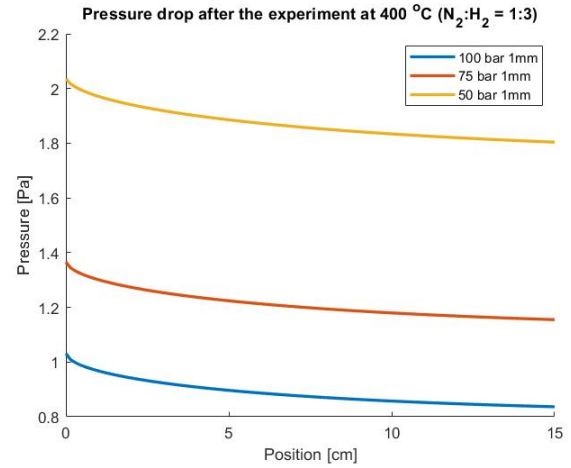


**Figure 5.17:** Fixed bed pressure after the experiment ( $N_2 : H_2 = 1 : 3$ ,  $d_p = 1$  mm)

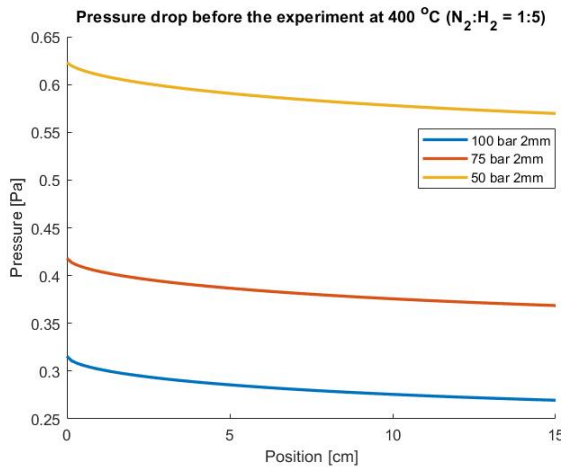


**Figure 5.18:** Fixed bed pressure before the experiment ( $N_2 : H_2 = 1 : 5$ ,  $d_p = 2$  mm)

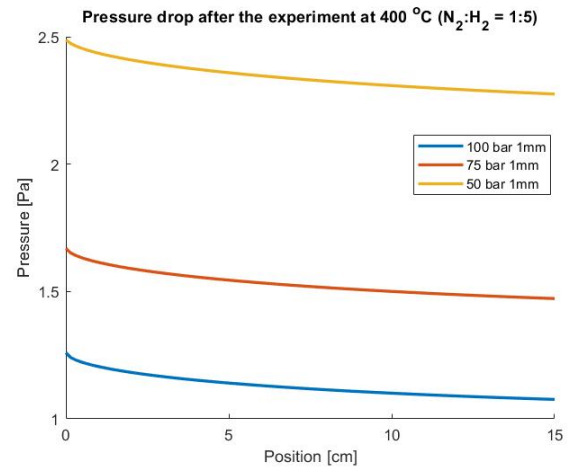


**Figure 5.19:** Fixed bed pressure after the experiment ( $N_2 : H_2 = 1 : 5$ ,  $d_p = 1$  mm)

The fixed bed pressure drop after one month of testing increased as a result of the catalyst particle size reduction. The small escalation in pressure drop can aid the auto-thermal circulation in the proposed small-scale ammonia synthesis reactor.

## 5.4. The experimental results comparison

The pressure decay test was performed right after the ammonia production test at the identical operation conditions. The main difference between the two tests is that ammonia production test has continued flow fed through the reactor. The results of the ammonia space time yield in the first two hours time should be coincident with each other. The space time yield from the pressure decay test can be determined using the equations mentioned in the subsection 5.2.4..

$$PV = nRT$$

$$n_0 = \frac{P_0 V}{RT_0}, \quad n_1 = \frac{P_1 V}{RT_1}, \quad \frac{n_0}{n_1} = \frac{P_0 V_0 T_1}{P_1 V_1 T_0} = \frac{P_0}{P_1}$$

where the unit of pressure is bar, temperature is K. The value of the gas constant is  $8.314 \times 10^{-2} [L \cdot \text{bar} / K / \text{mol}]$ .

	$N_2$	$H_2$	$NH_3$
Stoichiometric ratio	1	3	2
Initial mole ( $n_0$ )	$0.25n_0$	$0.75n_0$	0
Reacted mole	$x$	$3x$	$2x$
Remaining mole ( $n_1$ )	$0.25n_0 - x$	$0.75n_0 - 3x$	$2x$
$n_{NH_3}$		$n_0 - n_1$	

The space yield time value equals to:

$$SYT = \frac{n_{NH_3} * M_{NH_3}}{t * m_{catalyst}}$$

where  $t$  is time in hour,  $M_{NH_3}$  is the ammonia molar weight [g/mol] and  $m_{catalyst}$  is the total weight of catalyst in gram. The pressure difference in the first PD test hour is used to calculate the space time yield of the reaction. The results are illustrated in figures 5.20 and 5.21.

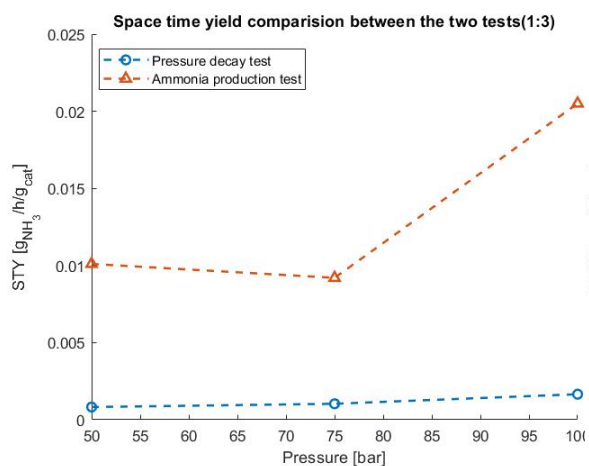


Figure 5.20: Space-time yield vs. pressure with  $N_2 : H_2 = 1 : 3$

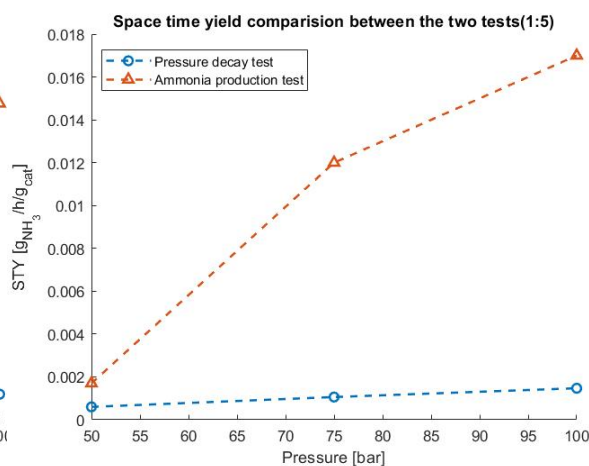


Figure 5.21: Space-time yield vs. pressure with  $N_2 : H_2 = 1 : 5$

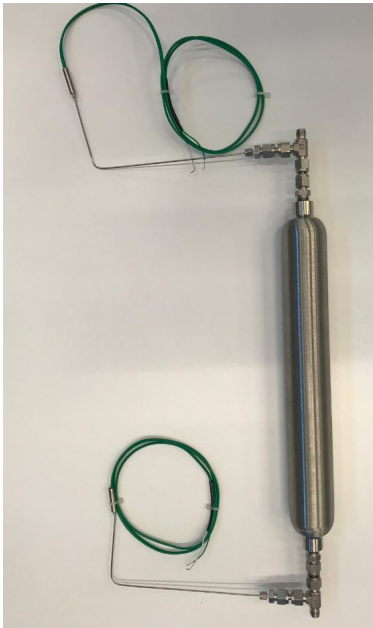
The mean space time yield values are distinguish between the two tests. The value in ammonia production test is much higher than those of the pressure decay test. The first reason could be that the space time yield of ammonia production test is an average value in 2 hours, while the data of pressure decay test is based on the first hour reaction. Secondly, during the ammonia production test reactant gases were fed continually to the reactor. There was sufficient nitrogen source for ammonia formation and the reaction pressure was kept at the target isobar operation conditions. However, in the pressure decay test, reactant gases were limited by the feed gas ratio and the initial total pressure of the system. Once the reaction started and ammonia was formed, the total pressure of the system declined, which had significant impact on the reaction kinetics. Hereafter are some of the photos that were taken before and after the experiments.



Figure 5.22: Catalyst weight loss



Figure 5.23: Reactor cross section cut after experiment



**Figure 5.24:** Reactor before the experiment



**Figure 5.25:** Reactor after weeks of experiments

# 6

## Micro-Ammonia Plant Techno-Economic Analysis

In this chapter, the techno-economic analysis is carried out in order to assess if a micro green ammonia synthesis plant concept is profitable and if it has a compatible market compared to that of current existing industrial scale ammonia plants. The green ammonia micro-plant is a fully automated production plant. It is modular, air to ammonia, and using renewable energy only. The nitrogen source is captured from the air. The hydrogen is obtained from water electrolysis. Ammonia is formed by nitrogen and hydrogen via Haber-Bosch process<sup>1</sup>.

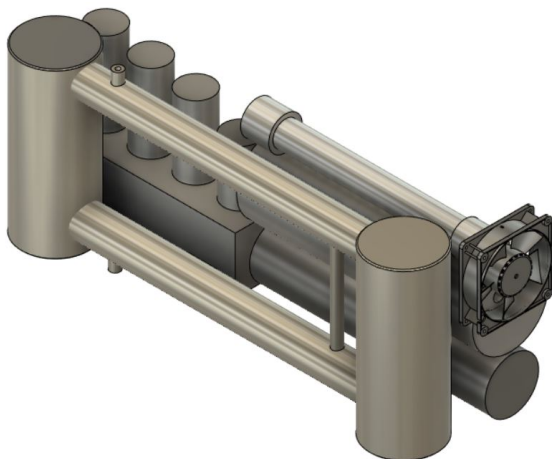


**Figure 6.1:** Ammonia micro-plant<sup>1</sup>: 350 g/day



**Figure 6.2:** Ammonia mini-plant: 65 kg/day [70]

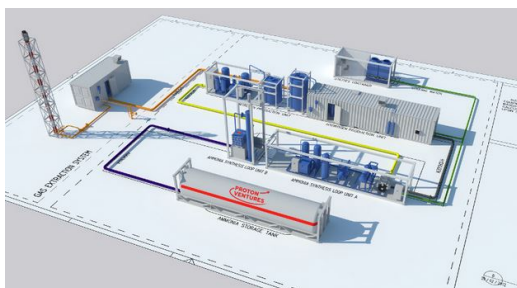


**Figure 6.3:** Ammonia pilot plant: 10 tons/day[68]



**Figure 6.4:** Ammonia industrial plant: 3300 tons/day[84]

<sup>1</sup>The drawing of the micro-plant (figure 6.1) is for illustration purpose only. The actual products of the compressor (ZEF B.V.), alkaline electrolysis cell (ZEF B.V.) and hydrogen buffer (ZEF B.V.) may vary due to product design and enhancement.

## 6.1. Methodology

The two optimal reactor design results from chapter 3 are adopted to the techno-economic analysis. Namely, a micro plant, including all the other subsystems, operates at 100 bar 400 °C and a micro-ammonia plant that runs at 50 bar 400 °C. A mass and energy balance is derived for both cases, from which the CAPEX and OPEX can be estimated. A sensitivity analysis is performed for both cases, and then the most economically profitable case is selected.

## 6.2. Micro-ammonia plant energy and mass balance

### 6.2.1. Energy balance

The energy balance for ammonia used directly as fuel can be illustrated in following tables. The lower heating value of ammonia as combustion fuel is 18.6 MJ/kg. Based on the production of the reactor system and the total required energy of the micro-plant, the energy efficiency of the complete system can be computed. The power of the equipment was taken from vendor specifications or advice. The reactor in the current model is assumed fully insulated during the production.

Ammonia	
LHV [kJ/kg]	18600
$NH_3$ production [g/h]	50
Power [W]	258
Equipment required power	
Electrolysis cell power [W]	750
Membrane separator power [W]	60
Compressor power [W]	40
Heater power [W]	15
Pump power [W]	0.05
Total plant required energy [W]	865
Efficiency	30%

**Table 6.1:** 50 bar micro-ammonia plant energy balance

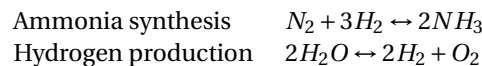
Ammonia	
LHV [kJ/kg]	18600
$NH_3$ production [g/h]	50
Power [W]	258
Equipment required power	
Electrolysis cell power [W]	750
Membrane separator power [W]	60
Compressor power [W]	100
Heater power [W]	6
Pump power [W]	0.04
Total plant required energy [W]	916
Efficiency	28%

**Table 6.2:** 100 bar micro-ammonia plant energy balance

In order to generate sufficient energy for the micro-plant, a minimum quantity of four 300 W off grid solar panels are required for operating a micro-ammonia plant. The total amount of sun hour is 7 in this calculation.

### 6.2.2. Mass balance

In accordance to the model in chapter 3, the daily production of the reactor system is 350 g  $NH_3$ /day. The mass balance can be derived from the chemical reactions.



Given that all the other subsystems have an efficiency of 70%, the mass of reactants, product and raw materials can be computed.

$N_2$ [g/day]	$H_2$ [g/day]	$NH_3$ [g/day]	Air [l/day]	Actual air [l/day]	$H_2O$ [g/day]	Actual $H_2O$ [g/day]
288	62	350	317	453	556	794

**Table 6.3:** Micro-ammonia plant mass balance

### 6.3. Capital cost

The fixed capital cost investment consists of the total cost of designing, constructing, plant installation and the associated modifications needed for the plant site preparation.

$$\text{Fixed capital investment} = \text{ISBL} + \text{offsite/OSBL} + \text{Engineering \& construction} + \text{Contingency} \quad (6.1)$$

The first step for a process capital cost estimation is the selection of construction materials. This can significantly influence the total cost of a process plant. There are many factors that need to be taken into account when selecting an engineering material, such as high temperature strength, corrosion resistance, ease of fabrication, availability in standard sizes, lowest cost over plant working life and so on.

Due to the gas composition in combination with high pressure and high temperature, a high reliability material is required for an ammonia synthesis converter. As chapter 4 stated, the concurrence of hydrogen attack and nitriding in the synthesis loop can cause damage to the ammonia converter. The higher the operation conditions (high temperature and high pressure), the larger the content of ammonia and hydrogen in the synthesis reactor, which reduces the reliability of the material. AISI 321 stainless steel is preferable for an ammonia synthesis converter because it is stabilized with titanium (a carbide-stabilizing element), which can prevent interior damage (embrittlement) to the steel caused by hydrogen. For thin elements, where stainless steel cannot be used due to the comparable thickness of the component to that of the nitride layer, inconel alloy 600 is advised to solve the problem. It remains high strength and has high oxidation resistance at high temperature. The use of superior welding (e.g. inconel alloy 600) is applied to all the expansion joints bellows. The same concerns subject to the heat exchangers, especially at the reactor outlet.

The reactor can be seen as a combination of vertical and horizontal pressure vessels and internals. In order to know the required wall thickness of the pressure vessels, the equation specified by ASME BPV Code is used. The design pressure for the vessels should be 10% above the highest operating pressure (125 bar).

$$t_w = \frac{P_i D_i}{2SE - 1.2P_i} \quad (6.2)$$

where  $S$  is the maximum allowable stress,  $P_i$  is the internal pressure and  $E$  is the welding joint efficiency. It is assumed here that the welding is fully radiographed which has a weld efficiency of 1. Substituting the values in the equation, the minimum value of the column wall thickness for a micro-plant ammonia reactor should be about 10 mm. The inner column has direct contact with the reactants and ammonia. It is operating at high pressure and high temperature. The outer column with cooling fluid or heating fluid is operating at ambient pressure. Therefore, the material used for inner and outer vessels are different. Inconel is chosen as the material for the inner column and SS321 for the outer columns. Given the density of 321 stainless steel  $8000 \text{ kg/m}^3$  and inconel density  $8900 \text{ kg/m}^3$ , the shell mass of the reactor system can be computed by using following equation.

$$\text{Shell mass} = \pi D_c L_c t_w \rho \quad (6.3)$$

where  $D_c$  is vessel diameter [m],  $L_c$  is vessel length [m],  $t_w$  is wall thickness [m] and  $\rho$  is the metal density [ $\text{kg/m}^3$ ]. The shell mass of the reactor system can be obtained.

Reactor System	Pressure [bar]	Material	Mass [kg]	Total mass [kg]
	50	Inconel	13.37	19.4
	SS321	6.073		
100	Inconel	14.54	21.1	
		SS321		6.6

**Table 6.4:** Reactor system shell mass

### 6.3.1. Base cases CAPEX estimation

Since the solubility of nitrogen and hydrogen in liquid ammonia is negligible. There is no analyzer needed after the condensation of ammonia. The price input of the electrolysis cell, compressor and the control system are provided by ZEF B.V.. The rest of the sections are based on the prices from AliExpress. All components need to be assembled in order to make a complete working product. An overview of the major plant equipment costs are shown in table 6.5.

Equipment	Cost [€] (50 bar)	Cost [€] (100 bar)
Reactor system	318	339
Nitrogen membrane separator	92	92
Nitrogen buffer	20	20
Electrolysis cell (ZEF -AEC)	150	150
Hydrogen buffer (ZEF)	25	25
Compressor (ZEF)	50	200
<b>Total</b>	<b>655</b>	<b>826</b>

**Table 6.5:** Overview of equipment cost

The most expensive part of a micro plant is the ammonia reactor system due to the use of expensive materials, which is responsible for about 49% of the total equipment cost. The second major cost is that of the electrolysis cell system, which contributes about 27% to the total equipment costs. Both costs are based on a 50 bar micro-plant.

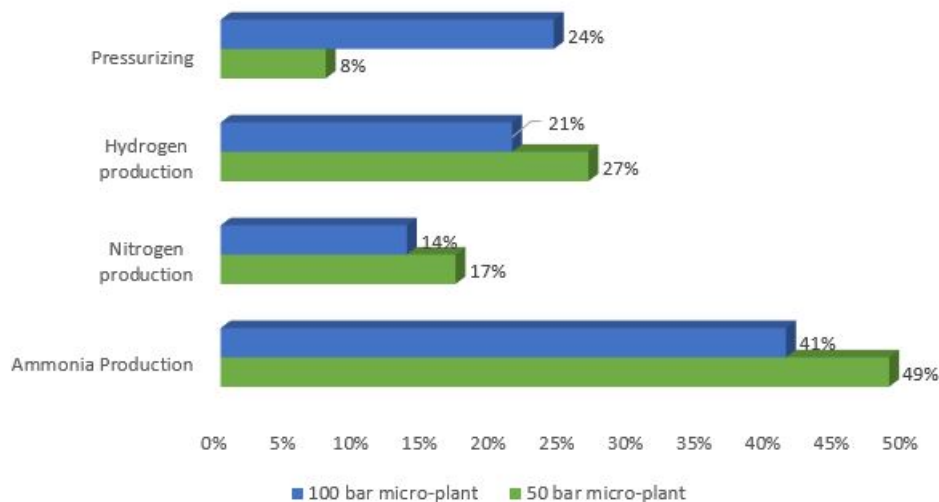


**Figure 6.5:** Equipment cost percentage in a 50 bar (green) and 100 bar (blue) operation reactor system

For a 100 bar micro-ammonia plant system, the compressor becomes the second expensive equipment, which is responsible for about 24% of the total equipment cost. It is clear that the hydrogen production system and the compressor for high pressure service should be improved and cheaper, which can significantly reduce the total cost of the micro-plant.

The OSBL cost for an initial estimation is usually in the range of 10% to 100% of ISBL cost. For a chemical plant in such a small-scale, a percentage of 10 is employed. As a rule of thumb for engineering costs, 10% of

IBSL plus OSBL cost is used. For the contingency charge, a minimum percentage of 10 of IBSL plus OSBL cost is used here. It is assumed that the total required installation time would be 1 hour by one person with an average wage of 10 €/h [12]. The rest of other CAPEX cost are estimated by using an approximation factor of the overall equipment cost.

Cost type	% of cost	% used	Cost [€]
Equipment	100	100	655
Equipment installation	-	-	10
Instrumentation and control (ZEF)	-	-	86
ISBL			751
OSBL	10 - 100	10	75
Engineering	10	10	83
Contingency charge	10 - 50	10	83
<b>Fixed capital investment</b>			991
Working capital	5 - 30	5	50
<b>Total CAPEX</b>			1041

**Table 6.6:** CAPEX estimation of a 50 bar micro-ammonia plant

Cost type	% of cost	% used	Cost [€]
Equipment	100	100	826
Equipment installation	-	-	10
Instrumentation and control (ZEF)	-	-	86
ISBL			922
OSBL	10 - 100	10	92
Engineering	10	10	101
Contingency charge	10 - 50	10	101
<b>Fixed capital investment</b>			1217
Working capital	5 - 30	5	61
<b>Total CAPEX</b>			1278

**Table 6.7:** CAPEX estimation of a 100 bar micro-ammonia plant

## 6.4. Base cases OPEX estimation

There are two types of production costs. One is the variable cost of production (VCOP), another one is the fixed cost of production (FCOP). VCOP consists of the costs of raw materials, utilities, consumables, effluent disposal, packaging and shipping. FCOP is independent of the plant operation rate or output. It is a cost combination of operating labor, supervision, direct salary overhead, maintenance, property taxes and insurance, rent of land, general plant overhead, allocated environment charges to cover superfund payments et al..

Cost type	Cost	Unit	Required amount	Unit	Cost [€/year]
Air	free	-	165	[m <sup>3</sup> /year]	0
Water	0.11	[€/tn]	290	[kg/year]	0.03
Electricity	0.02	[€/kWh]	2300	[kWh /year]	46
Catalyst	1	[€/kg]	4	[kg/year]	4
Zeolite	2	[€/kg]	26	[kg/year]	52
Silicone oil	50	[€/kg]	7	[kg/year]	0.36
R404A	1	[€/kg]	6	[kg/year]	0.01
<b>Variable cost of production (VCOP)</b>					102

**Table 6.8:** VCOP estimation of a 50 bar micro-ammonia plant

It is assumed that the micro-plant is controlled by software and operates 365 days per year. No labor and supervision are required.

Cost type	Range	Used value	Cost [€/year]
Maintenance (M)	3 - 5% (ISBL)	3%	23
Property taxes and insurance	1 - 2% (ISBL)	1%	8
Rent of land or buildings	1 - 2% (ISBL+OSBL)	1%	8
<b>Fixed cost of production (FCOP)</b>			<b>38</b>

**Table 6.9:** FCOP estimation of a 50 bar micro-ammonia plant

The cash cost of production (CCOP) for a 50 bar micro-ammonia plant is the sum of the fixed and variable production costs:

$$CCOP_{50bar} = VCOP + FCOP = 102 + 38 = 140 \quad [€/year]$$

The production cost for a 100 bar micro-ammonia plant changes slightly due to the higher equipment cost in CAPEX. Once the price for the compressor can be reduced. The total production cost of the 100 bar micro-plant can be decreased.

Cost type	Cost	Unit	Required amount	Unit	Cost [€/year]
Air	free	-	165	[m <sup>3</sup> /year]	0
Water	0.11	[€/tn]	290	[kg/year]	0.03
Electricity	0.02	[€/kWh]	2555	[kWh /year]	51
Catalyst	1	[€/kg]	4	[kg/year]	4
Zeolite	2	[€/kg]	26	[kg/year]	52
Silicone oil	50	[€/kg]	4	[kg/year]	0.18
R404A	1	[€/kg]	6	[kg/year]	0.01
<b>Variable cost of production (VCOP)</b>					<b>107</b>

**Table 6.10:** VCOP estimation of a 100 bar micro-ammonia plant

Cost type	Range	Used value	Cost [€/year]
Maintenance (M)	3 - 5% (ISBL)	3%	28
Property taxes and insurance	1 - 2% (ISBL)	1%	9
Rent of land or buildings	1 - 2% (ISBL+OSBL)	1%	10
<b>Fixed cost of production (FCOP)</b>			<b>47</b>

**Table 6.11:** FCOP estimation of a 100 bar micro-ammonia plant

The cash cost of production (CCOP) for a 50 bar micro-ammonia plant is the sum of the fixed and variable production costs:

$$CCOP_{100bar} = VCOP + FCOP = 107 + 47 = 154 \quad [€/year]$$

## 6.5. Annualized capital cost and total annualized cost

It is assumed that the micro-plant system has a 25 year lifetime. The cost of capital can be computed by applying below equation. Since it is a small scale plant, it is assumed that no debt is needed for operating the micro-plant.

$$i_c = (DR \times i_d) + ((1 - DR) \times i_e)$$

where DR is the debt ratio,  $i_d$  is the interest rate due on debt and  $i_e$  is the cost of equity. From reference [27], here  $i_c$  is taken the value of 8% from chemical basic category. The annual capital charge ratio can be determined[87].

$$ACCR = \frac{[i(1+i)^n]}{[(1+i)^n - 1]} = \frac{0.08 \times (1.08)^{25}}{[(1.08)^{25} - 1]} = 0.0937$$

Then, the annual capital cost of the two micro-plant can be calculated by applying the following equation.

$$ACC = ACCR \times \text{total fixed capital cost}$$

50 bar micro-plant	93 €/year
100 bar micro-plant	114 €/year

**Table 6.12:** Annualized capital cost of the micro-plants

The total annualized cost of production (TAC) can be derived by adding the annual operation cost to the annual capital costs.

50 bar micro-plant	233 €/year	1.8 €/kg $NH_3$
100 bar micro-plant	268 €/year	2 €/kg $NH_3$

**Table 6.13:** TAC of the micro-plants

Given that a corporate interest of 20%, the gross profit of the ammonia can be calculated.

$$\text{Gross profit} = \text{Main product revenues} - \text{CCOP}$$

	Main product revenues [€/year]	Gross profit [€/year]
50 bar micro-plant	280	140
100 bar micro-plant	322	168

**Table 6.14:** Gross profit of the micro-plants

## 6.6. Micro-ammonia plant economic performance analysis

It is assumed that the micro-ammonia plant is with a one-time fixed capital investment. The depreciation charge is calculated by using the 10 years recovery MACRS method. The plant is built at time zero and begins operation at full rate in year 1. A 20% of the corporate income tax rate is used here and the taxes are paid based on the previous year's income. The lifetime of the plant is 25 years. In the final year, the working capital is released and will be taken as a positive increment to the cash flow. A solution is solved into the spreadsheet shown below.

Year	Gross Profit [€]	Depreciation Charge [€]	Taxable Income [€]	Taxes Paid [€]	Cash Flow [€]	Discount Factor [€]	NPV [€]	Cum. NPV [€]
0	0	0	0	0	-991,00	1	-991,00	-991,00
1	140,00	99,10	40,90	-	140,00	0,925925926	129,63	-861,37
2	140,00	178,38	-38,38	8,18	131,82	0,85733882	113,01	-748,36
3	140,00	142,70	-2,70	-	140,00	0,793832241	111,14	-637,22
4	140,00	114,16	25,84	-	140,00	0,735029853	102,90	-534,32
5	140,00	91,37	48,63	5,17	134,83	0,680583197	91,76	-442,55
6	140,00	73,04	66,96	9,73	130,27	0,630169627	82,09	-360,46
7	140,00	64,91	75,09	13,39	126,61	0,583490395	73,87	-286,58
8	140,00	64,91	75,09	15,02	124,98	0,540268885	67,52	-219,06
9	140,00	65,01	74,99	15,02	124,98	0,500248967	62,52	-156,54
10	140,00	64,91	75,09	15,00	125,00	0,463193488	57,90	-98,64
11	140,00	-	140,00	15,02	124,98	0,428882859	53,60	-45,03
12	140,00	-	140,00	28,00	112,00	0,397113759	44,48	-0,56
13	140,00	-	140,00	28,00	112,00	0,367697925	41,18	40,63
14	140,00	-	140,00	28,00	112,00	0,340461041	38,13	78,76
15	140,00	-	140,00	28,00	112,00	0,315241705	35,31	114,06
16	140,00	-	140,00	28,00	112,00	0,291890468	32,69	146,76
17	140,00	-	140,00	28,00	112,00	0,270268951	30,27	177,03
18	140,00	-	140,00	28,00	112,00	0,250249029	28,03	205,05
19	140,00	-	140,00	28,00	112,00	0,231712064	25,95	231,01
20	140,00	-	140,00	28,00	112,00	0,214548207	24,03	255,04
21	140,00	-	140,00	28,00	112,00	0,198655748	22,25	277,29
22	140,00	-	140,00	28,00	112,00	0,183940507	20,60	297,89
23	140,00	-	140,00	28,00	112,00	0,170315284	19,08	316,96
24	140,00	-	140,00	28,00	112,00	0,157699337	17,66	334,62
25	140,00	-	140,00	28,00	162,00	0,146017905	23,65	358,28

**Figure 6.6:** Net present value of a 50 bar micro-plant system

The net present value equals to the difference between the present value of inflow cash and the present value of outflow cash over a period of time [87].

$$NPV = \sum_{n=1}^n \frac{CF_n}{(1+i)^n}$$

where  $n$  is the time of cash flow,  $i$  is the return that could be earned per unit of time on an investment with similar risk, CF is the net cash flow.

For the 100 bar micro-ammonia plant, the solution of NPV shows in the following figure 6.7.

Year	Gross Profit [€]	Depreciation Charge [€]	Taxable Income [€]	Taxes Paid [€]	Cash Flow [€]	Discount Factor [€]	NPV [€]	Cum. NPV [€]
0	0	0	0	0	0	1	€ -1.217,00	€ -1.217,00
1	€ 168,0	€ 121,70	€ 46,30	€ -	€ 168,00	0,925925926	€ 155,56	€ -1.061,44
2	€ 168,0	€ 219,06	€ -51,06	€ 9,26	€ 158,74	0,85733882	€ 136,09	€ -925,35
3	€ 168,0	€ 175,25	€ -7,25	€ -	€ 168,00	0,793832241	€ 133,36	€ -791,99
4	€ 168,0	€ 140,20	€ 27,80	€ -	€ 168,00	0,735029853	€ 123,49	€ -668,50
5	€ 168,0	€ 112,21	€ 55,79	€ 5,56	€ 162,44	0,680583197	€ 110,55	€ -557,95
6	€ 168,0	€ 89,69	€ 78,31	€ 11,16	€ 156,84	0,630169627	€ 98,84	€ -459,11
7	€ 168,0	€ 79,71	€ 88,29	€ 15,66	€ 152,34	0,583490395	€ 88,89	€ -370,22
8	€ 168,0	€ 79,71	€ 88,29	€ 17,66	€ 150,34	0,540268885	€ 81,23	€ -289,00
9	€ 168,0	€ 79,84	€ 88,16	€ 17,66	€ 150,34	0,500248967	€ 75,21	€ -213,79
10	€ 168,0	€ 79,71	€ 88,29	€ 17,63	€ 150,37	0,463193488	€ 69,65	€ -144,14
11	€ 168,0	€ -	€ 168,00	€ 17,66	€ 150,34	0,428882859	€ 64,48	€ -79,66
12	€ 168,0	€ -	€ 168,00	€ 33,60	€ 134,40	0,397113759	€ 53,37	€ -26,29
13	€ 168,0	€ -	€ 168,00	€ 33,60	€ 134,40	0,367697925	€ 49,42	€ 23,13
14	€ 168,0	€ -	€ 168,00	€ 33,60	€ 134,40	0,340461041	€ 45,76	€ 68,89
15	€ 168,0	€ -	€ 168,00	€ 33,60	€ 134,40	0,315241705	€ 42,37	€ 111,26
16	€ 168,0	€ -	€ 168,00	€ 33,60	€ 134,40	0,291890468	€ 39,23	€ 150,49
17	€ 168,0	€ -	€ 168,00	€ 33,60	€ 134,40	0,270268951	€ 36,32	€ 186,81
18	€ 168,0	€ -	€ 168,00	€ 33,60	€ 134,40	0,250249029	€ 33,63	€ 220,44
19	€ 168,0	€ -	€ 168,00	€ 33,60	€ 134,40	0,231712064	€ 31,14	€ 251,59
20	€ 168,0	€ -	€ 168,00	€ 33,60	€ 134,40	0,214548207	€ 28,84	€ 280,42
21	€ 168,0	€ -	€ 168,00	€ 33,60	€ 134,40	0,198655748	€ 26,70	€ 307,12
22	€ 168,0	€ -	€ 168,00	€ 33,60	€ 134,40	0,183940507	€ 24,72	€ 331,84
23	€ 168,0	€ -	€ 168,00	€ 33,60	€ 134,40	0,170315284	€ 22,89	€ 354,73
24	€ 168,0	€ -	€ 168,00	€ 33,60	€ 134,40	0,157699337	€ 21,19	€ 375,93
25	€ 168,0	€ -	€ 168,00	€ 33,60	€ 195,40	0,146017905	€ 28,53	€ 404,46

Figure 6.7: Net present value of a 100 bar micro-plant system

The net present values for both 50 bar and 100 bar micro-plants with a 8% cost of capital after 13 years of production become positive. For an operation lifetime longer than 15 years, the micro-ammonia plant of both operation pressures seems attractive investment.

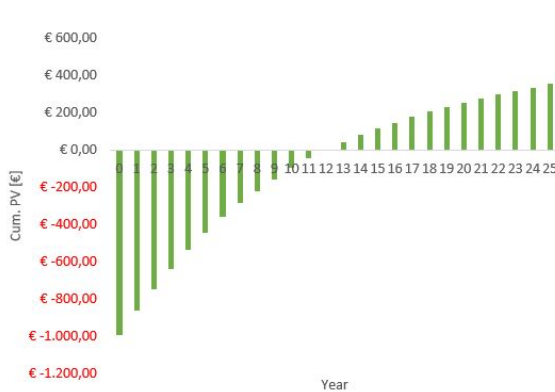


Figure 6.8: Cum. PV of a 50 micro-plant

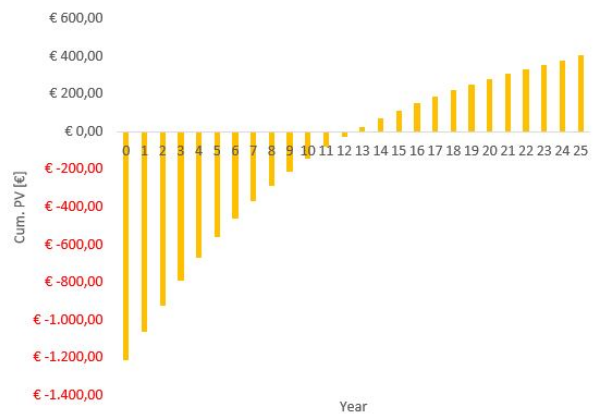


Figure 6.9: Cum. PV of a 100 micro-plant

The simple payback after tax can also be calculated from the total investment and the average annual cash flow.

	Average annual cash flow [€/year]	Simple after tax payback time [year]
50 bar micro-plant	80	13
100 bar micro-plant	95	13

Table 6.15: Simple after tax payback time of the micro-plants

The DCFROR (discount cash-flow rate of return) of the two micro-plants after 25 years of production at full capacity can be found by adjusting the interest rate at which the cumulative net present value at the end of the project year is zero. The results obtained from the calculation are 52% for a 50 bar micro-plant and 53% for a 100 bar micro-plant respectively.

## 6.7. Sensitivity analysis

In order to forecast on the viability of the micro-plant on different uncertainties, the sensitivity analysis is carried out. The sensitivity is investigated in a 15 -year NPV to variation in total fixed capital and electricity cost. The variation of annual ammonia production is also studied in order to see its impact on the cost of one kg ammonia. The results are plotted on the same graph for the two micro-ammonia plants.

### 6.7.1. Scenario I: the effect of the total capital investment on the micro-plant

In the first scenario, both of the systems have a positive 15 years NPV over the expected CAPEX range. At a lower total fixed capital cost ( $< \text{€}1000$ ), the 100 bar micro-plant is a more attractive investment. However, when the total fixed capital cost increases ( $> \text{€}1000$ ), then the 50 bar micro-ammonia plant is a better business option.

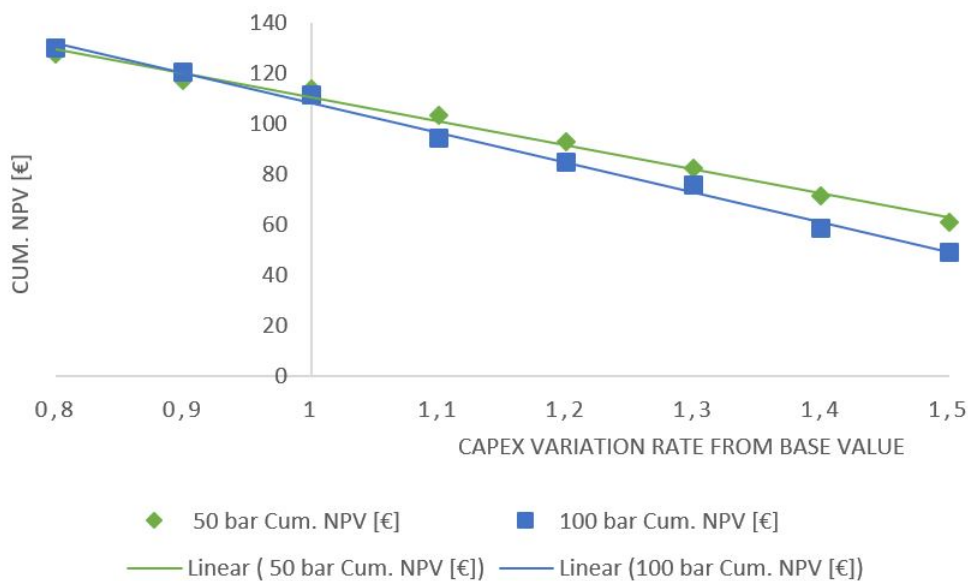
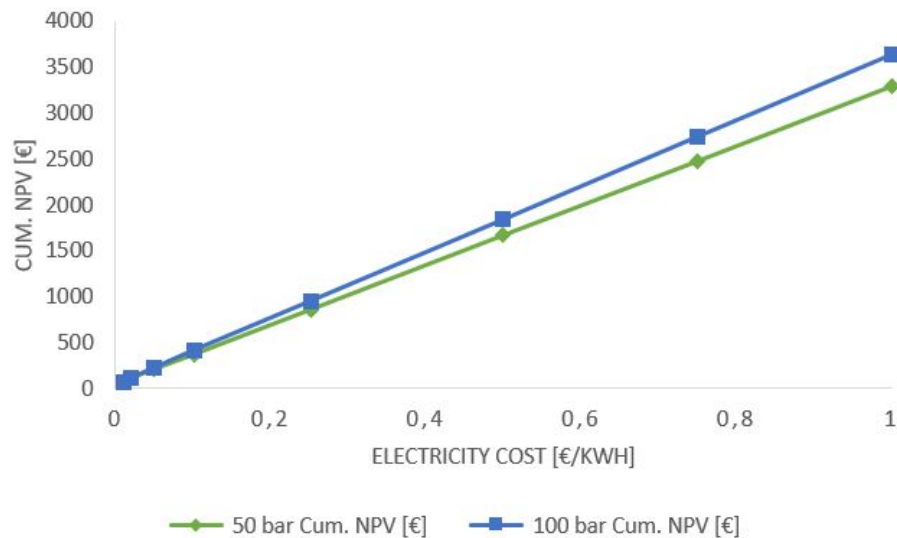


Figure 6.10: Micro-plant sensitivity analysis on CAPEX variation

### 6.7.2. Scenario II: the effect of electricity cost on the micro-plant

In the second scenario, the growth of electricity price, in accordance to the graph, will steadily increase the project NPV at the 15<sup>th</sup> year. When the renewable electricity price is less than 0.1 €/kWh, the cumulative 15 year NPV of the two systems are identical. However, once the electricity price goes up to 0.2 €/kWh, the 100 bar micro-ammonia plant turns into a much more beneficial investment plan.



**Figure 6.11:** Micro-plant sensitivity analysis on electricity cost variation

### 6.7.3. Scenario III: the effect of $NH_3$ production on the micro-plant

The productivity of the micro-ammonia plant is limited by the capacities of the equipment in the CAPEX list and the availability of renewable energy. It is assumed that there is enough sun light during the operation hours, the maximum production of ammonia is constrained only by the hydrogen production per day and the nitrogen separation system has sufficient capacity to supply the nitrogen demand. As the figure shows, the higher the ammonia productivity, the lower the ammonia cost per kilogram. There is less difference between the two systems as the production goes up. However, when the hydrogen demand is larger than the capacity of the electrolysis cell, then an additional cell should be added to the plant in order to reach the target production. In this case, the CAPEX and the variable operation cost increase because of the extra costs of the cell and energy consumption. Air and water are almost free, hence, the mass growth of air and water for the reactor system has negligible effect on the variable operational costs. The VCOP increases only if the amount of electricity consumption rises.

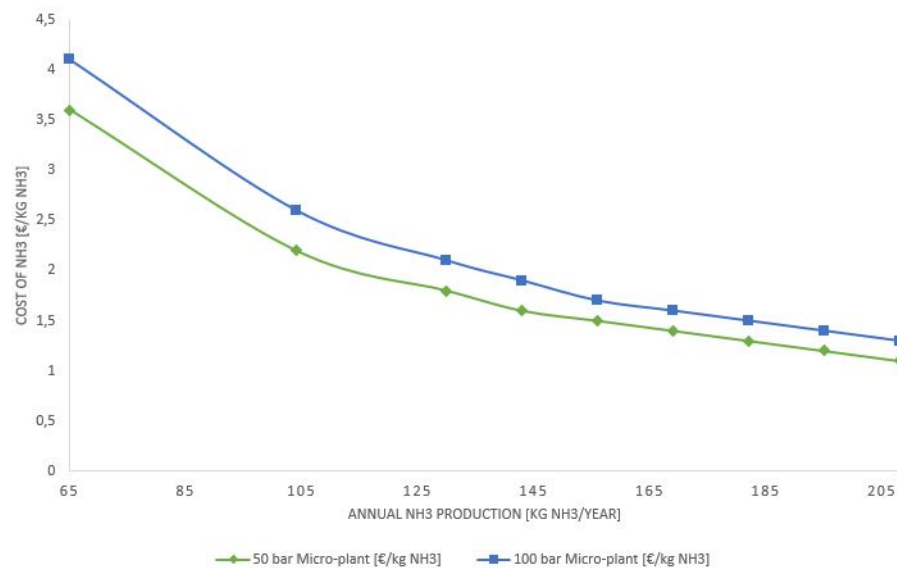


**Figure 6.12:** Micro-plant sensitivity analysis on  $NH_3$  production variation

### 6.7.4. Sensitivity analysis summary

Comparing the data of the three scenarios, the micro-plant operated at 50 bar is more suitable for a small-scale plant design. Using a better ammonia synthesis catalyst can significantly increase the yield of the product, which can accordingly reduce the cost per kg ammonia. A summary of three scenarios are plotted in the same graph for the 50 bar micro-plant. As the figure shows, the project economics for a 50 bar micro-ammonia plant are more sensitive to capital investment (CAPEX) and electricity cost than to annual production.

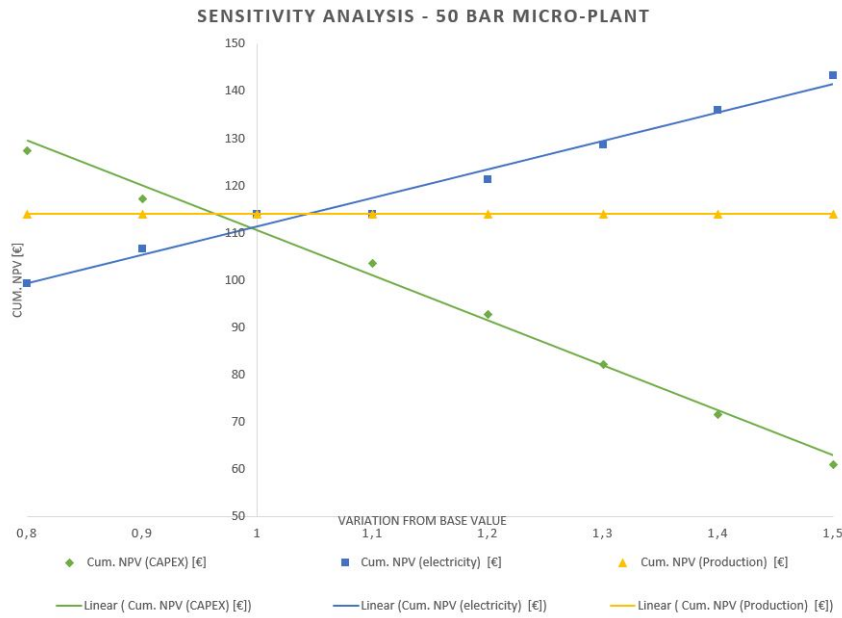


Figure 6.13: 50 bar micro-plant sensitivity analysis

## 6.8. Comparison of the micro-plant design

### 6.8.1. CAPEX and OPEX variations

The CAPEX and OPEX differences of the two micro-plants are depicted in the below figures. The system operating at lower pressure (50 bar) shows lower capital and operation investment compared to that of the higher pressure plant. The major cause for this is the costly compressor.

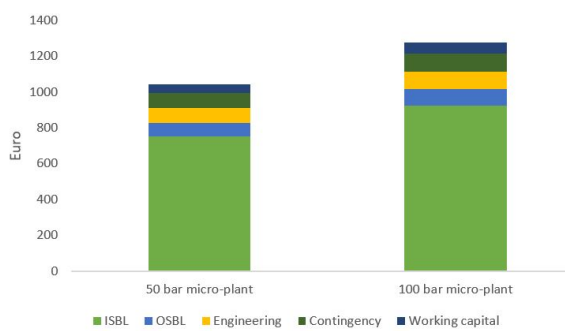


Figure 6.14: Two micro-plants CAPEX comparison

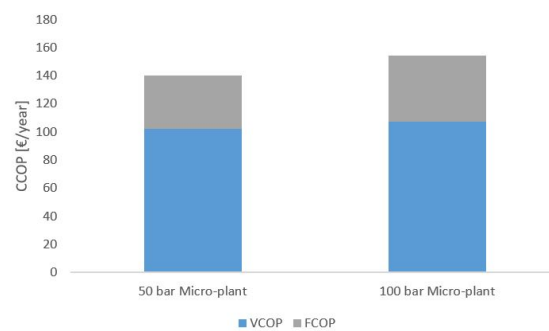
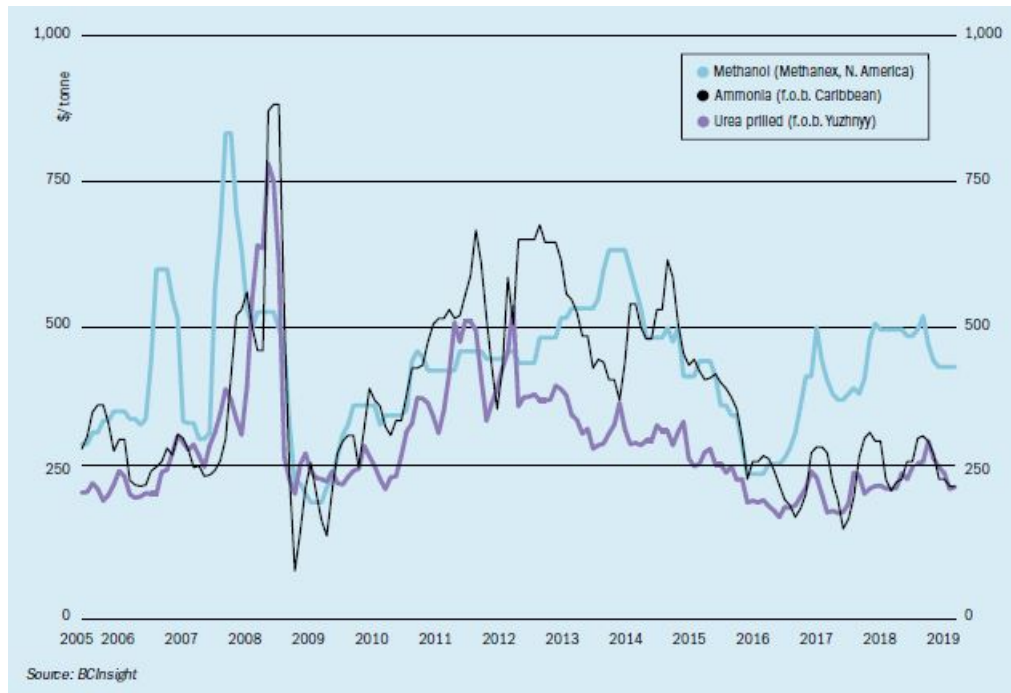


Figure 6.15: Two micro-plants OPEX comparison

### 6.8.2. Ammonia price

The global price of fossil ammonia in average is €410 per ton [10]. The actual ammonia cost varies. It depends on the type of energy sources and processes that are applied, the production location and the plant capacity. Ammonia produced from coal has the lowest cost range of €134 - €385 per ton. Natural gas is slightly higher with a cost of €359.5 - €627 per ton. Biomass produced ammonia has a cost range from €444 to €1688 per ton. Green ammonia produced by wind and solar energy currently has the highest cost with a range of

€600 to €2131 per ton and €755 - €5415 per ton, respectively [21]. For example, in 2019, the US ammonia applications have been fallen due to the poor weather in the Mid-West. The market was oversupplied and ammonia price dropped. The European ammonia producers have also been influenced by lower gas prices. The Caribbean f.o.b. prices were as low as \$200 per ton.



**Figure 6.16:** Ammonia average market cost [\$/ton] (Source: BCInsight)

To summarize and compare the prices with the proposed 50 bar version design system in this thesis, the results can be illustrated as following table 6.16.

Sources	Price [€/kg $NH_3$ ]
Coal	0.13 - 0.39
Natural gas	0.36 - 0.63
Biomass	0.44 - 1.7
Wind	0.6 - 2.1
Solar	0.76 - 5.4
* Proposed design (50 bar)	1.2 - 2.2

**Table 6.16:** Price comparison of ammonia from different sources

where \* is with a corporate interest of 20%. For one current module micro-ammonia plant, with ammonia production range from 130 kg/year to 200 kg/year, the cost of ammonia can be as low as 1 €/kg  $NH_3$  to 1.8 €/kg  $NH_3$ . By increasing the capacity of feed gas production or cost reduction in plant equipment can remarkably cut the cost to less than 1 €/kg  $NH_3$ .

### 6.8.3. Ammonia production

The top 10 ammonia producers have occupied more than 50% of the global sales (source: IFA). The global production is dominated by China, which was account for 56.1% of the total production in 2016. The other main producers are Russia (16.2%), India (14.1%) and USA (12.4%). The production of ammonia has been constantly growing in the last decades, peaking at 179 million tonnes in 2015 (see figure 6.17).

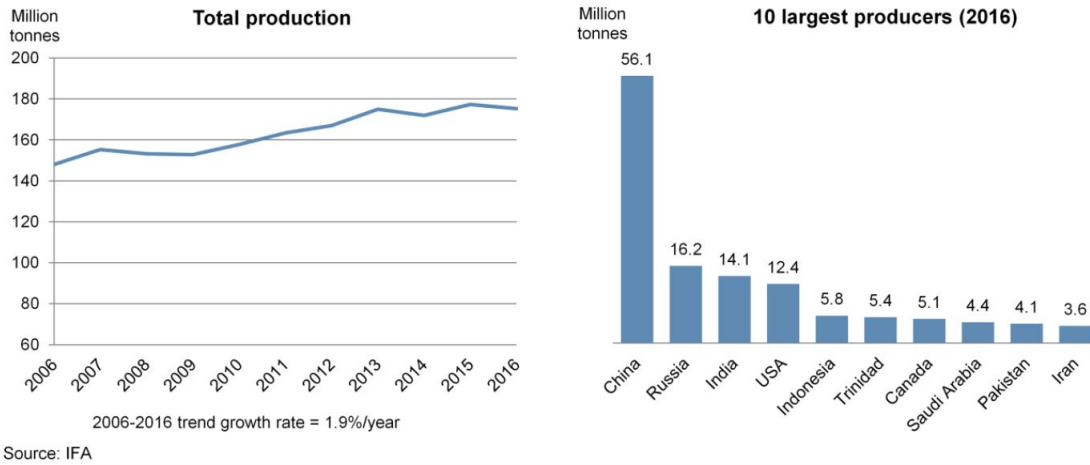


Figure 6.17: Ammonia global production and the top 10 producers (source:IFA)

The world's population in 2019 is about 7.7 billion[9]. Global annual ammonia consumption per person is approximately 23 kg  $NH_3$ /year. Let's assume that the future of ammonia is making its decentralized green micro-plant accessible for everyone in the world. Then, the proposed micro-plant design with a base production of 130 kg  $NH_3$ /year can sufficiently meet the demand.

### 6.9. Pro's and Con's of the proposed design

The ammonia production can be green and small. Based on the current work and design, some main pro's and con's of the micro-plant can be characterized from the large scale industrial ammonia plant.

#### 6.9.1. Pro's

##### (1) Decentralized ammonia production

Ammonia is the precursor to almost all nitrogen fertilizers. About 80% of the global ammonia production is consumed by the fertilizer industry, specifically, an average of 48% of the ammonia produced is used in urea production, 11% is for ammonium nitrate production, 20% is employed in the production of other fertilizers, such as ammonium sulfate, ammonium phosphate, diammonium phosphate and monoammonium phosphate [33]. Since acid is available almost everywhere, a decentralized green ammonia micro-plant makes fertilizer available for a farm's location where no transportation is permitted, such as at the top of the mountain. Besides, decentralized green ammonia micro-plants can encourage more small-scale green fertilizer businesses in developing countries where there is limited financial support to build a mega plant but with plenty of renewable resources. The micro-plant module can also be numbering up and become a green ammonia farm sharing the production facilities for the formation of existing different types of fertilizers, which is a good incentive for the industry to integrate horizontally.

Nitrogen fertilizer application by region and product

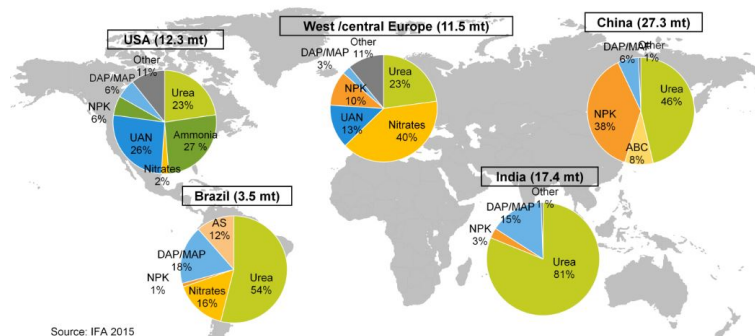


Figure 6.18: Nitrogen fertilizer application by region and product [24]

(2) Zero emission fuel market

Ammonia is also called the 2.0 version of hydrogen. It is a great energy carrier for renewable fuel blending. Furthermore, ammonia has an established transportation network and high flexibility, which can provide a full and cheaper energy transport system for energy storage and the use of power generation. Moreover,  $CO_2$  emission legislations are increasing, which creates the incentive for greener alternatives. The potential of ammonia as shipping fuel and truck fuel is high. For example, C-Job Naval Architects in the Netherlands has been researching viability of ammonia as clean sailing fuel for years and the result looks promising.

(3) Utilization of surplus energy sources

Because renewable energy production is influenced by fluctuations, surplus energy can be stored and released to a small-scale process, such as the proposed green ammonia micro-plant.

(4) Rapid development of hydrogen production electrolysis cell

The development of ZEF AEC for example, enables the ammonia production to become smaller, greener and cheaper.

(5) Avoidance of high logistic costs

One of the reasons that the OPEX of the proposed design is much lower than standard ammonia plant is due to its avoidance of shipping cost. Consequently, there is no additional cost for extra administration fee, custom duties, import taxes and so on.

(6) No operating labor cost

The total OPEX of a small-scale process can be dominant by the amount of the annual operating labor cost. However, the proposed green ammonia micro-plant is completely controlled by computer software. There is no operation labor needed for the production which significantly brings down the total capital investment of such a system.

### 6.9.2. Con's

(1) High ammonia price

This is the major disadvantage of the proposed green ammonia micro-plant. It is due to the low annual production and high fixed capital investment of the proposed design system. By using a better ammonia synthesis catalyst or finding cheaper equipment can considerably minimize the price.

# 7

## Conclusions & Recommendations

In this thesis, a conceptual design of a small-scale green ammonia synthesis reactor system is built. A set of research questions were formed at the beginning of the thesis. Conceptual process simulation in COCO and Aspen were performed so as to study if a small-scale ammonia reactor system under milder operation conditions works. After a broad process modeling and thorough HAZOP study, a reactor setup was designed and the setup was built in the TNO lab. The experimental work could validate the design concepts and answer part of the research questions. Last but not least, a techno-economic analysis was carried out to evaluate the feasibility of the integrated small-scale ammonia plant. In this chapter, the final conclusions and the according recommendations of this work are presented.

### 7.1. Conclusions

The research questions from the start of the thesis are stated as conclusions.

#### (1) What is the optimum operation condition for a small-scale ammonia synthesis reactor?

The conventional Haber-Bosch process relies on high temperature ( $>400\text{ }^{\circ}\text{C}$ ) and high pressure ( $>150\text{ bar}$ ). It requires masses of energy. Most of ammonia plants these days burn fossil fuels to obtain nitrogen and hydrogen for ammonia production. During the process, loads of carbon is being released to the atmosphere (around 3% of the global  $\text{CO}_2$  emissions). Plenty of surplus energy from the processes is wasted.

As the growth of the photovoltaics, the renewable energy capacity that is generated by the solar PV systems has reached 500 GW by 2018. As a consequence, cost of solar decreases remarkably due to the improvement in technology and economies of scale. The electricity cost from solar PV has declined from 96 \$/W in 1970 to nowadays in a range from 0.02 to 0.03 €/kWh. A typical home use solar system has a capacity of 5 kW. Besides, the availability of solar power in regions such as the Middle East is enormous. The Middle East has a minimum annual amount of 412.4 EJ. All in all, green ammonia production is possible at present and is necessary for future. A green ammonia plant in small-scale allows smart management and modification of arable fields along with expanding the approachability and affordability of ammonia products.

Ammonia synthesis is an exothermic reaction which has higher equilibrium value at a higher pressure and lower temperature (reference: table 3.2). In spite of that, this reactor, with a diameter of 3.6 cm and with a length of less than 50 cm, is able to yield more ammonia with a synthetic reaction conducting at an elevated temperature ( $400\text{ }^{\circ}\text{C}$ ) and a higher pressure (100 bar) (references: table 3.3 and table 3.4). The same conclusion is drawn from the reactor design validation experiment results (reference: chapter section 5.1). Employing smaller size catalyst particles ( $<1\text{ mm}$ ) can increase the pressure drop across the fixed bed, which leads to larger mass flow rate of the autothermal circulation reaction loop system (reference: chapter section 5.3).

The final conclusion of the first research question based on this work is that a reaction performed at 100 bar and  $400\text{ }^{\circ}\text{C}$  is the optimum operation condition for a small-scale ammonia synthesis reactor with a dimension of 3.6 cm in diameter and a bed length of 15 cm. According to the reactor experiment results, the optimal flow

rate of ammonia at 100 bar and 400 °C is 0.5 mol/h. The percent yield of ammonia is 15.4%. The conversion of nitrogen in the single pass fixed bed reactor is 15.4%. The table below (7.1) summarized the conversion values of the proposed small-scale reactor with an iron based catalyst bed length of 15 cm under optimum operation conditions.

Optimum operation condition	Conversion Modelling	Conversion Experiment	Conversion Industry	Equilibrium value
100 bar 400 °C	40%	9% - 15.4%	10% - 15% [2]	47%

**Table 7.1:** The single pass conversion values of a small-scale ammonia synthesis reactor

It can be seen that the applicability of the Temkin equation model is poor, but our experimental results are very close to the industrial conversion level.

### (2)What is the most favorable heat exchanger system?

There are two types of heat exchange system studied in this work. One is the heat pipe, another one is the double pipe heat exchanger. The heat pipe uses working fluid evaporation latent heat to achieve certain amount of energy transportation. Because of the large temperature difference between the reactor outlet gas and the condensation temperature of ammonia, making use of only one sort of heat transfer fluid is not sufficient (reference: chapter 2). Two working fluids were chosen for the modelling. One is water (20 - 200 °C) and the other one is DowthermA (100 - 450 °C). Results show that the capillary limitation is the dominant factor that decides the heat transfer capability of the heat pipes. For  $\phi = 90^\circ$ , the minimum heat transfer capability of a water heat pipe is 15 W and is about 7 W with a DowthermA heat pipe [52]. Depending on the operation condition, the quantity of heat pipes required for energy transportation from hot gas stream to cold gas stream is different, which brings extra complexity to the reactor design. Furthermore, heat pipe fabrication for a specific small-scale high temperature range process is relatively expensive.

The second option is the simplest form of a two-fluid heat exchanger, which is made up of two concentric circular tubes and is called double pipe heat exchanger. In this work, silicone oil is applied as the cooling fluid flowing through the outer tube of the heat exchanger. The gases flow into the inner tube and the two fluids run counter-currently. The double pipe heat exchanger has good flow distribution and can be cleaned easily by disassembly. It is a type of heat exchanger configuration that is suitable for one or both sides high pressure operation since it has a small-diameter tube and is less costly than a larger diameter shell. It is generally used for small-capacity applications where the total heat transfer surface area required is less than 50 m<sup>2</sup>. The two shortcut heat exchanger systems were simulated in ASPEN software. Simulation results suggest that two double pipe heat exchangers are sufficient for the proposed small-scale reactor system. One for removing the heat from the outlet hot gas and another one for pre-heating the reactor inlet feed gas. Silicone oil is recycled and is circulated back to the first heat exchanger outer tube by the pumping system. At the operation pressure of 100 bar and temperature of 400 °C, the total heat duty of each double pipe heat exchanger is about 51 W. The total required heat transfer area of one heat exchanger is on average 0.015 m<sup>2</sup> which is considerably less than 50 m<sup>2</sup>.

The study concludes that the double pipe heat exchanger is the most favorable heat exchanger system for the proposed small-scale ammonia synthesis reactor system.

### (3)What is the capital and operation cost for such a green ammonia micro-plant?

The green ammonia micro-plant consists of four main subsystems. They are the nitrogen production subsystem, the hydrogen production subsystem, the compression subsystem and the ammonia production subsystem respectively. Among all, only the ammonia production subsystem is in the scope of the current project. The techno-economic analysis of the green ammonia micro-plant is partly based on this work and the rest of the information is taken from expert advice (ZEF B.V.) and from the Alibaba vendor platform.

Two types of micro-plants are analyzed. One is an ammonia micro-plant operated at 100 bar, another one is a micro-plant with 50 bar operation pressure. Both of them have an annual productivity of 130 kg NH<sub>3</sub>/year. The analytic results are illustrated in the following table (7.2). According to the results, the 50 bar green ammonia micro-plant seems to be a more attractive business investment than that of the 100 bar micro-plant.

The total capital cost of both plants are predominant by the equipment cost. Once the costs of the compression subsystem and the reactor material can be reduced, then the 100 bar green ammonia micro-plant would be a better choice than 50 bar micro-plant. The cost of ammonia per kilogram can also be significantly reduced.

	50 bar micro-plant	100 bar micro-plant	Unit
CAPEX	1041	1278	€
OPEX	140	154	€/year
Cost of ammonia	1.8	2	€/kg

**Table 7.2:** A green ammonia micro-plant techno-economic analysis summary

## 7.2. Recommendations

In this section, recommendations for reactor system design optimizations and future work are provided in four main categories: reaction experiment, reaction catalyst, double pipe heat exchangers and separation process.

### 7.2.1. Reaction experiment

It is highly recommended to perform additional experimental work on various parameters, such as a wider range of temperature, a milder operating pressure, varying mass flow rate, fixed bed pressure drop measurement, effect of inner on the reaction, effect of catalyst type and size on the reaction, catalyst activity testing and so on. An accurate ammonia analyzer for the experiment is greatly advised for obtaining more precise results of the ammonia conversions.

In this work, the experiment has been carried out in a small-scale single fixed bed plug flow reactor. The current results show that the reactor is able to produce 6% to 15% percent yield of ammonia under the tested conditions. Since temperature has stronger impact on the reaction rate than that of pressure, an investigation of a multi-beds small-scale reactor system in series or in parallel at different reaction temperatures seems to be a valuable further research for this project and for the improvement of the production.

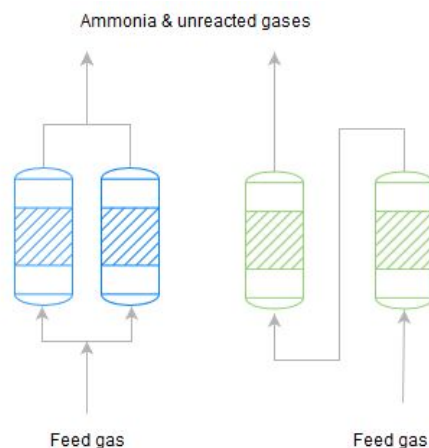


**Figure 7.1:** Multi-bed reactor: in series or in parallel

### 7.2.2. Reaction catalyst

It is clear that using a much smaller iron based catalyst particle ( $< 1$  mm) can have one main advantage to the ammonia auto-thermal synthesis loop design. The reduction in the catalyst size can lead to higher fixed bed pressure drop which can increase the mass flow rate in the synthesis loop. Furthermore, one of the targets for this work is to design a reactor system which is able to produce ammonia at a much milder operation condition. In such circumstances, the use of a better catalyst, such as the Ru-based catalyst, could be an alternative for the process optimization. For example, study of RENRC in Japan [57] shows that ammonia synthesis process using  $Ru/CeO_2$  operated at 25 bar and  $400$  °C can have a space time yield value of 0.072 g

$NH_3/g_{cat}/h$  which is nearly three times higher than the best space time yield value  $0.026 g NH_3/g_{cat}/h$  this work achieved at 100 bar and  $400^\circ C$ . According to Alibaba platform, a self made  $Ru/CeO_2$  catalyst requires a minimum cost of €330 per 300 gram, while the iron base catalyst costs only about €1 per 300 gram.

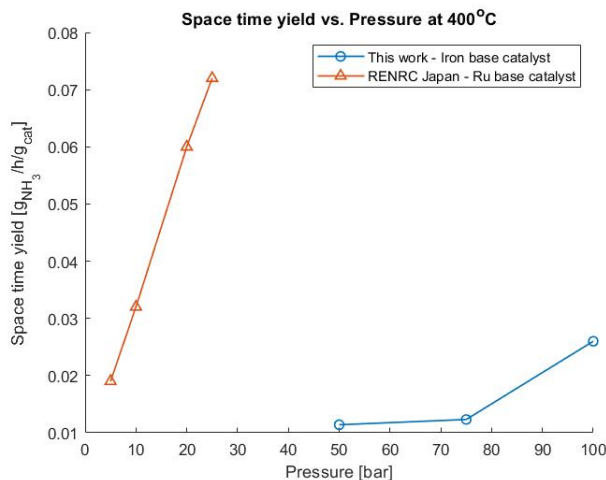


**Figure 7.2:** Comparison between iron base catalyst and Ru base catalyst at  $400^\circ C$

### 7.2.3. Double pipe exchangers

The double pipe heat exchanger should be further designed based on the simulation results. The current model of the double pipe heat exchangers is designed with completed insulation which is not possible in reality. Since the silicone oil which meets the requirement of this application is available in the commercial market, a laboratory setup of the reactor in combination with the heat exchangers system can be built. Then, a further design validation can be achieved. The efficiency of the system and the heat loss can be calculated.

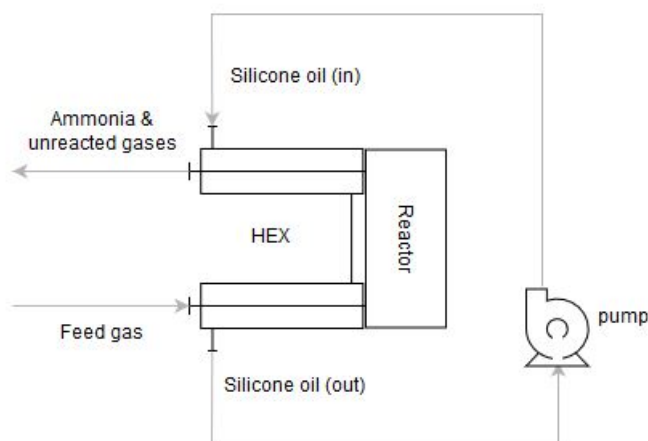


**Figure 7.3:** Setup system of reactor in combination with heat exchanger system

### 7.2.4. Separation process

Reducing the pressure in the Haber-Bosch process synthesis loop is difficult because it leads to the decline of ammonia conversion per single pass. In this case, the condensation temperature of ammonia from unreacted gases decreases. Correspondingly, more refrigerant is needed for removing the heat. An alternative is to apply ammonia absorption as a separation process, which can occur at temperature above  $200^\circ C$ . As a result, a more economic and environmental friendly heat transfer fluid can be taken into account, such as water, and less heat transfer area is required. The lower the synthesis loop operation pressure, the less wall thickness of the reactor system and a cheaper pressurizing system can be employed. The total capital cost of an ammonia micro-plant can be significantly reduced.

# A

## Reactor Development

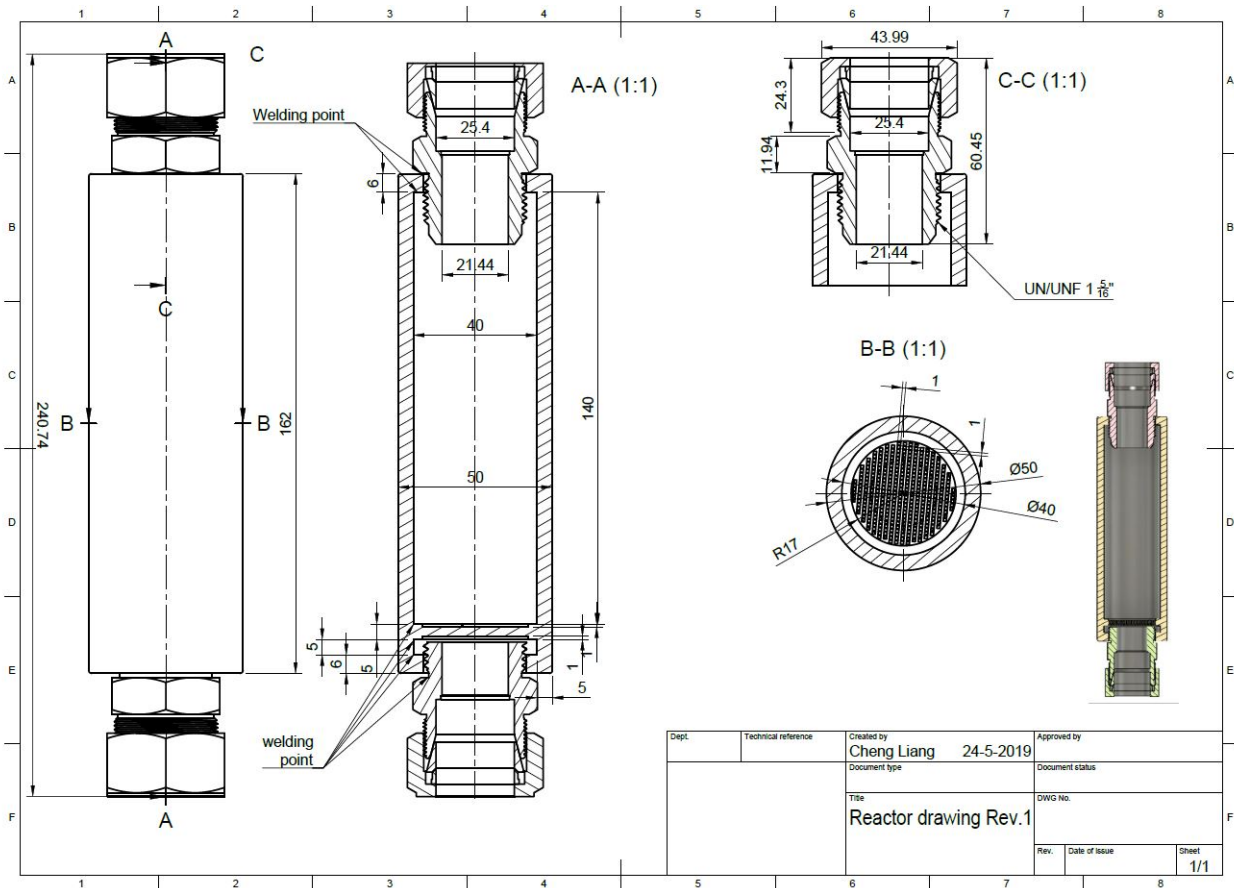
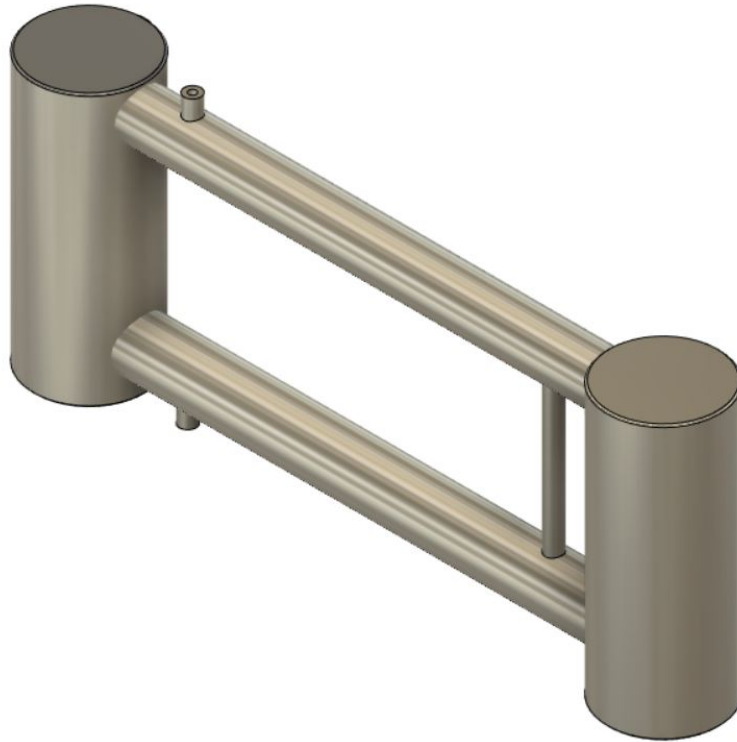
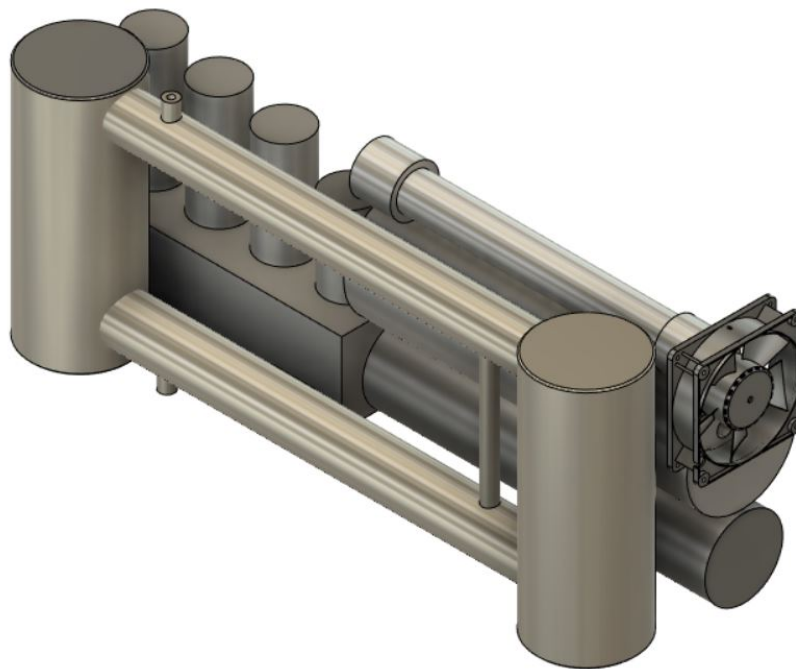


Figure A.1: Reactor design revision 1 - single pass plug flow reactor for experiment



**Figure A.2:** Reactor design revision 2 with double pipe heat exchanger in accordance to ASPEN process simulation results



**Figure A.3:** Green ammonia micro-plant (50 bar) without solar panel<sup>2</sup>

<sup>2</sup>The drawing of the micro-plant (figure A.3) is for illustration purpose only. The actual products of the compressor (ZEF B.V.), alkaline electrolysis cell (ZEF B.V.) and hydrogen buffer (ZEF B.V.) may vary due to product design and enhancement.

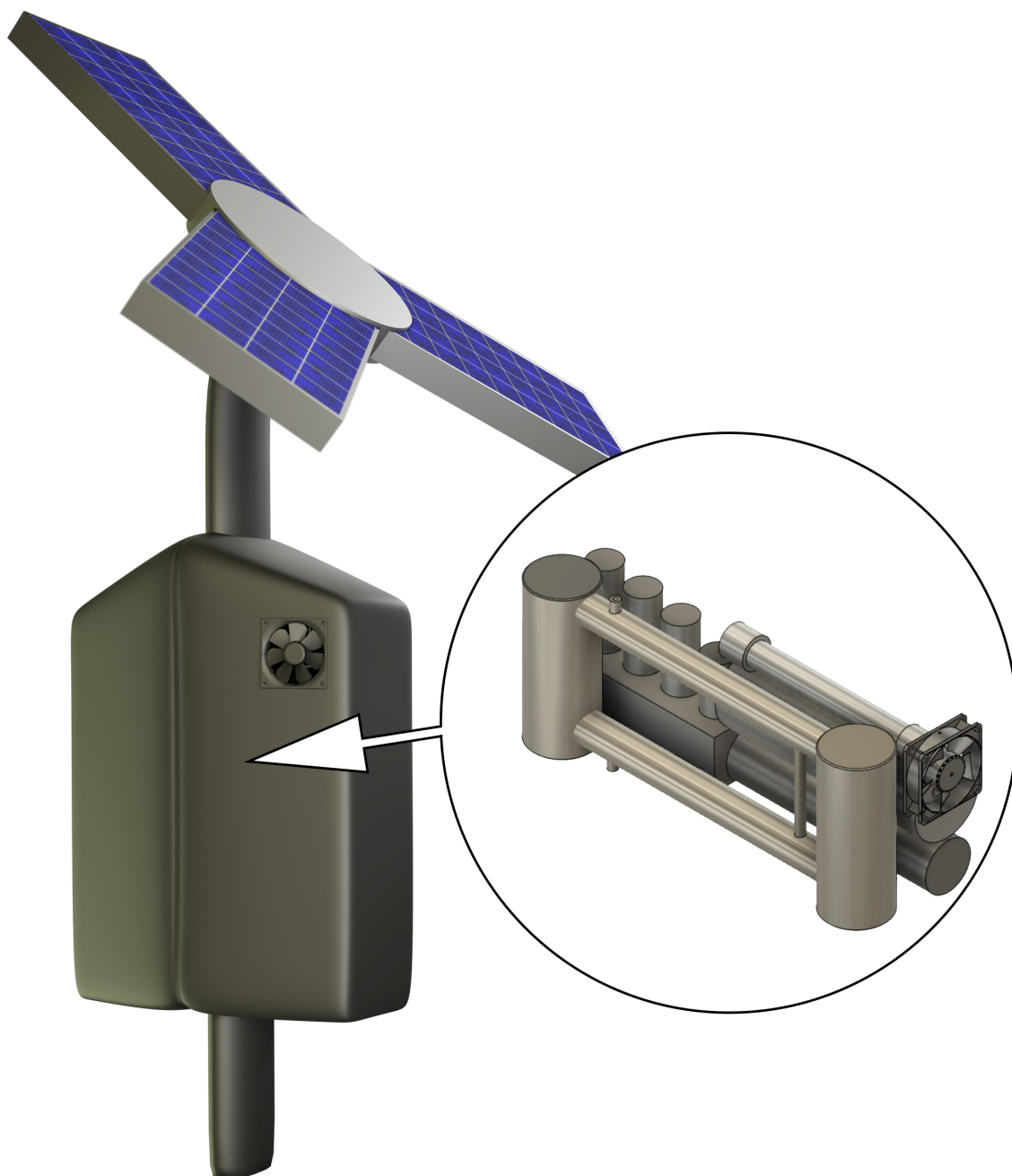


**Figure A.4:** Green ammonia micro-plant (50 bar) with solar panel



# B

## Reactor Material Properties

	Properties	AISI 316L	AISI 321	Inconel 600
Mechanical	Elastic modulus [GPa]	200	200	190
	Elongation at break	9% – 55%	34% – 50%	3.4%
	Fatigue strength [MPa]	170 – 450	220 – 270	300
	Tensile strength: ultimate (UTS) [MPa]	530 – 1160	590 – 690	990
	Tensile strength: yield (proof) [MPa]	190 – 870	220 – 350	760

**Table B.1:** Material mechanical properties in comparison with SS316L [54]

	Properties	AISI 316L	AISI 321	Inconel 600
Thermal	Max. corrosion temperature [ $^{\circ}C$ ]	410	480	-
	Max. mechanical temperature [ $^{\circ}C$ ]	870	870	1100
	Melting onset (solidus) [ $^{\circ}C$ ]	1380	1400	1350
	Specific heat capacity [ $J/kg - K$ ]	470	480	460
	Thermal conductivity [ $W/m - K$ ]	15	16	14
	Thermal expansion [ $\mu/m - K$ ]	16	17	13

**Table B.2:** Material thermal properties in comparison with SS316L [54]

To have corrosion resistance, the chromium content must be above 12% and the higher the chromium content, the more resistance the alloy gains in oxidizing conditions. Additional nickel can improve the material corrosion resistance in non-oxidizing environments.

Alloy Composition	AISI 316L	AISI 321	Inconel 600
Carbon (C)	0 – 0.03%	0 – 0.08%	0 – 0.15%
Chromium (Cr)	16 – 18%	17 – 19%	14 – 17%
Iron (Fe)	62 – 72%	65.3 – 74%	6 – 10%
Manganese (Mn)	0 – 2%	0 – 2%	0 – 1%
Molybdenum (Mo)	2 – 3%	0	-
Nickel (Ni)	10 – 14%	9 – 12%	72 – 80%
Nitrogen (N)	0 – 0.1%	0 – 0.1%	-
Phosphorus (P)	0 – 0.045%	0 – 0.045%	-
Silicon (Si)	0 – 0.75%	0 – 0.75%	0 – 0.5%
Sulfur (S)	0 – 0.03%	0 – 0.03%	0 – 0.015%
Titanium (Ti)	0	0 – 0.7%	-
Copper (Cu)	-	-	0 – 0.5%

**Table B.3:** Alloy compositions in comparison with SS316L [54]



# Bibliography

- [1] BASF.
- [2] Haber process.
- [3] NFPA.
- [4] Sodium hydroxide.
- [5] Ammonia, .
- [6] Sulfuric acid, .
- [7] Climate in Saudi-arabia.
- [8] Silicone oil.
- [9] Current world population.
- [10] Zauba.
- [11] The Netherlands annual weather averages, 2019.
- [12] Hourly wage for select jobs in construction in the middle east, 2019.
- [13] Ballance Agri-Nutrients. Kapuni hydrogen project seen as catalyst for NZ market.
- [14] AISI. High-temperature characteristics of stainless steels. In *A Des. Handb. Ser.*, page 47. 1979.
- [15] K. L. M. Al-Malah. *Aspen plus chemical engineering application*. John Wiley & Sons, Inc., New Jersey, 2017.
- [16] AmsterCHEM. Matlab CAPE-OPEN Thermo Import.
- [17] M. Appl. *Ammonia principles and industrial practice*. Wiley-VCH, Weinheim, 1999.
- [18] H. Araki, Y. Kataoka, and M. Murase. Measurement of condensation heat transfer coefficient inside a vertical tube in the presence of noncondensable gas. *J. Nucl. Sci. Technol.*, 32(6):517–526, 1995.
- [19] ARENA. Renewable hydrogen could power Moranbah ammonia facility.
- [20] B. V. Babu and R. Angira. Optimal design of an auto-thermal ammonia synthesis reactor. *Comput. Chem. Eng.*, 29(5):1041–1045, 2005.
- [21] J. R Bartels. A feasibility study of implementing an ammonia economy. *Digit. Repos. @ Iowa State Univ.*, page 102, 2008.
- [22] L. K. Boerner. Industrial ammonia production emits more  $CO_2$  than any other chemical-making reaction. Chemists want to change that, 2019.
- [23] M. Boudart. Kinetics of chemical processes. page 17. 1991.
- [24] T. Brown. If green ammonia, whence urea? Stamicarbon's innovation agenda.
- [25] T. Brown. Small-scale ammonia: where the economics work and the technology is ready, 2018.
- [26] I. I. Cheema and U. Krewer. Operating envelope of Haber-Bosch process design for power-to-ammonia. *RSC Adv.*, 8(61):34926–34936, 2018.
- [27] A. Damodaran. Cost of capital by sector.

- [28] A. R. Dehghani-Sani, E. Tharumalingam, M. B. Dusseault, and R. Fraser. Study of energy storage systems and environmental challenges of batteries. *Renew. Sustain. Energy Rev.*, 104:192–208, 2019.
- [29] Delft University of Technology. First battery for electricity storage and hydrogen production thanks to Waddenfonds in Groningen, 2018.
- [30] C. J. Doonan, D. J. Tranchemontagne, T. G. Glover, J. R. Hunt, and O. M. Yaghi. Exceptional ammonia uptake by a covalent organic framework. *Nat. Chem.*, 2(3):235–238, 2010.
- [31] D. C. Dyson and J. M. Simon. A kinetic expression with diffusion correction for ammonia synthesis on industrial catalyst. *Ind. Eng. Chem. Fundam.*, 7(4):605–610, 1968.
- [32] Fisher Science Education. Sulfuric Acid Safety Data Sheet. 2015.
- [33] C. Egenhofer, L. Schrefler, V. Rizos, A. Marcu, F. Genoese, A. Renda, J. Wiczorkiewicz, S. Roth, F. Infelise, G. Luchetta, L. Colantoni, W. Stoefs, J. Timini, and F. Simonelli. *Composition and drivers of energy prices and costs in energy intensive industries : the case of ceramics , flat glass and chemical industries CEPS special report*. 2014.
- [34] Enaex. ENAEX & ENGIE: on the path to a smooth zero carbon transition in the Chilean mining sector.
- [35] J. A. Finneran. Process for the production of hydrogen-rich gas, 1969.
- [36] C. G. Gachet, G. Cavalletto, and L. D. E. Mourgues. Ammonia synthesis and related reactions for iron-cobalt and iron-nickel alloy catalysts. Part I. catalysts reduced at 853 K. *Appl. Catal. A Gen.*, 3:57–64, 1982.
- [37] W. Gao, P. K. Wang, J. P. Guo, F. Chang, T. He, Q. R. Wang, G. T. Wu, and P. Chen. Barium hydride-mediated nitrogen transfer and hydrogenation for ammonia synthesis: a case study of cobalt. *ACS Catal.*, 7(5):3654–3661, 2017.
- [38] L. J. Gillespie and J. A. Beattie. The thermodynamic treatment of chemical equilibria in systems composed of real gases. II. A relation for the heat of reaction applied to the ammonia synthesis reaction. The energy and entropy constants for ammonia. *Phys. Rev. Lett.*, 36(246):1008–1013, 1930.
- [39] L. J. Gillespie and J. A. Beattie. The thermodynamic treatment of chemical equilibria in systems composed of real gases. III. Mass action effects. The optimum hydrogen: Nitrogen ratio for ammonia formation in the haber equilibrium. *J. Am. Chem. Soc.*, 52(11):4239–4246, 1930.
- [40] W.A. Glover and J. P. Yoars. Adiabatic ammonia synthesis converter. pages 77–81, 1972.
- [41] J. B. Hansen and P. Han. The SOC4NH3 Project in Denmark. *NH3 Event*, pages 1–22, 2019.
- [42] D. Harris. Hydrogen energy value chains : ammonia as an enabling hydrogen carrier. CSIRO energy, 2019.
- [43] J. Helminen, J. Helenius, E. Paatero, and I. Turunen. Comparison of sorbents and isotherm models for  $NH_3$ -gas separation by adsorption. *AIChE J.*, 46(8):1541–1555, 2000.
- [44] J. Ikäheimo, J. Kiviluoma, R. Weiss, and H. Holttinen. Power-to-ammonia in future North European 100% renewable power and heat system. *Int. J. Hydrogen Energy*, 43(36):17295–17308, 2018.
- [45] Mordor Intelligence. Ammonia market - growth, trends, and forecast (2019 - 2024).
- [46] IRENA. Hydrogen and ammonia ' IEA. International Energy Agency, 2019.
- [47] IRENA. Renewable capacity statistics 2019. *IRENA*, page 60, 2019.
- [48] J. R. Jennings. *Catalytic Ammonia Synthesis*. Springer Science and Business Media, New York, 1991.
- [49] M. Kitano, Y. Inoue, M. Sasase, K. Kishida, Y. Kobayashi, K. Nishiyama, T. Tada, S. Kawamura, T. Yokoyama, M. Hara, and H. Hosono. Self-organized ruthenium – barium core – shell nanoparticles on a mesoporous calcium amide matrix for efficient low-temperature ammonia synthesis. *Angew. Chemie*, 130:2678–2682, 2018.

- [50] I. F. Kurunov, V. R. Ansheles, and S. V. Svitko. Production of ammonia from top gas. *Metallurgist*, 43 (11-12):529–533, 1999.
- [51] A. T. Larson and R. S. Taur. Contributions to the study of ammonia catalyst. *Chem. Met. Eng.*, 26(14):647, 1922.
- [52] C. Liang. Haber-Bosch Process : Ammonia synthesis Small scale ammonia reactor design. Technical report, Delft University of Technology, Delft, 2019.
- [53] H. Z. Liu. Ammonia synthesis catalyst 100 years : Practice , enlightenment and challenge. *Chinese J. Catal.*, 35(10):1619–1640, 2014.
- [54] MakeltFrom.com. AISI 316 stainless steel vs. AISI 321 stainless steel.
- [55] M. Malmali, Y. M. Wei, A. V. McCormick, and E. L. Cussler. Ammonia Synthesis at Reduced Pressure via Reactive Separation. *Ind. Eng. Chem. Res.*, 55(33):8922–8932, 2016.
- [56] S. H. Mark, L. W. Andrew, A. V. McCormick, and E. L. Cussler. Ammonia absorption at Haber process conditions. *AIChE J.*, 59(11):215–228, 2012.
- [57] H. Matsumoto, J. Rahat, Y. Manaka, M. Ishii, and T. Nanba. Analysis of influence of operating pressure on dynamic behavior of ammonia production over ruthenium catalyst under high pressure condition. In *2018 AIChE Annu. Meet.*, page 16, Japan, 2018. AIIST.
- [58] A. F. Mills. *Basic heat and mass transfer*. Pearson Education Limited, Essex, 2 edition, 2014.
- [59] A. Mittasch and W. Frankenburger. The historical development and theory of ammonia synthesis. *J. Chem. Educ.*, 6(12):7, 1929.
- [60] J. M. Modak. Haber process for ammonia synthesis. *Resonance*, 16(12):1159–1167, 2011.
- [61] N. Nagalingam. Methanol from Sunlight and Air Condenser 1D Model. Technical report, Delft University of Technology, Delft, 2019.
- [62] Con Narcot. Port Lincoln green  $H_2/NH_3$  supply chain demonstrator. 2019.
- [63] G. A. Nelson and R. T. Effinger. Blistering and embrittlement of pressure vessel steels by hydrogen. *Weld. Res. Supplement*, 34(1):125–219, 1955.
- [64] A. Nielsen. *An investigation on promoted iron catalysts for the synthesis of ammonia*. The Haldor Topsoe Research Laboratory, Vedbak, 1968.
- [65] A. Nielsen. *Ammonia catalysis and manufacture*. Springer-Verlag Berlin Heidelberg, 1995.
- [66] J. U. Nwalor, J. G. Goodwin, and P. Biloen. Steady-state isotopic transient-kinetic analysis of iron-catalyzed ammonia synthesis. *J. Catal.*, 117(1):121–134, 1989.
- [67] Y. Ogura, K. Tsujimaru, K. Sato, S. Miyahara, T. Toriyama, T. Yamamoto, S. Matsumura, K. Nagaoka, K. Tsujimaru, K. Sato, S. Miyahara, T. Toriyama, T. Yamamoto, S. Matsumura, and K. Nagaoka.  $Ru/La)_{0.5}Pr_{0.5}O_{1.75}$  catalyst for low-temperature ammonia synthesis. *ACS Sustain. Chem. Eng.*, 6: 17258–17266, 2018.
- [68] A. Patil, L. Laumans, and H. Vrijenhoef. Solar to ammonia - Via Proton's NFuel units. *Procedia Eng.*, 83: 322–327, 2014.
- [69] S. S. Rashwan, A. M. Shaaban, and F. Al-Suliman. A comparative study of a small-scale solar PV power plant in Saudi Arabia. *Renew. Sustain. Energy Rev.*, 80:313–318, 2017.
- [70] M. Reese. Lessons Learned in Developing a Wind to Ammonia Pilot Plant. West Central Research and Outreach Center, 2012.
- [71] M. Reese, C. Marquart, M. Malmali, K. Wagner, E. Buchanan, A. V. McCormick, and E. L. Cussler. Performance of a Small-Scale Haber Process. *Ind. Eng. Chem. Res.*, 55:3742–3750, 2016.

- [72] Riogen. MSDS catalyst.pdf. 2019.
- [73] H. Ritchie. How many people does synthetic fertilizer feed?, 2017.
- [74] S. Rokni, J. Sehested, P. Stoltze, C. J.H. Jacobsen, and E. Törnqvist. Ammonia synthesis over a multipromoted iron catalyst: extended set of activity measurements, microkinetic model, and hydrogen inhibition. *J. Catal.*, 188(1):83–89, 2002.
- [75] I. E. Sampson. Design and operation of double pipe heat exchanger. *TLEP Journals*, 3:1–26, 2017.
- [76] R.W. Serth. Design of double-pipe heat exchangers. In *Process heat Transf. Princ. Appl.*, chapter 4, pages 128–186. Elsevier Ltd, Kingsville, Texas, 2007.
- [77] R. K. Shah and P. S. Dusan. *Fundamentals of heat exchanger design*. John Wiley & Sons, Inc., New Jersey, 2003.
- [78] V. E. Sharonov, J. V. Veselovskaya, and Y. I. Aristov. Ammonia sorption on composites 'CaCl<sub>2</sub> in inorganic host matrix': isosteric chart and its performance. *Int. J. Low-Carbon Technol.*, 1(3):191–200, 2009.
- [79] Siemens. Green Ammonia and Hydrogen at Scale. In *Siemens Hydrog. Solut.*, page 21. Siemens, 2019.
- [80] C. Smith, M. Malmali, C. Y. Liu, A. V. McCormick, and E. L. Cussler. Rates of ammonia absorption and release in calcium chloride. *ACS Sustain. Chem. Eng.*, 6(9):11827–11835, 2018. ISSN 21680485.
- [81] P. Stephan. *VDI Heat Atlas*. Springer, Berlin Heidelberg, 2 edition, 2010.
- [82] P. Stoltze and J. K. Nørskov. Bridging the "pressure gap" between ultrahigh-vacuum surface physics and high-pressure catalysis. *Phys. Rev. Lett.*, 55(22):2502–2505, 1985.
- [83] P. Stoltze and J. K. Nørskov. The surface science based ammonia kinetics revisited. *Top. Catal.*, 1(3-4): 253–263, 1994.
- [84] Thyssenkrupp Industrial. One of the largest single-train ammonia plants worldwide.
- [85] M. M. Tokarev, J. V. Veselovskaya, H. Yanagi, and Yu I. Aristov. Novel ammonia sorbents "porous matrix modified by active salt" for adsorptive heat transformation: 2. Calcium chloride in ACF felt. *Appl. Therm. Eng.*, 30(8-9):845–849, 2010.
- [86] Haldor Topsoe. Ammonia converter baskets S-300.
- [87] G. Towler and R. Sinnott. *Chemical engineering design*. 2012. doi: 10.1016/b978-0-08-096659-5.00019-5.
- [88] A. Tummala, R. K. Velamati, D. K. Sinha, V. Indrajaya, and V. H. Krishna. A review on small scale wind turbines. *Renew. Sustain. Energy Rev.*, 56:1351–1371, 2016.
- [89] Cairo University. Chapter 9: Forced convection correlations.
- [90] A. van Wijk. Green hydrogen economy ammonia as a hydrogen carrier. Rotterdam, 2019.
- [91] J. S. Vanick and J. G. Thompson. Deterioration of steels in the synthesis of ammonia. *Technol. Pap. Bur. Stand.*, 22(361):39, 1927.
- [92] K. Wagner, M. Malmali, C. Smith, A. V. McCormick, E. L. Cussler, and N. C. A. Seaton. Column absorption for reproducible cyclic separation in small scale ammonia synthesis. *AIChE*, 63(7):11, 2017.
- [93] Yara. Green hydrogen feed for Haber Bosch ammonia synthesis. 2019.
- [94] S. Zhang. A Chemical reaction revolutionized farming 100 years ago. Now it needs to go.



**Green Haber-Bosch Process:**  
A Small-Scale Ammonia Reactor  
System Design

---

C. Liang